

# **A weather system perspective on winter-spring rainfall variability in southeastern Australia during El Niño**

Master's thesis  
of

**Seraphine Hauser**

June 2019



INSTITUTE OF METEOROLOGY AND CLIMATE RESEARCH  
KARLSRUHE INSTITUTE OF TECHNOLOGY (KIT)

Referent:

Dr. Christian Grams

Co-referent:

Prof. Dr. Peter Knippertz



*This document is licenced under the Creative Commons Attribution-ShareAlike 4.0 International Licence.*

# Abstract

The southeastern Australian rainfall variability is prominent for its strength compared to other places in the world that are located in similar climate zones. The very high rainfall variability on intraseasonal, interannual and interdecadal time scales can be attributed to processes on different temporal and spatial scales. Local weather systems (cut-off low pressure systems and extratropical cyclones) are the main contributors to rainfall and affect the sub-monthly rainfall variability in southeastern Australia. Multiple drivers that include the El Niño-Southern Oscillation (ENSO), the Indian Ocean Dipole (IOD) and the Southern Annular Mode (SAM) influence rainfall in southeastern Australia on intraseasonal-to-interannual time scales. ENSO is the leading driver and its positive phase, El Niño, is typically associated with below-average cool-season (April-October) rainfall in southeastern Australia. However, the El Niño of 1997 with near-average rainfall points to a large case-to-case variability. Despite recent progress in understanding the linkage of remote climate drivers and rainfall variability, the dynamic processes that govern rainfall during El Niño are not fully understood. With this study, we aim to advance the dynamic understanding by combining a set of four clusters of monthly rainfall anomalies over southeastern Australia with a novel data set of objectively identified weather systems derived from ERA-Interim reanalyses. We want to investigate in particular the effect of El Niño on rainfall from a weather system perspective.

We find that above-average winter-spring (June-November) rainfall over southeastern Australia during El Niño (Cluster 1) is associated with a shift of the westerly wind belt towards Antarctica (positive SAM) and the increased frequency of midlatitude atmospheric blocking southeast of Australia. From a weather system perspective, above-average rainfall over southeastern Australia results from the enhanced activity of cut-off low pressure systems (cut-off lows) forming over the Great Australian Bight west of a blocking anticyclone and an increased frequency of warm conveyor belts over southeastern Australia. Conversely, below-average winter-spring rainfall over southeastern Australia during El Niño (Cluster 2) is related to anomalous high pressure over almost the entire continent that suppresses the eastward movement of rain-producing weather systems. Significant decreases of extratropical cyclone and warm conveyor belt frequencies and reduced moisture flux are observed over the eastern half of Australia and over maritime areas to the east of Australia. Below-average rainfall inland and above-average rainfall along the East Coast of southeastern Australia (Cluster 3) is associated with a broad area of anomalous high pressure south of central Australia during El Niño. This anomalous pattern relates to the positive SAM and favors the development of cut-off lows over the Tasman Sea bringing rainfall to southeastern Australia. During the occurrence of above-average (below average) rainfall along the South (East) Coast

---

in Cluster 4, anomalous low geopotential south of Australia points to enhanced westerlies along the South Coast of southeastern Australia that is associated with the negative SAM phase during El Niño. The increased frequency of extratropical cyclones along the South Coast indicates the enhanced contribution on rainfall in the south of southeastern Australia. In contrast, the decreased frequency of rain-producing systems over the Tasman Sea points to below-average rainfall along the East Coast of Australia.

The results of this study add to a better understanding of the processes that affect rainfall variability during El Niño. Since previous studies have focused on the statistical links between large-scale remote drivers and rainfall in southeastern Australia, the results of this thesis allow a significant step forward in understanding the weather system variability during El Niño.

# Zusammenfassung

Im Vergleich zu anderen Orten mit ähnlichen Klimabedingungen ist die Niederschlagsvariabilität in Australien für ihre herausragende Stärke bekannt. Insbesondere im Südosten von Australien ist sie sehr hoch, was auf eine Vielzahl von Prozessen auf unterschiedlichen zeitlichen und räumlichen Skalen zurückzuführen ist. Lokale Wettersysteme (Cut-off Tiefdruckgebiete und außertropische Zyklonen) sind für den größten Anteil des Niederschlags verantwortlich und beeinflussen die Niederschlagsvariabilität in Südostaustralien auf synoptischer Zeitskala. Weitere Faktoren beeinflussen den Niederschlag in Südostaustralien auch auf deutlich längeren Zeitskalen, darunter das ozeanisch-atmosphärische Phänomen El Niño-Southern Oscillation (ENSO), der Indian Ocean Dipole (IOD) und der Southern Annular Mode (SAM). Dabei dominiert der Einfluss von ENSO auf die Niederschlagsvariabilität in Südostaustralien. Die positive Phase von ENSO ist El Niño und wird typischerweise mit negativen Niederschlagsanomalien über Südostaustralien zwischen April und Oktober verbunden. Der El Niño von 1997 führte jedoch zu fast durchschnittlichen Niederschlagsmengen und verdeutlicht die hohe Variabilität der Auswirkungen von El Niño auf Niederschlag in Südostaustralien. Obwohl jüngste Forschungen Fortschritte beim Verständnis der Verknüpfung von großskaligen atmosphärischen und ozeanischen Phänomenen und der Niederschlagsvariabilität zeigen, sind die dynamischen Prozesse, durch welche die Phänomene ihren Einfluss auf den Niederschlag übertragen, nicht vollständig verstanden. Mit dieser Studie wollen wir das dynamische Verständnis verbessern, indem wir aus monatlichen Niederschlagsanomalien über Südostaustralien vier Cluster formen. Mit einem neuartigen Datensatz objektiv identifizierter Wettersysteme aus ERA-Interim Reanalysen wollen wir insbesondere den Einfluss von El Niño auf Niederschlag aus Sicht der Wettersysteme untersuchen.

Die Ergebnisse zeigen, dass überdurchschnittlich viel Niederschlag im Winter und Frühling (Juni-November) über Südostaustralien während El Niño (Cluster 1) mit einer Verschiebung der Westwindzone in Richtung Antarktis (positive SAM-Phase) verbunden sind. Dabei tritt auch ungewöhnlich oft ein blockierendes Hochdruckgebiet in den mittleren Breiten südöstlich von Australien auf. Aus Sicht der Wettersysteme resultiert der überdurchschnittlich hohe Niederschlag über Südostaustralien aus der verstärkten Frequenz von Cut-off Tiefdruckgebieten, die sich über der Großen Australischen Bucht westlich einer blockierenden Antizyklone bilden, und aus einer erhöhten Häufigkeit von "Warmluft-Förderbändern" (engl. warm conveyor belts) über Südostaustralien. Negative Niederschlagsanomalien im Frühling und im Winter über Südostaustralien (Cluster 2) stehen während El Niño im Zusammenhang mit ungewöhnlich hohem Geopotential, das sich fast über dem gesamten Kontinent erstreckt und die Ostwärtsbewegung von Wet-

---

tersystemen unterdrückt. Im Osten Australiens und über den Gewässern östlich von Australien ist eine signifikante Abnahme der Frequenzen von außertropischen Zyklonen, warm conveyor belts und Feuchtigkeitsflüssen zu beobachten. Ungewöhnlich wenig Niederschlag im Landesinneren und überdurchschnittlich viel Niederschlag an der Ostküste Südostaustraliens (Cluster 3) stehen während El Niño in Verbindung mit einem weitläufigen Gebiet, das durch anomal hohes Geopotential südlich von Westaustralien charakterisiert ist. Diese Geopotentialanomalie ist mit der positiven SAM-Phase verbunden und begünstigt die Entwicklung von Cut-off Tiefdruckgebieten über der Tasmanischen See, die einen hohen Anteil des Niederschlags in den Südosten Australiens bringen. Anomal viel Niederschlag entlang der Südküste und anomal wenig Niederschlag an der Ostküste in Cluster 4 ist mit negativen Geopotentialanomalien südlich von Australien verbunden. Dies deutet auf verstärkte Westwinde über Südostaustralien hin, die typischerweise mit der negativen SAM-Phase assoziiert werden. Erhöhter Niederschlag im Süden von Südostaustralien kann auf das erhöhte Auftreten außertropischer Zyklonen zurückgeführt werden. Im Gegensatz dazu ist eine verringerte Häufigkeit von Wettersystemen über der Tasmanischen See zu beobachten, die mit ungewöhnlich wenig Niederschlag an der australischen Ostküste verbunden ist.

Die Ergebnisse dieser Studie tragen zu einem besseren Verständnis der Prozesse bei, die die Niederschlagsvariabilität während El Niño in Südostaustralien beeinflussen. Da sich frühere Studien auf die statistischen Zusammenhänge zwischen großskaligen Klimamoden und Niederschlag im Südosten Australiens konzentrierten, ermöglichen die Ergebnisse dieser Arbeit einen bedeutenden Fortschritt beim Verständnis der Variabilität von Wettersystemen während El Niño.

# Contents

<b>1</b>	<b>Introduction</b>	<b>1</b>
<b>2</b>	<b>Background information</b>	<b>5</b>
2.1	Rainfall in southeastern Australia . . . . .	5
2.2	Influences on southeastern Australian rainfall . . . . .	6
2.2.1	Large-scale remote drivers . . . . .	7
2.2.2	Weather systems . . . . .	17
<b>3</b>	<b>Data and methodology</b>	<b>23</b>
3.1	Data . . . . .	23
3.1.1	ERA-Interim reanalysis . . . . .	23
3.1.2	Climatology of Eulerian and Lagrangian flow features . . . . .	23
3.1.3	Australian rainfall analyses . . . . .	25
3.1.4	Sea surface temperature data set HadISST1 . . . . .	26
3.1.5	Climate indices . . . . .	26
3.1.6	Data set for outgoing longwave radiation . . . . .	28
3.2	Methods . . . . .	28
3.2.1	K-means clustering and optimal number of clusters . . . . .	28
3.2.2	Monte Carlo approach . . . . .	29
3.2.3	Lagrangian parcel trajectories with LAGRANTO . . . . .	29
<b>4</b>	<b>Monthly rainfall variability in southeastern Australia</b>	<b>31</b>
4.1	Data base and clustering region . . . . .	31
4.2	Statistical tests about finding the most physically sensible number of clusters . . . . .	32
4.3	Introduction of rainfall anomaly clusters . . . . .	32
4.4	The El Niño subset of clusters . . . . .	33
4.5	Insights into the cluster sets . . . . .	37
<b>5</b>	<b>Large-scale patterns and influences of climate modes</b>	<b>43</b>
5.1	SST anomalies and climate modes . . . . .	43
5.1.1	SST anomalies in the Pacific Ocean and the role of PDO and IPO . . . . .	43
5.1.2	SST anomalies in the Indian and Southern Ocean and the role of IOD . . . . .	46
5.1.3	SST anomalies around Australia . . . . .	47
5.1.4	The role of SAM . . . . .	47
5.2	Large-scale atmospheric patterns . . . . .	48
5.2.1	Geopotential and streamlines . . . . .	49

5.2.2	Convection and irrotational winds . . . . .	52
<b>6</b>	<b>Weather system occurrence during El Niño</b>	<b>55</b>
6.1	A climatology of synoptic activity in the Australian region . . . . .	55
6.2	Characteristic weather systems during El Niño . . . . .	57
6.2.1	Wet Cluster 1 . . . . .	57
6.2.2	Dry Cluster 2 . . . . .	60
6.2.3	Wet East Coast Cluster 3 . . . . .	62
6.2.4	Wet South Coast Cluster 4 . . . . .	65
<b>7</b>	<b>The origin of rainfall during El Niño</b>	<b>69</b>
7.1	Contribution of weather systems to rainfall . . . . .	69
7.2	Synoptic patterns of rainfall during El Niño . . . . .	74
7.3	Backward trajectories for rainfall events . . . . .	78
<b>8</b>	<b>Conclusions and outlook</b>	<b>87</b>
<b>A</b>	<b>Appendix</b>	<b>93</b>
	<b>Bibliography</b>	<b>95</b>

# 1 Introduction

The population and main agricultural production of Australia are highly concentrated in the south-east of the continent, as the climate conditions are more moderate there compared to the rest of the continent (Murphy and Timbal, 2008; Risbey et al., 2009a). The crop yield of rainfed agriculture strongly varies in wet and dry years and is therefore closely related to interannual rainfall (Risbey et al., 2009a). Changes in rainfall are also a threat to water resources for the population and to natural ecosystems (CSIRO, 2010). As the Australian rainfall variability is prominent for its strength compared to other places in the world that are located in a similar climate zone, an understanding of the processes that drive rainfall variability is crucial to make a precise forecast on seasonal and sub-seasonal time scales (Risbey et al., 2009b).

Southeastern Australia receives most of its annual rainfall during the grain growing season period of April-October (Murphy and Timbal, 2008). Drivers of rainfall variability in Australia are split in higher frequency synoptic processes (cut-off low pressure systems and extratropical cyclones) and lower frequency large-scale phenomena that are oceanic and atmospheric in nature (Risbey et al., 2009b). The lower frequency remote drivers of intraseasonal-to-interannual rainfall variability are the El Niño-Southern Oscillation (ENSO), the Indian Ocean Dipole (IOD), the Southern Annular Mode (SAM) and atmospheric blocking. For most of Australia, one or two of the remote drivers are associated with rainfall variability at a specific time of the year. However, rainfall in southeastern Australia is influenced by multiple drivers: ENSO, IOD and SAM affect rainfall between March and November (Risbey et al., 2009b).

ENSO is the primary driver of interannual rainfall variability in Australia as it explains the rainfall variability to a large part and is consistent through the seasons (Risbey et al., 2009b). Rainfall is mainly affected by ENSO in particular over central eastern Australia during the austral winter-spring season that comprises the months between June and November (Murphy and Timbal, 2008). During El Niño (La Niña), cool-season (April-October) rainfall is usually reduced (enhanced) in the eastern and extreme southern parts of Australia (Murphy and Timbal, 2008; Risbey et al., 2009a). However, the relationship of Australian rainfall with El Niño is weaker compared to the relationship with La Niña which points to the strength of El Niño as a poor indicator for rainfall deficiency (Power et al., 2006; Murphy and Timbal, 2008; Chung and Power, 2017).

The El Niño of 1982 was one of the three strongest El Niño events of the satellite area and led to a significant rainfall deficit over eastern Australia (Van Rensch et al., 2019). The slightly stronger event of 1997 was associated with near-average rainfall especially over eastern Australia. In particular, September 1997 had unusual above-average rainfall over southeastern Australia (Fig. 1.1a). The most recent event of 2015 brought only weak below-average rainfall to eastern Australia. In

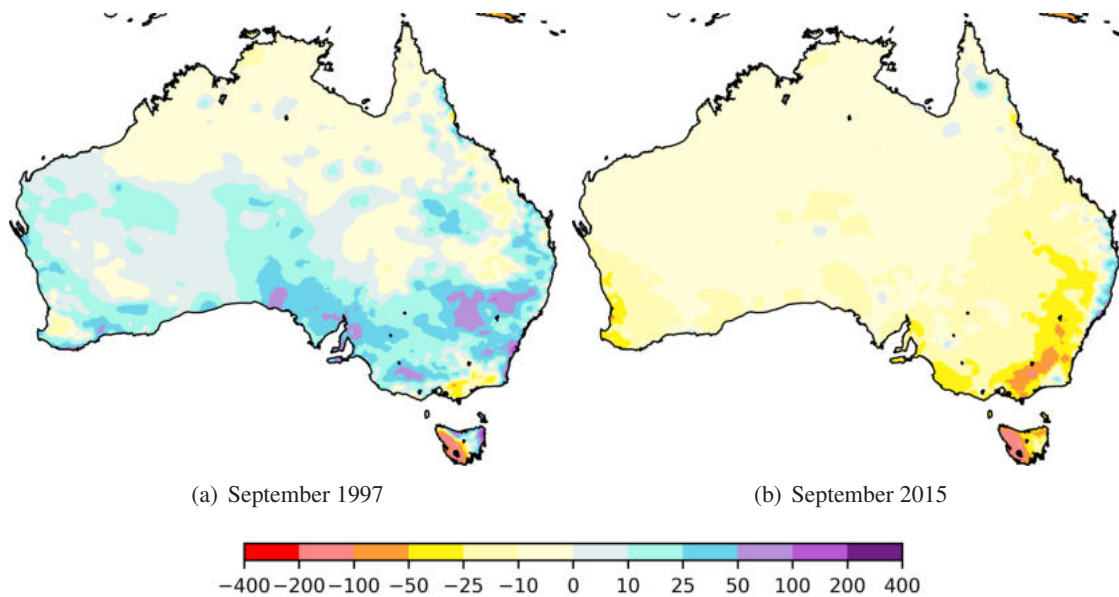


Figure 1.1: Monthly mean rainfall anomaly (in mm) over southeastern Australia for (a) September 1997 and (b) September 2015. The data is from the Bureau of Meteorology and will be introduced in Chapter 3.

contrast to 1997, rainfall anomalies were strongly negative in September 2015 (Fig. 1.1b). This points to the non-linear relationship of El Niño strength and the impact on east Australian rainfall. There is an important lack of knowledge about the processes that drive interannual rainfall variability in east Australia, as ENSO flavor alone cannot explain it (Brown et al., 2009; Van Rensch et al., 2019).

The differences in the processes that link El Niño and rainfall in southeastern Australia require further examination (Van Rensch et al., 2019). Previous studies about rainfall variability in southeastern Australia document statistical relationships between an index of a large-scale mode and rainfall in this region (e.g., Taschetto and England, 2009; Risbey et al., 2009b; Ashcroft et al., 2016). In this thesis, we take a different approach that aims to develop a dynamic understanding of interacting processes during El Niño. A clustering of monthly rainfall anomaly patterns will allow a more separate and detailed dynamic analysis of processes during different rainfall patterns in southeastern Australia. We investigate the effect of El Niño on rainfall variability from a weather system perspective by addressing the following research questions:

- What characterizes the monthly rainfall anomaly patterns during the winter-spring season in southeastern Australia?
- Which effect do large-scale climate modes (ENSO, IOD, SAM) and blocking have on rainfall in southeastern Australia? Is there evidence of teleconnection patterns between the tropical ENSO and IOD signals and the large-scale circulation in higher latitudes of southeastern Australia?
- How do the weather system patterns over Australia change during El Niño?

- 
- Which weather systems produce rainfall in southeastern Australia during El Niño and what characterizes the synoptic surface patterns during rainfall?
  - Where is the origin of air masses during rainfall events? Are there specific pathways that determine the strength of rainfall?

The remainder of this thesis is organized as follows. Chapter 2 provides the background information on rainfall in southeastern Australia and the processes that drive rainfall variability. The data and methods are described in Chapter 3. The results are split in four parts. We first introduce the clustering of rainfall anomalies over southeastern Australia in Chapter 4. It follows the investigation of large-scale climate modes and circulation patterns during El Niño in Chapter 5. A weather system perspective of rainfall variability is given in Chapter 6. A broader view on the origin of rainfall during El Niño is presented in Chapter 7. The thesis completes in Chapter 8 with a summary of the findings and an outlook with further directions for future work.



## 2 Background information

For the purpose of this thesis, it is important to know the characteristics and influencing factors of rainfall in southeastern Australia. This chapter introduces the meteorological background of rainfall variability and its drivers. All seasons in this thesis refer to austral seasons. Winter comprises the months June-August and spring includes the months from September to November. We first present the distribution of annual and winter-spring rainfall over southeastern Australia. It follows a characterization of the different processes that affect rainfall with focus on large-scale remote drivers and weather systems. Finally, the effect of El Niño on southeastern Australian rainfall is introduced, since El Niño is the basic framework of this study.

### 2.1 Rainfall in southeastern Australia

The population of Australia and the most productive agricultural regions are concentrated in the southeast of Australia (Murphy and Timbal, 2008). Although Murphy and Timbal (2008) define southeastern Australia as the mainland south of 33°S and east of 135°E (south of dashed dark red line in Fig. 2.1a), the definition varies between the different studies (e.g., McIntosh et al., 2007; Cowan et al., 2013; Risbey et al., 2013; Ashcroft et al., 2016). This might affect direct comparisons with our results. Irrespective of the exact definition, the region under consideration encompasses the state of Victoria and parts of South Australia and New South Wales (Murphy and Timbal, 2008).

Warm, dry summers and cool, wet winters characterize the climate of southeastern Australia and resemble the general Mediterranean climate pattern (Risbey et al., 2009a). There is a huge contrast of annual rainfall between the coastal areas and the inland (Fig. 2.1a). The coastal stripe east of the Great Dividing Range, a mountain range along the East Coast of Australia, receive much more rainfall than the regions inland (Risbey et al., 2009a). The coastal areas of New South Wales and Victoria can gain up to 2000mm of rainfall per year. More inland, some areas are characterized by a dry climate as they do not receive more than 100mm of annual rain.

Southeastern Australia receives a significant amount of its rainfall in the cool season that is important for the growing season from April to November (Pook et al., 2006; Murphy and Timbal, 2008). A large percentage of the annual rainfall is especially observed over the coastal parts in the south where winter-spring rainfall contributes more than 60% to the annual mean (Fig. 2.1b). Further inland, the share of winter-spring rainfall on annual rainfall becomes considerably lower. Some inland areas receive less than 30% of rainfall in winter and spring, which indicates that they receive most of the annual rainfall in austral summer (December-February) and austral autumn (March-May).

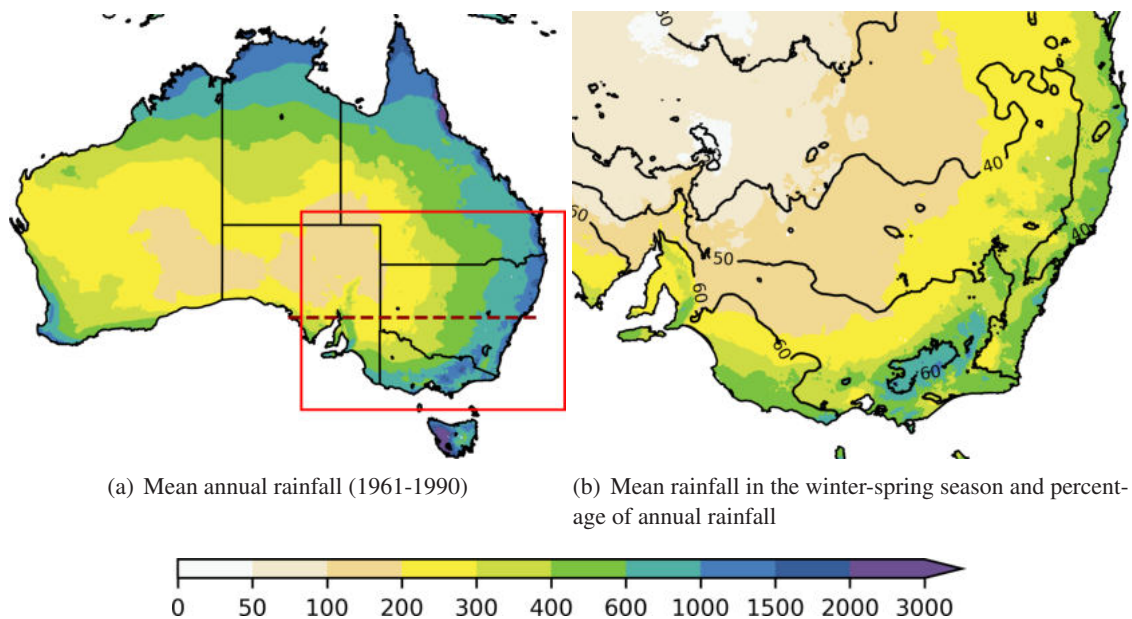


Figure 2.1: (a) Average annual rainfall of Australia over the period 1961 to 1990 (color shading in mm). (b) Average winter-spring rainfall over the period 1961 to 1990 in the southeast of Australia (area in red box,(a) in mm (shading in uneven intervals) and percentage of annual rainfall (contour lines every 10%). The southeastern Australian definition of Murphy and Timbal (2008) is displayed by the land mass south of the dark red dashed line. The data is from the website of the Bureau of Meteorology and will be introduced in Chapter 3.

Murphy and Timbal (2008) describe the latest changes in rainfall in their study about recent climate variability and climate change in southeastern Australia. Increased annual rainfall over southeastern Australia has been observed from 1910 to 1995 with a jump to an even higher rainfall regime in 1946. The abrupt fall of annual rainfall around 1997 indicates the transition in a new regime in southeast Australia (Murphy and Timbal, 2008). From 1997 to 2006, rainfall has been 11.4% below the long-term average. Although all months between March and October were concerned by this drier period, the majority of the rainfall decline occurred during the autumn months (Murphy and Timbal, 2008; Timbal and Drosowsky, 2013).

## 2.2 Influences on southeastern Australian rainfall

Rainfall in southeastern Australia is influenced by a variety of drivers which can be attributed to high-frequency processes or lower frequency phenomena (Risbey et al., 2009b). Figure 2.2 gives a schematic representation of the main drivers. The lower frequency phenomena contain large-scale oceanic and atmospheric modes. We focus here on ENSO, IOD, SAM, further oscillations in the Pacific Ocean and atmospheric blocking. High-frequency processes include the synoptic-scale weather systems that are embedded in the westerlies and usually bring most of the rainfall in southeastern Australia (Risbey et al., 2009b).

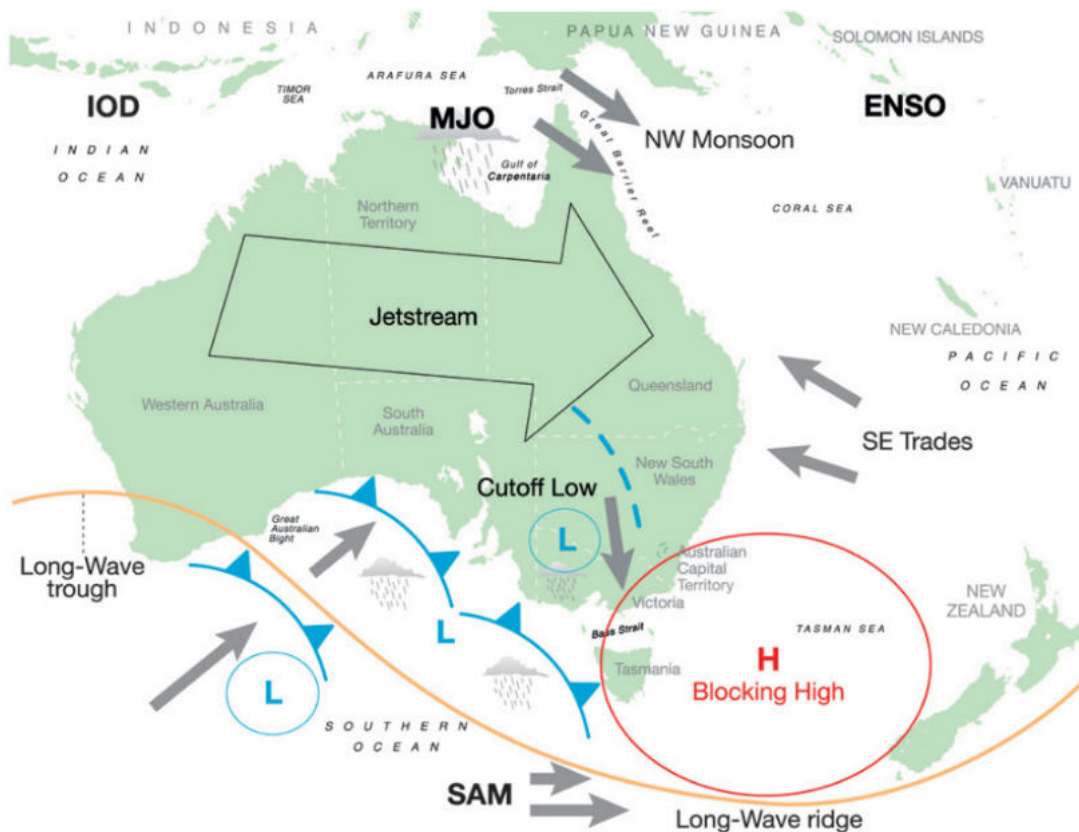


Figure 2.2: A schematic representation of the main drivers of rainfall variability in the Australian region. The figure is adapted from Risbey et al. (2009b, Fig. 1).

### 2.2.1 Large-scale remote drivers

Tropical and extratropical large-scale remote drivers affect intraseasonal-to-interannual rainfall in southeastern Australia. Most of them are of tropical origin like ENSO, IOD and further oscillations in the Pacific Ocean. Extratropical drivers include SAM and atmospheric blocking. In the following, we will introduce the large-scale remote drivers and present their correlation with rainfall in the winter-spring season using the results of Risbey et al. (2009b).

#### The El Niño-Southern Oscillation

On average, southeasterly trade winds over the tropical Pacific Ocean converge on the low pressure zone over Indonesia and northern Australia leading to enhanced cloudiness and rainfall (Fig. 2.3a). At higher altitudes, the air moves eastward and sinks over the cold, dry high pressure zone over the eastern equatorial Pacific Ocean. This zonally arranged cell was discovered by Gilbert Walker and is therefore known as the Walker circulation (Philander, 1983). As the atmosphere and ocean are coupled, the wind stress at the surface leads to divergence and causes cold upwelling in the upper oceanic layer in the eastern equatorial Pacific. In contrast, sea surface temperatures (SSTs) in the so-called 'warm pool' in the West Pacific are high (Kiladis and Kingtse, 1998).

Much of the rainfall variability in Australia is related to ENSO (Nicholls et al., 1997). The 'delayed oscillator' theory is one of the theories about the initiation of an ENSO event and suggests

that oceanic waves determine the transition between different events (Kiladis and Kingtse, 1998). In this concept, the initiation of an El Niño starts with downwelling equatorial Kelvin waves that are stimulated over the Western Pacific and transport warm water from the warm pool eastward. The oceanic Kelvin waves lower the thermocline in the central and Western Pacific and cause an increase of SSTs. Convection sets in near the date line and produces westerly surface winds that further trigger downwelling Kelvin waves and eastward oceanic flow leading to a further increase of SSTs in the central and eastern Pacific. When the Kelvin wave reaches the eastern boundary of the Pacific Ocean, the warm water is deflected to the north and south and cools down. Off-equatorial oceanic Rossby waves, that are stimulated by Kelvin waves, transport the cooled water to the west. After 6-12 months, the Rossby waves reach the Western Pacific and mark the transition to a new ENSO phase. They are reflected off the western boundary of the Pacific as Kelvin waves and generate upwelling Kelvin waves, which move eastward and transport cold water towards the eastern Pacific (Kiladis and Kingtse, 1998). With a focus on the atmosphere, higher SSTs and increased convection during El Niño results in lower pressure over the eastern Pacific and higher pressure over Australasia which indicates the displacement of the upward branch of the Walker Circulation (Fig. 2.3b).

Further precursors of El Niño exist, for example a shift of the Intertropical Convergence Zone (ITCZ) to the south that is associated with unusual high SSTs, a deep thermocline near the coast of Peru and weak winds. These anomalous conditions off the coast of Peru and Ecuador expand westward and the previously explained precursors over the westerly equatorial Pacific Ocean grow in amplitude and lead to El Niño (Kiladis and Kingtse, 1998). The well-developed phase of El Niño is connected with unusually warm SSTs in the eastern equatorial Pacific Ocean, a further southward shifted ITCZ, an intensified Hadley Cell and weak trade winds over most of the equatorial Pacific Ocean (Philander, 1983).

The term 'El Niño' origins from the Spanish word for 'the boy Christ-child' as the phenomenon and especially anomalous SSTs usually develop around Christmas time (Trenberth, 1997). About 6 months later, the El Niño conditions are spread over the entire tropical Pacific (Kiladis and Kingtse, 1998). The connection between the ENSO and rainfall in southeastern Australia is of high complexity and non-linear (Ashcroft et al., 2016). Rainfall in Australia is in general below-average during El Niño with the greatest effects in the peak ENSO impact months between June and December (Brown et al., 2009; Cai et al., 2010). This is due to the eastward shift of the Walker circulation and the higher surface pressure that results in anomalous subsidence over Australia (Wang and Hendon, 2007). The impact of El Niño on cool-season rainfall is strongest in southeastern Australia (Risbey et al., 2009a). The correlation between El Niño and decreased rainfall is stronger during spring, especially along the East Coast area (Fig. 2.4). Although the region is too remote to notice the direct effect of the SST anomalies in the tropical Pacific, ENSO seems to affect rainfall by SST-induced pressure and circulation anomalies (Van Rensch et al., 2019). An examination of past El Niño events by the Bureau of Meteorology demonstrated that the mean winter-spring rainfall totals were lower than 90% of previous winter-spring rainfall observations in particular in central southeastern Australia (Fig. 2.5). However, the effect of El Niño on rainfall along the coasts of southeastern Australia is smaller (Ashcroft et al., 2016).

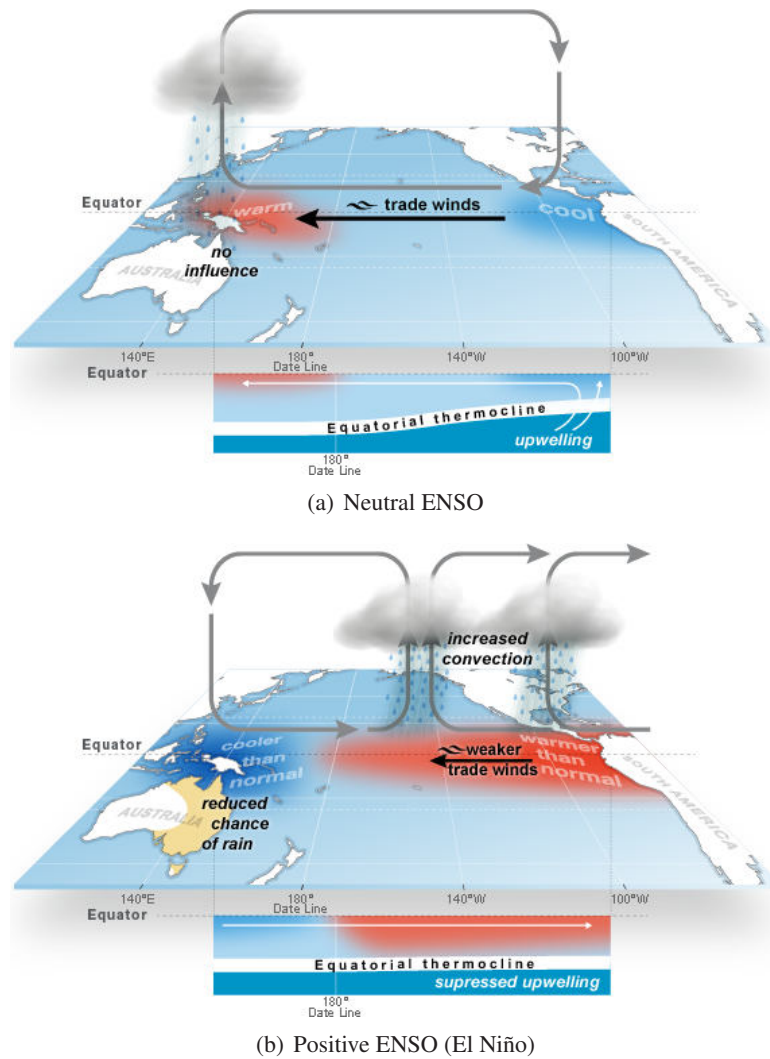


Figure 2.3: Schematic overview of (a) the neutral ENSO phase and (b) the positive phase (El Niño) (Commonwealth of Australia Bureau of Meteorology, 2019[c]).

The counterpart of El Niño (negative ENSO phase) is called La Niña and represents basinwide cooling of the equatorial Pacific Ocean (Trenberth, 1997). During La Niña, rainfall over most of Australia is above-average (Nicholls et al., 1997). This is in accordance with the negative correlation between ENSO and rainfall in Figure 2.4.

A phenomenon in the tropical Pacific, that is different from the canonical El Niño, has recently been discovered (Ashok et al., 2009). It is characterized by anomalously cold and persistent SSTs in the eastern tropical Pacific and in the western tropical Pacific and warm SSTs in the central tropical Pacific. In contrast to the canonical El Niño, the greatest positive SST anomalies persist in the central tropical Pacific. This phenomena is named as El Niño Modoki and got attention due to an increased intensity and frequency since the 1980s (Ashok et al., 2009). During El Niño Modoki, two Walker circulation cells exist over the tropical Pacific with the core rising branch over the central Pacific. The connected descending branch is located over the maritime continent. Previous studies demonstrated that the teleconnections of El Niño Modoki events are stronger and

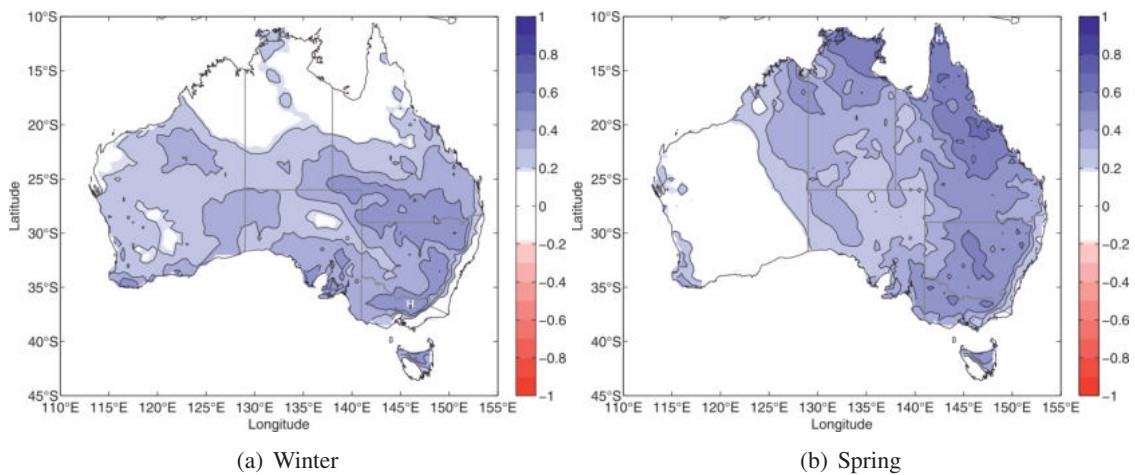


Figure 2.4: Correlation between ENSO and Australian rainfall for the data period 1889-2006 (a) in winter and (b) in spring. Positive correlations illustrate the coherence of El Niño (La Niña) and decreased (increased) rainfall. The figure is adapted from Risbey et al. (2009b, Fig. 2c-d) and only shows significant correlations at the 95 % level.

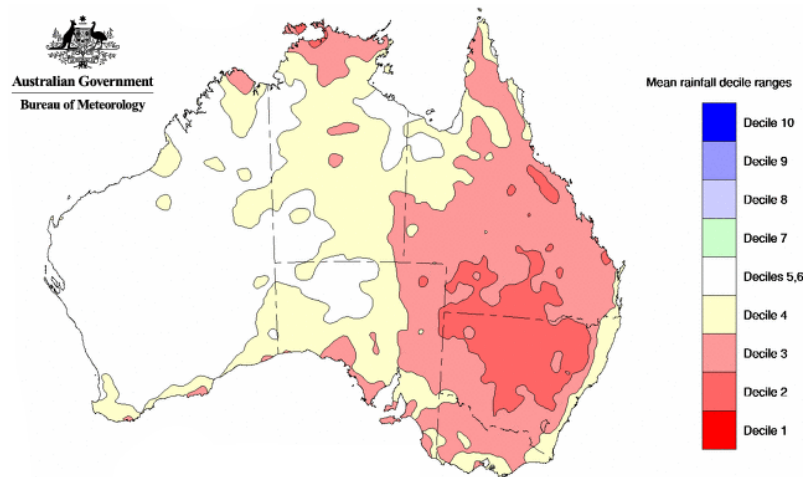


Figure 2.5: Mean rainfall deciles in winter-spring of 12 classical moderate-strong El Niño events: 1905, 1914, 1940, 1941, 1946, 1965, 1972, 1977, 1982, 1991, 1994, 1997. The figure is taken from the website of the Bureau of Meteorology (Commonwealth of Australia Bureau of Meteorology, 2019[b]).

more widespread in Australia during winter (Cai et al., 2010). The effect of the El Niño Modoki on Australia in winter differs from the effects of the canonical El Niño. The two anomalous Walker circulation cells in the troposphere during El Niño Modoki lead to a more effective suppression of rainfall over Australia (Cai et al., 2010). A further examination showed the existence of atmospheric blocking over central eastern Australia. The associated suppression of the storm track activity leads to the reduction of frontal rainfall in the southeast during the El Niño Modoki events (Ashok et al., 2009). A further difference to the canonical events is the maximum rainfall response of Modoki events in autumn instead of winter and spring (Taschetto and England, 2009). Nevertheless, Brown et al. (2009) highlight that the processes which influence rainfall are more complicated than just different flavors of El Niño.

The average-known impacts fit for most of the previous observed El Niño events. Rainfall was significant low in spring during a very strong canonical El Niño event in 1982 (Van Rensch et al., 2019). The modest El Niño Modoki of 2002 also led to exceptionally dry conditions with near-record drought in eastern Australia (Wang and Hendon, 2007; Brown et al., 2009). Paradoxically, the strong canonical El Niño of 1997 effected Australia with only slightly below-average rainfall (Brown et al., 2009). The latest El Niño of 2015 led to only slightly below-average rainfall and indicates the diversity of responses from equally strong El Niños on Australian rainfall (Van Rensch et al., 2019).

### **The Indian Ocean Dipole**

The IOD is one of the remote climate drivers that modulate interannual rainfall variability in southeastern Australia (Cowan et al., 2013). It can be measured by taking the difference in SST anomalies between the tropical western Indian Ocean and the tropical southeastern Indian Ocean (Risbey et al., 2009b). This tropical mode, that can develop prematurely since the 1970s from mid-autumn on, significantly influences rainfall over a broad area from northwest to southeast Australia (Ashok et al., 2003; Cowan et al., 2013). The main effect of the IOD on Australian rainfall occurs during winter and spring (Ummenhofer et al., 2011).

Warm SST anomalies in the western Indian Ocean and cold SST anomalies in the eastern Indian Ocean define a positive IOD event (Fig. 2.6a). Ashok et al. (2003) studied the mechanism on the influence of a positive IOD on rainfall over southeastern Australia. They point out that the relatively cold SST anomalies in the eastern tropical and subtropical Indian Ocean induce an anomalous near-surface anticyclonic circulation that covers a large part of Australia. The baroclinic response of the atmosphere leads to subsidence over southern Australia and reduces rainfall (Ashok et al., 2003). Negative correlations of the IOD with rainfall over Australia reflect this relationship (Fig. 2.7). Especially extreme positive IOD events are connected to very much below average rainfall over western and central Victoria and below-average rainfall in most areas of southern Australia except the East Coast (Murphy and Timbal, 2008).

Cold SST anomalies in the western Indian Ocean and warm SST anomalies in the eastern Indian Ocean define a negative IOD event (Murphy and Timbal, 2008). During a negative IOD event, when SSTs are anomalously warm northwest of Australia, rainfall is enhanced over large parts of the continent (Fig. 2.7). Early studies pointed out that above-average rainfall across Australia results from the interaction with the tropics and especially the increased moisture advection into the Extratropics of Australia (Ummenhofer et al., 2009). Northwest cloudbands, that spread across Australia, reflect this relationship (Fig. 2.6b). In winter, negative IOD events are one of the main drivers of southeastern Australian rainfall variability (Cowan et al., 2013).

In their study about remote drivers, Risbey et al. (2009b) investigated the correlation of IOD and ENSO. A combination of both climate modes leads to a more extreme effect on rainfall: below-average (above-average) rainfall over Australia during El Niño (La Niña) occurs in conjunction with a positive (negative) IOD event (Risbey et al., 2009a; Risbey et al., 2009b). By

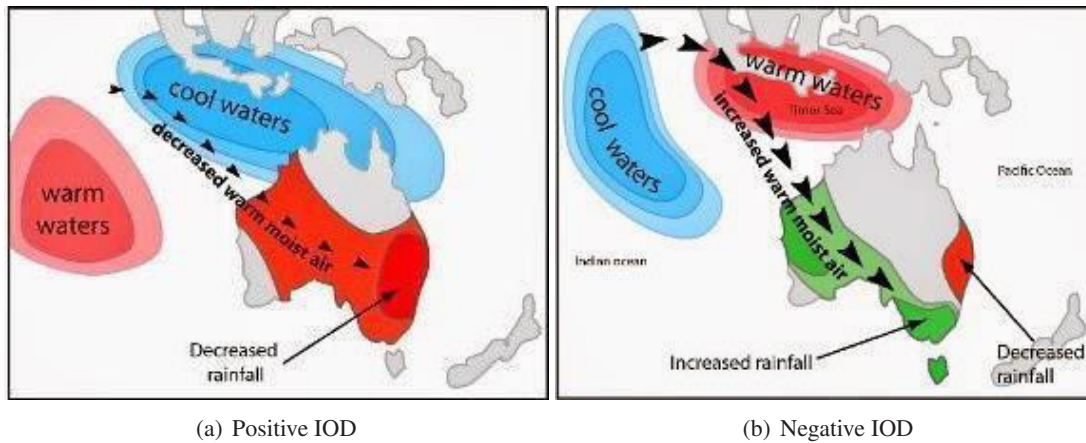


Figure 2.6: Schematic representation of the IOD and the observed effects of (a) the positive phase and (b) the negative phase on Australian rainfall (Beale, 2009).

removing the effect of ENSO, the IOD predominantly influences the southwestern parts of south-eastern Australia (Fig. 2.7b).

Cai et al. (2011) point out that the Indian Ocean affect southeastern Australian rainfall by the generation of Rossby wave trains (RWTs). Diabatic heating anomalies induced by tropical SST anomalies play a crucial role on the stimulation of RWTs, that propagate from the Tropics into the Extratropics. These wave trains seem to influence rainfall in southeastern Australia by changing the circulation in Australian latitudes (Cai et al., 2011). Figure 2.8 illustrates schematically the RWTs and their sources. For El Niño, the primary wave train emanates from the central equatorial Pacific and does not impact Australia which means that the impact is only due to the western pole of the Southern Oscillation (Fig. 2.8a). The positive phase of IOD is associated with the development of a RWT from the eastern Indian Ocean that results in an equivalent barotropic ridge over southern Australia (Fig. 2.8b). In spring, when IOD and ENSO are strongly correlated, two primary RWTs from the equatorial Indian Ocean share a common anomaly center south of Australia (Fig. 2.8c).

### The Southern Annular Mode

SAM measures the strength and location of mid-latitude westerly winds and is an extratropical source of rainfall variability (Risbey et al., 2009b; Ashcroft et al., 2016). As a dominant mode of atmospheric variability of the Southern Hemisphere, it represents the north-south shift of the westerly wind belt and points to zonal wind anomalies between 30°S and 60°S (Risbey et al., 2009b).

Enhanced westerlies and decreased pressure over southern Australia characterize the negative phase of SAM (Fig. 2.9b). An equatorward shift of the mid-latitude jet is usually connected with increased rainfall around 140°E in southeastern Australia (Fig. 2.10), as enhanced westerlies over southern Australia can bring more frontal rainfall due to embedded cyclones (Risbey et al., 2009a; Ashcroft et al., 2016). In addition, regions east of the Great Dividing Range get less rainfall due

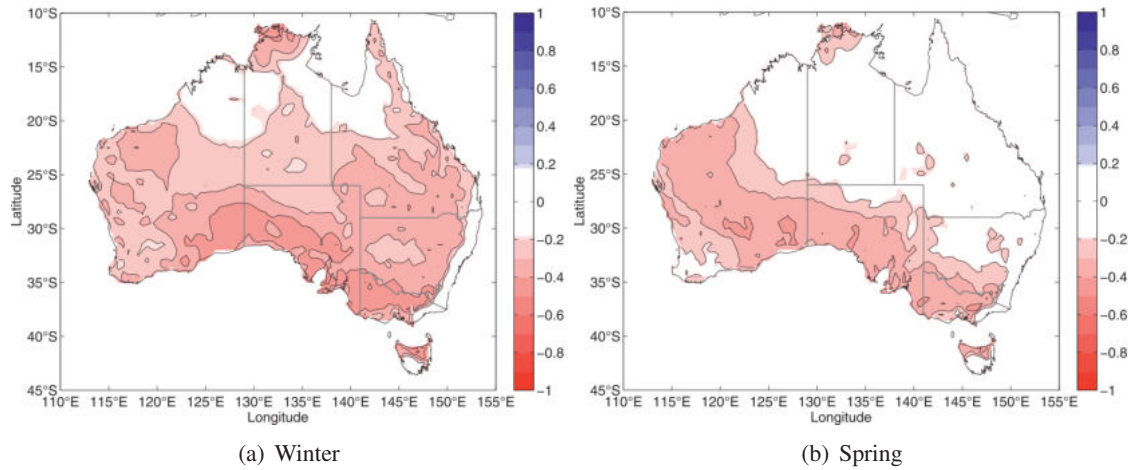


Figure 2.7: (a) Correlation between the IOD and Australian rainfall for June-October. (b) Same correlation but with removed effect of ENSO. The data period spans 1889-2006. Negative correlations illustrate the coherence of a positive (negative) IOD phase and and decreased (increased) rainfall. The figure is adapted from Risbey et al. (2009b, Fig. 5) and only shows significant correlations at the 95 % level.

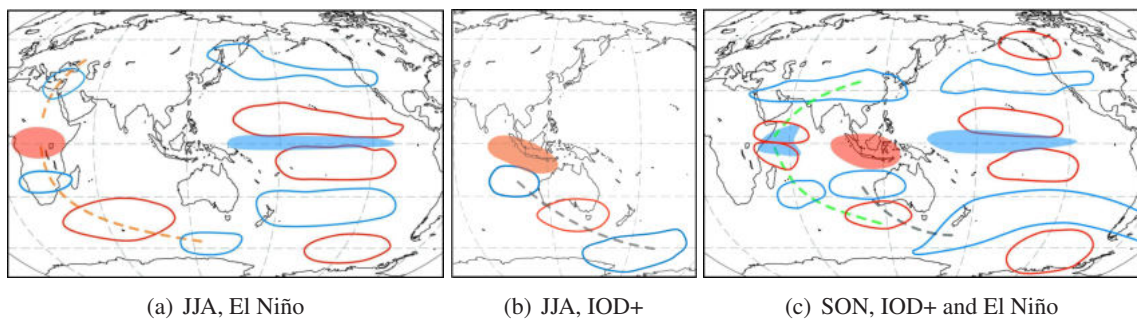


Figure 2.8: A schematic illustration of the RWTs (a) for the positive phase of ENSO in winter (JJA), (b) for the positive phase of IOD in winter and (c) for a combination of both in spring (SON). Shaded blue (red) areas indicate areas with increased (decreased) tropical convection. Blue (red) contours show anomalous low (high) geopotential in upper levels. Dashed lines trace the analyzed RWTs. The figure is adapted from Cai et al. (2011, Fig. 9).

to decreased onshore moisture flux from the Coral Sea and dynamically induced subsidence over the subtropics (Lim and Hendon, 2015; Ashcroft et al., 2016).

The positive SAM phase results in lower pressure in the polar regions and higher pressure over the Australian continent (Risbey et al., 2009b). This is due to a poleward shift of the maximum of mid-latitude westerlies (Fig. 2.9a). Previous studies examined the relationship between SAM and rainfall in southeastern Australia. They pointed out that this relationship comprise a reduction in winter rainfall in the south of Australia (Risbey et al., 2009b; Ashcroft et al., 2016). However, a positive SAM phase is also associated with increased spring rainfall along the East Coast of New South Wales (Risbey et al., 2009b; Ashcroft et al., 2016). Figure 2.10b displays this behavior with high positive correlation between SAM and rainfall along the East Coast. Positive pressure anomalies and enhanced blocking southeast promotes onshore subtropical flow and favors the development of cut-off low pressure systems (cut-off lows) over southeastern Australia, which

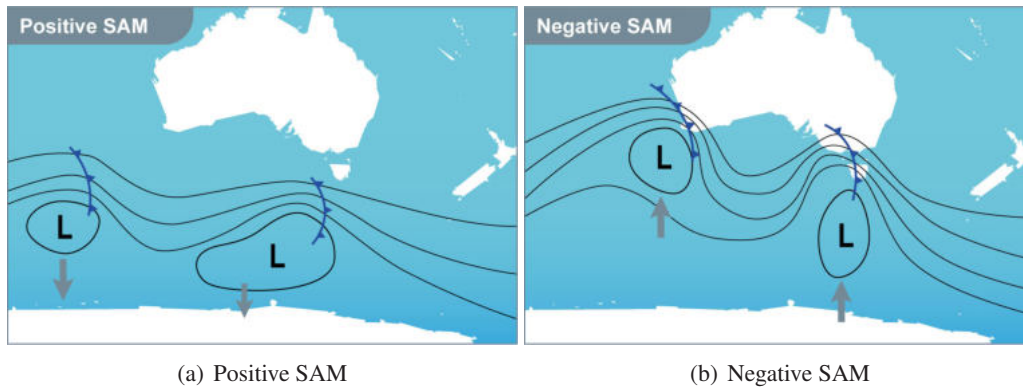


Figure 2.9: Schematic representation of (a) the positive SAM and (b) the negative SAM phase (Agriculture Victoria, 2019).

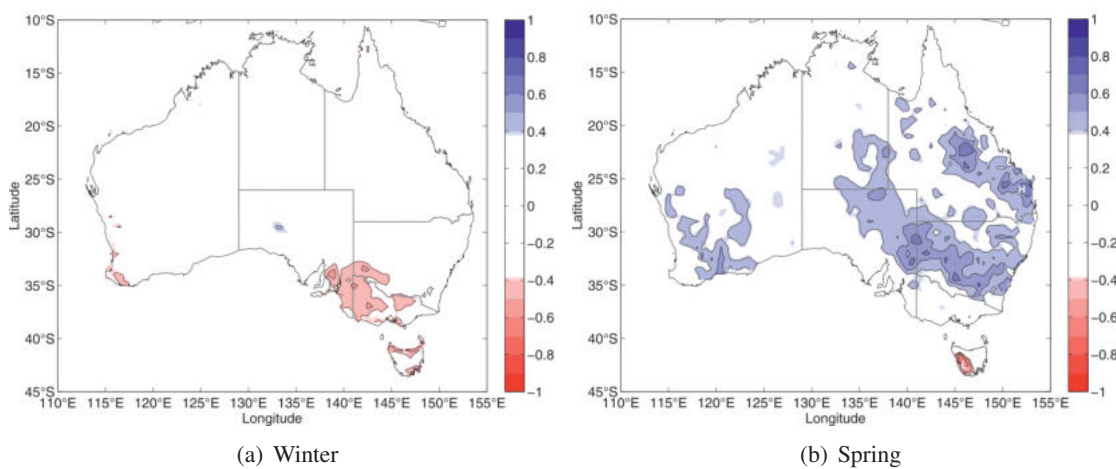


Figure 2.10: Correlation between SAM and Australian rainfall for the data period 1979-2005 in (a) winter and (b) spring. The figure is adapted from Risbey et al. (2009b, Fig. 12) and only shows significant correlations at the 95% level.

are very efficient rain-bringing systems for the Australian region (Risbey et al., 2009a; Cowan et al., 2013; Ashcroft et al., 2016). The increase in rainfall at the East Coast can be explained by anomalous easterly winds, enhanced moisture advection from the Tasman Sea and orographic rainfall at the eastern side of the Great Dividing Range (Cowan et al., 2013).

A strong trend towards the positive phase of the SAM has been observed since 1958 (Nicholls, 2010). However, the trend was predominantly observed in summer and autumn (Murphy and Timbal, 2008).

### Oscillations in the Pacific Ocean

The Pacific Decadal Oscillation (PDO) and the Interdecadal Pacific Oscillation (IPO) are the two main modes of decadal to interdecadal variability in the Pacific Ocean (Henley et al., 2015). Despite their different temporal scales, they have statistical links with ENSO and significant impacts on rainfall in Australia (Mantua and Hare, 2002). The PDO is known as a long-lived El Niño-like

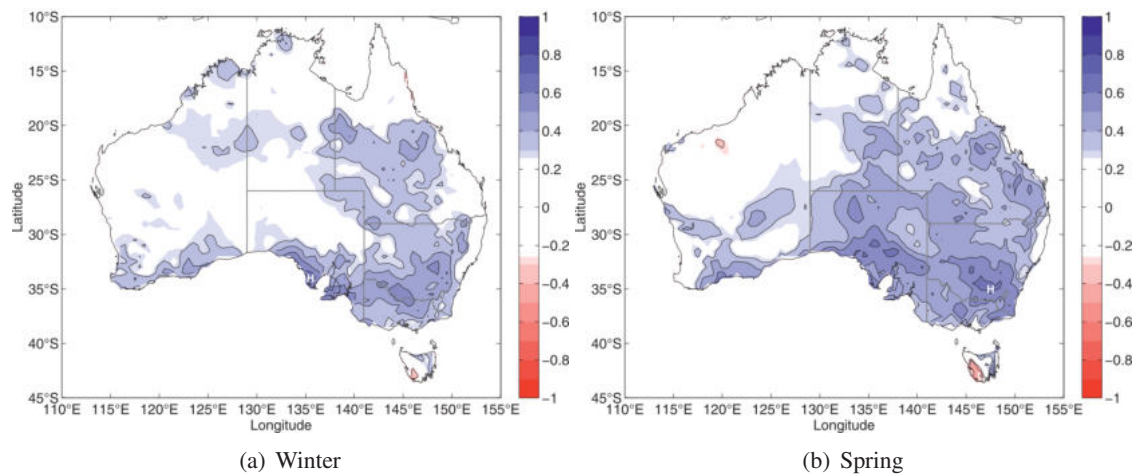


Figure 2.11: Correlation between atmospheric blocking at 140°E and Australian rainfall in winter (a) and spring (b) for the data period 1948-2006. The figure is adapted from Risbey et al. (2009b, Fig. 13c-d) and only shows significant correlations at the 95 % level.

pattern in the decadal Pacific climate variability based on SST patterns in the North Pacific. The mode is defined as the leading principal component of Pacific SSTs poleward of 20°N (Mantua and Hare, 2002; Westra et al., 2015). The second principle component of low-frequency filtered SST is the IPO that often shows ENSO-like decadal patterns (Westra et al., 2015).

During a warm (cold) PDO phase, SSTs are anomalous low (high) in the central North Pacific and anomalous high (low) along the west coast of America. Warm (cold) phases of the PDO are associated with warm-dry (cool-wet) conditions in eastern Australia (Mantua and Hare, 2002). When ENSO is in phase with the PDO, the induced impacts of ENSO are intensified (Kim et al., 2013). The modulation of ENSO by the IPO is more complex, as IPO indices are a smoothed version of ENSO (Westra et al., 2015).

### Atmospheric blocking

Atmospheric blocking is a term that describes the situation when anticyclones occasionally become stationary (Pook, 1994). A split of the upper-tropospheric westerly stream into two branches characterizes the pattern of blocking, where an extensive high pressure system forms at higher latitudes and blocks approaching weather systems from the west (Pook, 1994; Cowan et al., 2013). The Tasman Sea and the southwest Pacific region are the dominant zone for blocking activity in the southern hemisphere with occurrence frequency maxima in winter and early spring (Pook, 1994).

Atmospheric blocking is a mechanism to influence rainfall variability in southeastern Australia. Periods of blocking often manifest as dry spells over southern Australia as there is a tendency for weaken and distract approaching cold-fronts to the southeast (Risbey et al., 2009b; Cowan et al., 2013). Nevertheless, there exists a strong relationship with the development of cut-off lows (Risbey et al., 2013). The effect of blocking on rainfall in southeastern Australia strongly depends on the nature and location of the blocking (Cowan et al., 2013). Wetter conditions over Australia

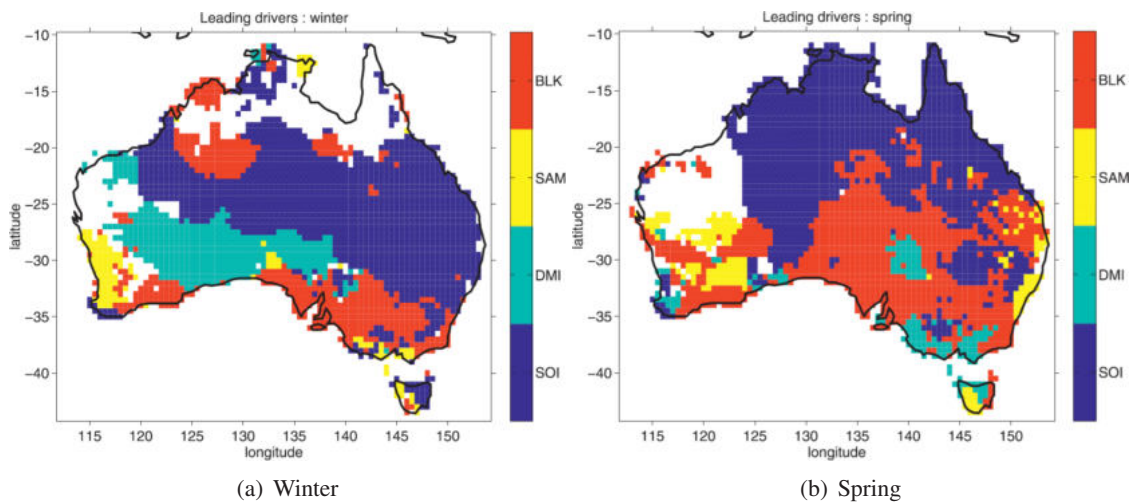


Figure 2.12: Leading drivers in terms of correlation with monthly rainfall at each grid cell for winter (a) and spring (b): atmospheric blocking (BLK), IOD (DMI), SAM (SAM) and ENSO (SOI). Only correlations that are significant at the 95% level are considered when selecting the leading driver. The data span the period from 1957 to 2006. The figure is adapted from Risbey et al. (2009b, Fig. 15c-d).

are associated with enhanced blocking at around  $160^{\circ}\text{E}$  that favor the development of cut-off lows (Risbey et al., 2009a). In contrast, weaker blocking in Tasman Sea longitudes leads to drier conditions over Australia. Blocking in the Great Australian Bight region ( $130^{\circ}\text{E}$ ) favors rainfall in western Australia, but not in southeastern Australia (Risbey et al., 2009b). The correlation of blocking at  $140^{\circ}\text{E}$  and rainfall shows that there is a significant positive relationship in winter and in spring (Fig. 2.11).

### Combined and leading drivers

The presented remote drivers and their effect on Australian rainfall are not independent of one another. Risbey et al. (2009b) demonstrated that ENSO and IOD have the strongest relationship. Their interaction makes it hard to study the impact on rainfall independently although it is known that their primary impact region differs. The other large-scale drivers are weakly correlated with one another (Risbey et al., 2009b). Local topography and various large-scale remote drivers influence rainfall variability at the same time, so it is hard to assess the leading driver of rainfall in Australia. For most parts of Australia, one or two large-scale modes have an influence on rainfall. One exception is southeastern Australia, where ENSO, IOD, SAM and atmospheric blocking affect rainfall in all seasons (Risbey et al., 2009b; Ashcroft et al., 2016). In their study, Risbey et al. (2009b) compare the main large-scale drivers conforming to the strength of their correlation with rainfall and present a qualitative overview of leading drivers. With focus on southeastern Australia, atmospheric blocking is the leading driver in terms of spatial coverage and consistency through the two seasons (Fig. 2.12). In winter, ENSO is the leading driver in northern New South Wales and SAM shows the highest correlation with rainfall along the South Coast (Fig. 2.12a). The IOD seems to take over the leading role of SAM along the South Coast of Victoria in spring (Fig. 2.12b). However, the effect of ENSO gets smaller along the East Coast in spring with SAM as a leading driver along the coastal areas of New South Wales. Risbey et al. (2009b) further

examined how much of the rainfall variability can be explained by the leading remote drivers. In winter and spring, ENSO and blocking can explain a higher level of rainfall variance compared to SAM and IOD (Risbey et al., 2009b).

### 2.2.2 Weather systems

The presented large-scale remote climate drivers (apart from blocking) influence rainfall in southeastern Australia on monthly, seasonal and interannual time scales. Local weather systems are the main mechanism that affect the sub-monthly rainfall variability in southeastern Australia (Murphy and Timbal, 2008). Following Wright (1997), extratropical cyclones and the passage of cold-fronts influence the rainfall along the southeastern coastal areas. More inland, cut-off lows and tropical-extratropical interactions provide the major rainfall amounts. There exist a few studies about the identification of synoptic systems associated with rainfall over southeastern Australia, but they all focus on just a small part within southeastern Australia. Nevertheless, we want to present the results of the few studies to gain a basic knowledge.

Wright (1989) classified in his study rainfall over Victoria during June-September from 1971 to 1982 into one of five synoptic types: interacting fronts, non-interacting fronts, post-frontal rain, cut-off lows and heat-lows. He outlines the importance of cut-off lows and frontal rain for the cool-season rainfall and points out the variation of the contributions with location (Wright, 1989). More recently, Pook et al. (2006) identified the main synoptic systems that were responsible for rainfall in northwestern Victoria between April and October in the period 1970-2002. Their resulting climatology shows that cut-off lows are responsible for around 50% of the rainfall in this months. However, the contribution of extratropical cyclones to the cool-season rainfall is about a third (Pook et al., 2006).

In the following, we will present the characteristics of the two dominant weather systems around Australia and their contributions to rainfall in southeastern Australia. Furthermore, we present the results of previous studies about the origin of air masses from weather systems.

#### Cut-off low pressure systems

In one of the first synoptic classification of rainfall over southeastern Australia in the cool season, Wright (1989) points out the importance of ‘cold lows’, which are better known as ‘cut-off’ lows. These systems are closed low pressure systems in the upper troposphere, that formed on the equatorward side of the westerly current in the jet stream and have been ‘cut-off’ (Nieto et al., 2008). Isolated centers of high cyclonic potential vorticity on an isentropic surface near the tropopause indicate the presence of a cut-off low. When the system moves over a region of potentially unstable low-level air, it can produce strong winds and intense rainfall. Cut-off lows can extend to the surface, but do not necessarily create convective cloudiness and rainfall. Processes like diabatic heating, friction or the motion back into high latitudes damp and wipe out the system (Fuenzalida et al., 2005).

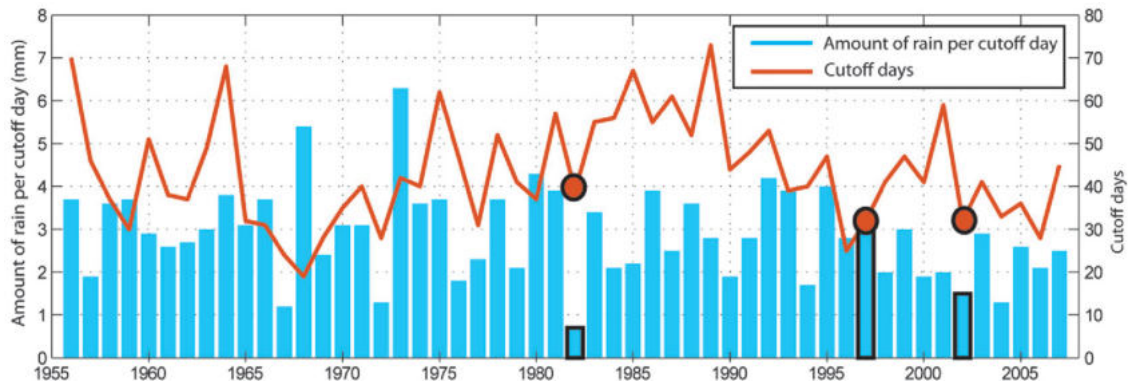


Figure 2.13: Analysis of April-October rainfall (in mm) for the period 1956-2007 in the Mallee region in the north of Victoria, Australia. The rainfall values are averaged over multiple stations in the Mallee region. The figure is adapted from Brown et al. (2009, Fig. 3).

Climatological studies about cut-off lows around Australia outline the importance on rainfall of these systems (Qi et al., 1999; Fuenzalida et al., 2005). Along the South Coast of Australia, the maximum frequency of cut-off lows is during May – October with a main genesis area (75%) between 110°E and 130°E. Most of the cut-off lows move eastwards or southeastwards but the movement velocity of the systems strongly varies between 2° and 10° latitude in 24 hours (Qi et al., 1999; Nieto et al., 2008). Cut-off lows are short-lived and only 10% of the systems last longer than 5 days (Nieto et al., 2008).

A few studies exist about the contribution of cut-off lows to rainfall in southeastern Australia. Wright (1989) connected synoptic systems to rainfall and found out, that cut-off lows are responsible for more than 50% of winter rainfall in southeastern Victoria. Two decades later, Pook et al. (2006) related daily rainfall from April-October over a 33-year period to cut-off lows and confirmed the results of Wright (1989) for the southeastern Australian region. The contribution of cut-off lows on rainfall is highest in spring with about 75%. In addition, rainfall from cut-off lows in the cold season account for 80% of daily rainfall events that exceed 25 mm per station (Pook et al., 2006). McIntosh et al. (2007) suggest that cut-off lows produce more rainfall as they propagate slower than fronts and stay longer in a particular region where it generates high rainfall amounts. They also intensify in regions with increased baroclinicity and through the interaction with the subtropical jet (Risbey et al., 2009a).

The occurrence of cut-off lows and the associated rainfall per cut-off low is highly variable (Pook et al., 2006; Brown et al., 2009). An analysis of April-October cut-off lows rainfall displays the non-linear relationship between rain per cut-off day and the number of cut-off days (Fig. 2.13). Risbey et al. (2009a) highlighted that wet years in southeastern Australia may result from enhanced rainfall of cut-off lows. With focus on the ‘dry period’ between 1996 and 2009, cut-off lows account for about two-third of the rainfall reduction in southeastern Australia due to a decreased frequency of cut-off lows and blocking in the Tasman region (Risbey et al., 2013).

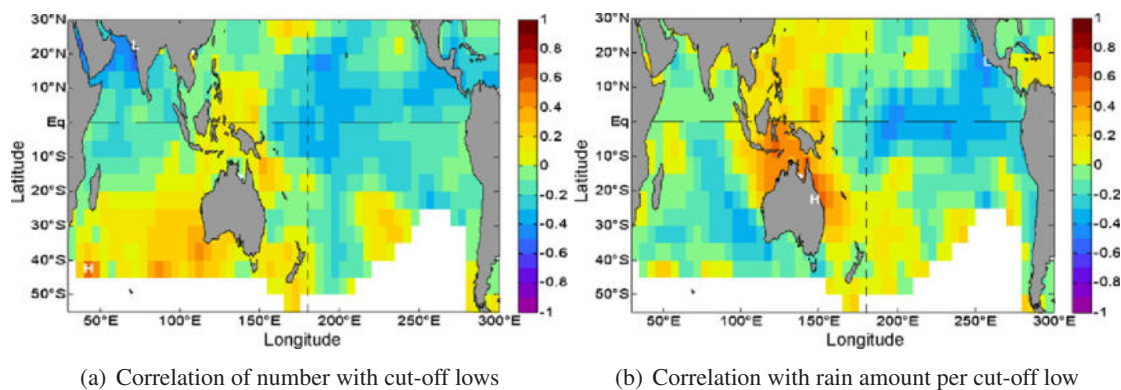


Figure 2.14: Simultaneous correlation between SSTs and (a) number of cut-off low systems and (b) amount of rainfall per cut-off low system for the period April-October over southern Australia. Correlation values that are greater than 0.28 are significant at a 90% level. The figure is adapted from McIntosh et al. (2007, Fig. 5).

### Extratropical cyclones and associated features

The dominant feature of the mid-latitudes are extratropical cyclones, that are associated with strong precipitation during their passage (Ulbrich et al., 2009). The belt of strong westerly winds establishes over southern Australia and is associated with an increased frequency of cyclones that delivers regular rainfall over southern Australia in the growing season (Pook et al., 2006). Fronts and warm conveyor belts (WCBs) are the associated features and link extratropical cyclones with precipitation in the midlatitudes (Catto et al., 2015).

Pook et al. (2006) studied the contribution of extratropical cyclones to rainfall in the growing season and found out that a third of the rain can be explained by frontal rain. In coastal regions of South Australia and Victoria, the fraction of frontal rainfall even reaches 45% (Pook et al., 2014). In addition, frontal rain brings light to medium daily rainfall (<10mm per station). A spatial examination on the contribution of frontal rainfall to growing season rainfall shows values up to 45% at the coastal stripes of South Australia and Victoria (Pook et al., 2014). However, extratropical cyclones account for one-third of the rainfall reduction during the dry period in 1996-2009 (Risbey et al., 2013). The reduction is due to a decrease of rain per extratropical cyclone and not due a decrease in the overall number of cyclones and can be explained by the observed decrease of baroclinicity and contraction of the Southern Hemisphere storm track (Risbey et al., 2013).

The WCB is the dominant ascending airstream associated with extratropical cyclones and plays a key role in the formation of precipitation (Madonna et al., 2014). WCBs typically ascend ahead of the cold front and over the warm front so that especially dynamically active fronts are more likely to show WCBs and rainfall extremes at the surface (Catto et al., 2015). On a climatological view, WCBs around Australia are more frequent in the cool season and start their ascent mainly over oceans between 17°S and 42°S with a predominant transport from the Subtropics. During their ascent, that is more likely to start east of the continent, air masses are transported southeastward towards the pole (Madonna et al., 2014). Pfahl et al. (2015) examined in their study the link of WCBs and rainfall in the period 1979-2010 and found that around 20-40% of the total rainfall over

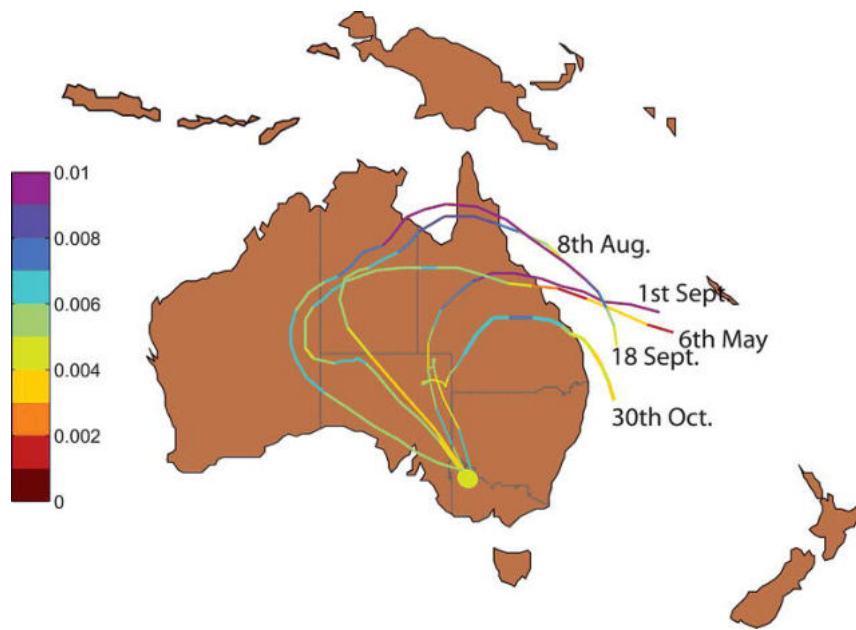


Figure 2.15: Backward trajectories (10 days) for 5 large wet events in 1997 in the Mallee region in the north of Victoria. Air parcels over the Mallee are backtracked at a starting height of 700hPa from several stations with a semi-Lagrangian algorithm. The colors indicate the specific humidity in  $\text{g kg}^{-1}$ . The dates relate to the day on which rain occurred and therefore the starting day of the trajectories. The figure is adapted from Brown et al. (2009, Fig. 6).

southeastern Australia is produced by WCBs. In addition, up to 60% of the number of extreme precipitation events are associated with WCBs. Over the Tasman Sea, the values are even higher with up to 90% (Pfahl et al., 2014). Catto et al. (2015) investigated the relationship between WCBs and fronts and showed that up to 80% (30%) of WCBs are linked to cold (warm) fronts in a region around Australia during winter. However, the WCBs over the Tasman Sea region are an exceptional case: most WCBs do not show links with any fronts but appear to be related to cut-off lows (Catto et al., 2015).

### Source of moisture for synoptic systems

After the introduction of the two main rain-bringing weather systems (cut-off lows, extratropical cyclones and associated WCBs), it is of interest to determine the moisture sources of these systems as most of southern Australia is relatively dry (Qi et al., 1999). Previous studies investigated the moisture source for a limited number of rainfall events over southeastern Australia. They calculated 10-days backward trajectories of particular cut-off low and extratropical cyclone events and compared the pathways. Many studies indicate that air parcel trajectories come from the north and northeast of Australia during high rainfall events related to cut-off lows (Fig. 2.15), where they pick up moisture over the Tasman and the Coral Sea (McIntosh et al., 2007; Brown et al., 2009; McIntosh et al., 2012). In addition, air parcels seem to descend over the marine boundary layer off the East Coast where they take up moisture. They travel westward at low levels over the continent before they turn south and reach the northeast quadrant of the cut-off low where they get lifted up again (McIntosh et al., 2012). In contrast, cut-off low trajectories from the southwest, south and southeast of Australia are not always associated with rainfall (Brown et al., 2009). McIntosh et al.

(2007) found in their study that more intense rainfall events over southeastern Australia can show a split of trajectories with proportions from the northwest and north. A clear difference between the cut-off low trajectories and extratropical cyclone trajectories is the length of the path: the trajectories of fronts have a 10-20 % longer path due to their greater propagation speed in comparison with the cut-off lows. Apart from that, the trajectories of fronts and cut-off lows are nearly similar (McIntosh et al., 2007). However, these results represent the mean trajectories. Single trajectories are also observed from the Southern and Indian Ocean.

As most of the trajectories seem to pick up moisture over the ocean, it raises the question if the SSTs around Australia are linked to the high variations of rainfall due to cut-off lows. McIntosh et al. (2007) suggest that there are different physical mechanism that control the number and behavior of cut-off lows. Some areas south and west of Australia reveal high correlations between SSTs and the number of cut-off lows (Fig. 2.14a). However, the SSTs north and east of Australia might have an stronger correlation with the amount of rainfall per cut-off low (Fig. 2.14b).

Pfahl et al. (2014) investigated the moisture origin of WCBs between 1979 and 2010 for southern-hemispheric winter. They found that the total moisture uptake in winter is highest to the east of Australia over the Coral Sea with a maximum at New Zealand longitudes. In addition, strong latent heat fluxes from the surface into the atmosphere occur along the coast lines to the north, east and west of Australia (Pfahl et al., 2014).



## 3 Data and methodology

We briefly introduce the data sets at the beginning of this chapter. The description of the used data sets is followed by an introduction of the primary methods that were applied in this thesis.

### 3.1 Data

#### 3.1.1 ERA-Interim reanalysis

Atmospheric reanalysis provides a best estimate of the true state of the atmosphere by reprocessing observational data from past decades with the use of a modern numerical weather prediction model. The benefits of reanalysis include the temporal and spatial consistency of the resulting long-term data set in comparison to the analysis. The data sets are heavily used in weather and climate research, as the reanalysis is not influenced by a constant improvement of the model and measurement methods over time (Parker, 2016).

An essential data source used in this thesis is the ERA-Interim reanalysis produced by the European Centre for Medium-Range Weather Forecasts (ECMWF) (Dee et al., 2011). It covers the data-rich period with the start of satellite measurements since 1979 and continues in real-time. The project was initiated in 2006 to replace the ECMWF's former reanalysis ERA-40. Currently, ERA-Interim is being replaced by the new ECMWF climate reanalysis ERA-5. The ERA-Interim reanalysis is produced with the cycle 31r2 data assimilation system of ECMWF's Integrated Forecast System (IFS) which uses a 4-dimensional variational analysis to apply a forecast model to limit the analysis (Dee et al., 2011). The gridded data products include estimates of three-dimensional meteorological parameters on 60 levels up to 0.1 hPa (Berrisford et al., 2009). Further details about the processes and parameters of ERA-Interim are documented in Dee et al. (2011) and Berrisford et al. (2009). In this thesis we use global, six-hourly data interpolated to a regular longitude-latitude grid with  $1^\circ$  horizontal resolution.

#### 3.1.2 Climatology of Eulerian and Lagrangian flow features

We make extensive use of a global collection of flow features created and kindly provided by the Atmospheric Dynamics group at ETH Zurich based on ERA-interim (Sprenger et al., 2017). In essence, different flow features are identified and then occurrence frequencies derived from binary fields. The collection provides a six-hourly climatology (1979-2015) of 15 different atmospheric flow features and allows us to study their variability and climatological frequency in the Australian region. The features are computed from the raw ERA-Interim data interpolated to a regular  $1^\circ \times 1^\circ$  grid. We consider two categories of features. These are Eulerian climatologies of cyclones, anticyclones, blocks, cut-off lows and enhanced moisture transport. The calculation of large ensembles of air parcel trajectories enable to derive Lagrangian climatologies of WCBs. In the following

sections, we present a short description of the algorithms that are used for the identification of Eulerian and Lagrangian flow features.

#### **Cyclones**

Cyclones are identified based on their minimum in mean sea level pressure (MSLP). The algorithm of Wernli and Schwierz (2006) first identifies local minima in MSLP as cyclone center candidates. Then, an outermost closed MSLP contour that encloses this MSLP minimum is identified. The length of the outermost pressure contour is limited to 7500km. For each time step, the outermost closed MSLP contour that encloses the MSLP minimum defines the cyclone area. In addition, the minimum center MSLP is tracked to determine the cyclone's track (Wernli and Schwierz, 2006; Pfahl et al., 2014).

#### **Cut-off lows**

Stratospheric potential vorticity (PV) cut-offs are associated with cut-off lows (Wernli and Sprenger, 2007). The contour searching algorithm by Wernli and Sprenger (2007) identifies stratospheric cut-off lows on isentropic surfaces between 305 K and 365 K and provides information about the structure of stratospheric air. Starting at the equator, the first grid point poleward with  $|PV| > 2\text{PVU}$  ( $1\text{PVU} = 10^6\text{K m}^2\text{kg}^{-1}\text{s}^{-1}$ ) and its neighborhood is examined. If the structure extends over the pole, the grid point would not represent a cut-off as the structure is categorized as a main stratospheric body. Otherwise, the structure can be identified as a cut-off when the detected structure does not extend to the equator (Wernli and Schwierz, 2006).

#### **Atmospheric blocking**

Regions of vertically averaged PV between 150 and 500hPa are considered for the identification of atmospheric blocking (Schwierz et al., 2004). In terms of PV, blocking is characterized by anomalous anticyclonic PV values. Anomalies are calculated as deviations from the monthly climatology of vertically averaged PV. The conditions for blocking in the southern hemisphere are satisfied when the anomaly at a grid point exceeds a certain threshold value and persists over at least 5 days (Schwierz et al., 2004). Previous studies often worked with a threshold of 1.3PVU. However, we use the threshold of 0.7PVU to further capture weak atmospheric blocking.

#### **Enhanced moisture transport**

Enhanced moisture transport is identified as a flow feature through the algorithm of Wernli and Knippertz (2019). In this Eulerian approach, a grid point is a candidate when the vertically integrated water vapor exceeds  $20\text{kg m}^{-2}$  and the value for the vertically integrated vapor transport is larger than  $250\text{kg m}^{-1}\text{s}^{-1}$ . Areas of enhanced moisture transport poleward of  $20^\circ\text{N/S}$  with a spatial expansion of at least 2000km are defined as Atmospheric Rivers (ARs) (Wernli and Knippertz, 2019). Although these criteria are in line with other studies, there is no commonly agreed definition of ARs and the AR community is currently comparing the different definitions (Shields et al., 2018).

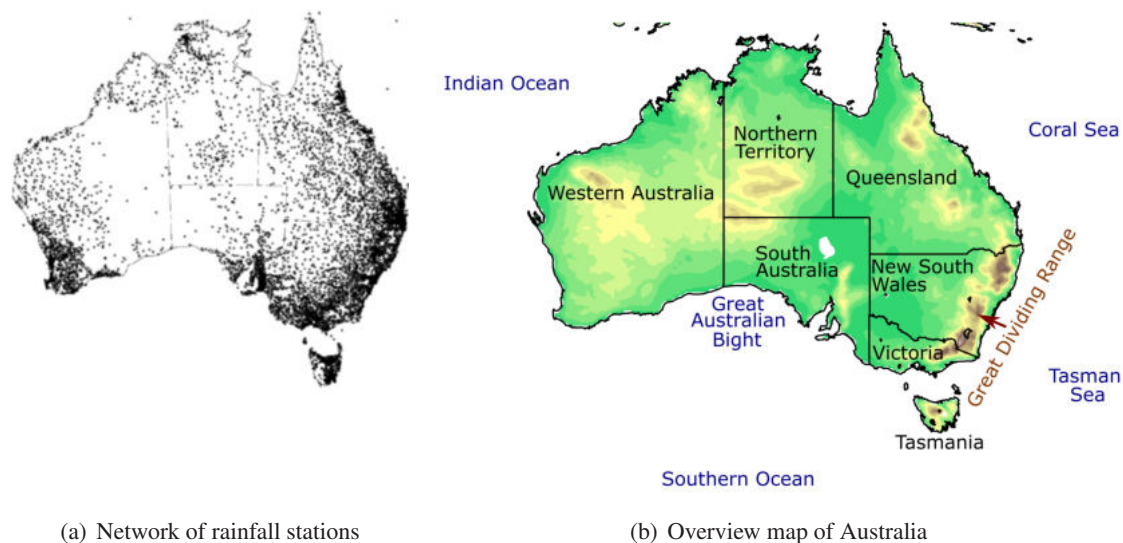


Figure 3.1: (a) The network of rainfall stations in Australia contributing to the analyses from 1980 to 2007. The figure is adapted from Jones et al. (2009, Fig. 2a). Each point represents a rainfall station. (b) Overview map of Australia with shaded elevation (in meters), the Australian states and territories and the surrounding seas and oceans. The  $0.25^\circ \times 0.25^\circ$  elevation data TerrainBase is from the National Center for Atmospheric Research and provided by the University of Washington (National Center for Atmospheric Research, 2014).

### Warm conveyor belts

We use the Lagrangian Analysis Tool (LAGRANTO) from ETH Zurich to calculate WCB trajectories from the lower troposphere for the identification of WCBs (Madonna et al., 2014). The criterion of WCBs is based on the rapid ascent of the trajectories near an extratropical cyclone: trajectories of an air parcel have to ascend more than 600hPa in 2 days from the boundary layer to the upper troposphere (Madonna et al., 2014). Different WCB frequencies are calculated and distinguished based on the height of the trajectories at a certain time: WCB inflow (pressure is higher than 800hPa), WCB outflow (pressure is less than 400hPa) and the mid-tropospheric area connecting the inflow and outflow (pressure is between 400-800hPa) (Madonna et al., 2014).

### 3.1.3 Australian rainfall analyses

The gridded rainfall data used in this thesis is from the Australian Data Archive for Meteorology, a national climate databank of the Bureau of Meteorology. Specific for rainfall, the data include total precipitation accumulated to 9am local time over a 24 hours period. The rainfall data set is available at daily and monthly temporal resolution with a spatial resolution of  $0.05^\circ \times 0.05^\circ$ . This thesis discusses daily and monthly rainfall amounts in the period 1979-2015. The monthly reference climatology to compute monthly anomalies is 1961-1990, according to the Bureau of Meteorology (Jones et al., 2009).

More than 3000 stations contribute to the rainfall analysis over Australia since 1900. Due to the increasing and evolving network, the number of stations reporting rainfall amounts exceeded 6000 in 1955 (Jones et al., 2009). Figure 3.1a shows the network of rainfall stations contributing

to the analyses from 1980 to 2007. Even the amount of high altitude stations in locations like the Great Dividing Range along the East Coast of Australia (Fig. 3.1b) has increased due to the installation of automatic weather stations that contribute to an improved analysis in more isolated high altitude locations (Jones et al., 2009). The rainfall analyses are computed using the Barnes analysis technique described in Jones et al. (2009). The analysis technique provides for each grid square the average and allows useful estimates for regions where data is sparse (e.g., central Australia). In data-rich regions (e.g., southeast Australia), the smoothing of the data leads to a slight variance of grid point values compared to the measurements of the exact rainfall amount at the stations. For additional information concerning the rainfall data set, the interested reader is referred to the work by Jones et al. (2009).

### **3.1.4 Sea surface temperature data set HadISST1**

The Met Office Hadley Centre provides global, monthly averaged SSTs. The data is available on a  $1^\circ$  latitude-longitude grid and covers the period of 1871 to real-time (Rayner et al., 2003). The SST analysis is based on quality-controlled in situ observations including ships' observations and observations from other in situ platforms. In addition, data from the Comprehensive Ocean-Atmosphere Data Set are used to increase data coverage. For the analysis in data-sparse regions, the reduced space optimal interpolation is applied (Rayner et al., 2003). The climatological reference period for calculating monthly anomalies is 1979-2015.

### **3.1.5 Climate indices**

Interactions between different components of the earth system can influence the systems variability. There exist climate indices that characterize different modes of variability. We want to investigate the climate modes that influence rainfall in southeastern Australia with the usage of data sets from the National Oceanic and Atmospheric Administration (NOAA).

#### **Southern Oscillation Index and Niño3.4 index**

The Southern Oscillation Index (SOI) and the Niño3.4 index measure the state of ENSO and the strength of the respective phase. Both indices are available at the website of NOAA (NOAA Physical Sciences Division, 2019[f]; NOAA Physical Sciences Division, 2019[d]). The SOI is calculated on the method given by Ropelewski and Jones (1987) and is based on the normalized pressure difference between Tahiti and Darwin (see red dots in Fig. 3.2). The Niño3.4 SST index measures the presence and strength of ENSO by monitoring the tropical SST variations (see green box in Fig. 3.2). Based on HadISST SSTs, anomalies are calculated and averaged over  $170^\circ$ - $120^\circ$ W and  $5^\circ$ S- $5^\circ$ N (Ropelewski and Jones, 1987)). The time period used for the climatology of SSTs in this region is 1981-2010.

#### **Dipole Mode Index**

The strength and phase of the IOD is represented by the anomalous SST gradient between two areas in the equatorial Indian Ocean (Saji and Yamagata, 2003). The Dipole Mode Index (DMI) demonstrates the SST anomaly difference between the western ( $60^\circ$ - $80^\circ$ E,  $10^\circ$ S- $10^\circ$ N) and the

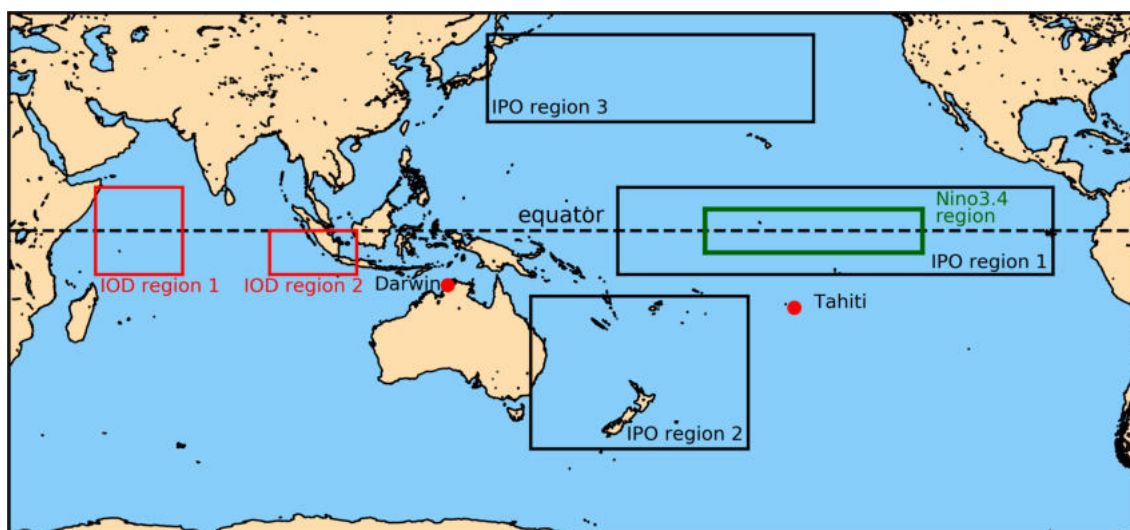


Figure 3.2: Regions and specific measurement points to monitor the different climate modes. The red boxes show the regions for the DMI, the black boxes are the three regions used to calculate the TPI and the green box shows the region used for the Niño3.4 index. Red dot points to the locations of Darwin and Tahiti.

southeastern ( $90^{\circ}$ - $110^{\circ}$ E,  $10^{\circ}$ S- $0^{\circ}$ ) equatorial Indian Ocean (see red boxes in Fig. 3.2). Anomalous low SSTs in the southeastern equatorial Indian Ocean (eastern red box in Fig. 3.2) and anomalous high SSTs in the western equatorial Indian Ocean (western red box in Fig. 3.2) indicate the presence of a positive IOD phase (Saji and Yamagata, 2003). The data is downloaded from the NOAA website (NOAA Physical Sciences Division, 2019[b]).

### Southern Annular Mode Index

SAM is measured by the difference of zonal averaged monthly normalized MSLP between  $40^{\circ}$ S and  $65^{\circ}$ S (Risbey et al., 2009b; Gong and Wang, 1999). The monthly data is available at the website of NOAA (NOAA Physical Sciences Division, 2019[a]). Each month's zonal mean is standardized using the mean deviation for the period 1981-201. For every month, the  $65^{\circ}$ S value is subtracted from the value at  $40^{\circ}$ S (Gong and Wang, 1999).

### PDO index and Tripole Index

The PDO index is defined by calculating the empirical orthogonal function (EOF) analyses of the monthly SST anomalies poleward of  $20^{\circ}$ N (Mantua and Hare, 2002). The Tripole Index (TPI) describes the interdecadal variability in the Pacific and is a measurement for the IPO that influences climate variability in the Pacific basin (Henley et al., 2015). Both indices are available at the website of NOAA (NOAA Physical Sciences Division, 2019[e]; NOAA Physical Sciences Division, 2019[c]). For the calculation of the TPI, SST anomalies (climatological reference period: 1971 to 2000) are averaged over the central equatorial Pacific ( $10^{\circ}$ S- $10^{\circ}$ N,  $170^{\circ}$ E- $90^{\circ}$ W), in the Northwest Pacific ( $25^{\circ}$ N- $45^{\circ}$ N,  $140^{\circ}$ E- $145^{\circ}$ W) and in the Southwest Pacific ( $15^{\circ}$ S- $50^{\circ}$ S,  $150^{\circ}$ E- $160^{\circ}$ W). The three regions are marked as black boxes in Figure 3.2. The TPI itself represents the difference between equatorial SST anomalies and in particular SST anomalies in the North Pacific (Henley et al., 2015).

### 3.1.6 Data set for outgoing longwave radiation

The emitted thermal radiation at the top of the atmosphere to space is also known as the outgoing longwave radiation (OLR) (Dewitte and Clerbaux, 2018). In general, positive (negative) OLR anomalies are connected with decreased (increased) cloudiness. For the detection of clouds, NOAA provides daily temporal interpolated OLR data at the top of atmosphere with a spatial resolution of  $2.5^\circ \times 2.5^\circ$  on a global grid that are available at the website of NOAA (Liebmann and Smith, 1996; NOAA Physical Sciences Division, 2019[g]).

## 3.2 Methods

### 3.2.1 K-means clustering and optimal number of clusters

The k-means algorithm is a centroid-based clustering method where different observations are allocated to k clusters so that a prescribed number of squares within a cluster is minimized (Hartigan and Wong, 1979). Therefore, the algorithm requires randomly selected k initial cluster centers. Each input field is assigned to the nearest cluster by calculating the Euclidean distance between the data point and each cluster center. Subsequently, the assigned points of a cluster are averaged to define a new cluster center. These steps are repeated until none of the cluster assignments change (Hartigan and Wong, 1979; Clark et al., 2018). The above method was previously used by Clark et al. (2018) for the clustering of rainfall data over northwestern Australia and will be utilized in this study for rainfall anomalies over southeastern Australia.

The most important input variable for the clustering algorithm is the number of clusters. Therefore, the calculation of the silhouette coefficient presents an approach to choose the number of clusters in an objective way (Clark et al., 2018). The silhouette coefficient  $s(i)$  is defined as:

$$s(i) = \frac{b(i) - a(i)}{\max(a(i), b(i))}, \quad (3.1)$$

where  $b(i)$  is the distance of an object  $i$  to the next closest cluster and  $a(i)$  the distance of an object to the remaining objects in the cluster. A value of 1 indicates that the data points represents the centroid, while a value of 0 would suggest that the data point does not fit any of the created cluster, as the distance to any cluster center is the same (Clark et al., 2018).

In addition to this method, we calculate the dissimilarity index as a function of the number of clusters. The dissimilarity index expresses the minimum of the average inter-cluster distance (Stefanon et al., 2012). A pseudometric definition is required to define a distance  $d'$  between two maps  $\mathbf{p}$  and  $\mathbf{q}$  as:

$$d'(\mathbf{p}, \mathbf{q}) = 1 - r(\mathbf{p}, \mathbf{q}) = 1 - \frac{\sum_{i=1}^N \sum_{j=1}^M p_{i,j} q_{i,j}}{\left( \sum_{i=1}^N \sum_{j=1}^M p_{i,j}^2 \right)^{\frac{1}{2}} \left( \sum_{i=1}^N \sum_{j=1}^M q_{i,j}^2 \right)^{\frac{1}{2}}}. \quad (3.2)$$

The term  $r(\mathbf{p}, \mathbf{q})$  is the anomaly correlation coefficient and is also known as cosine similarity. The maps are matrices of size  $M$  by  $N$  along the latitudinal and longitudinal axes and the quantities  $p_{i,j}$  and  $q_{i,j}$  are the values with dependence on longitudinal and latitudinal coordinates (Stefanon et al.,

2012). The distance  $d$  between two cluster  $C_1$  and  $C_2$  is the distance between the two farthest members:

$$d(C_2, C_1) = \max(d'(\mathbf{p}, \mathbf{q})), \quad \text{for all } \mathbf{q} \in C_1, \mathbf{p} \in C_2. \quad (3.3)$$

The index makes it possible to determine a suitable number of clusters that represent clearly different patterns. A noticeable jump of the dissimilarity index to smaller values by increasing the number of clusters means that the split of a current cluster into two clusters would lead to very similar clusters. This split would not provide different patterns and would therefore be unnecessary (Stefanon et al., 2012).

### 3.2.2 Monte Carlo approach

A Monte Carlo statistical significance test randomly samples reference sets whose dimensions match corresponding observed data (Scherrer et al., 2006; Martius et al., 2008). The Monte Carlo approach is used to rank an observed value among a random sample of values. In this study, 1000 random composites for different variables and clusters are created. For each cluster, all 1000 composites contain the same number of months as the examined cluster. As a first step, we randomly pick months in the considered period from 1979 to 2015 in the winter-spring season. For the ranking of the sampling data, the referred observed data is the mean over all months in the cluster composite. The comparison between the mean sampling data set and the mean observed data allows the percentile ranking (Scherrer et al., 2006; Martius et al., 2008). Values that fall below or exceed the upper and lower 2% (or in some cases 5%) percentiles of the Monte Carlo composites are defined as statistically significant.

### 3.2.3 Lagrangian parcel trajectories with LAGRANTO

A set of backward trajectories is computed with the Lagrangian analysis tool LAGRANTO by Sprenger and Wernli (2015) to investigate the origin of air masses. LAGRANTO uses ERA-Interim three-dimensional wind fields at 60 model levels to calculate the 240h (10 days) backward trajectories (Sprenger and Wernli, 2015). Three-dimensional Lagrangian backward trajectories are started 6-hourly between 970 and 490hPa at 17 levels over southeastern Australia. The grid width at the starting point of the trajectories is 60km and the starting point of the trajectories is referred to  $t = 0$ h in the following. As this paper focuses on the examination of rainfall over land, only trajectories ending on a grid point over land at  $t = 0$ h are considered. Physical properties traced along the computed backward trajectories include potential temperature, specific humidity and relative humidity.



# 4 Monthly rainfall variability in southeastern Australia

Different patterns of monthly rainfall anomalies over southeastern Australia form the basis of this study. Therefore, this chapter introduces different clusters and its characteristics, which are fundamental for the next chapters. First, the application of the k-means clustering algorithm (see Chapter 3.2.1) on the rainfall data is explained. After statistical methods are used to select the final number of clusters, we present the results and characterize the clusters.

## 4.1 Data base and clustering region

The focus of the subsequent examination is on the winter-spring season in the time period of 1979 to 2015. Monthly rainfall anomalies relative to the monthly 1961-1990 climatology (see Chapter 3.1.3) are the input data for the k-means clustering (see Chapter 3.2.1). The clustering region ( $29^{\circ}\text{S}$  to  $40^{\circ}\text{S}$ ,  $140^{\circ}\text{E}$  to  $154^{\circ}\text{E}$ ) is part of southeastern Australia and covers parts of the states Victoria, New South Wales and Southern Australia (red box in Fig. 4.1a). When we refer in the following discussion to the East Coast (South Coast), we point to the coastal areas of New South Wales (Victoria).

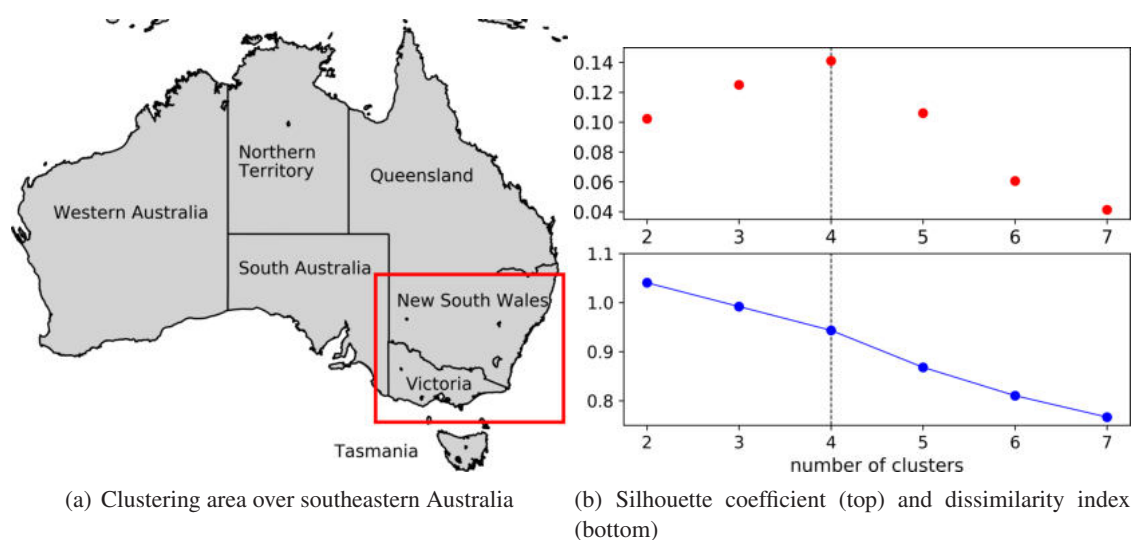


Figure 4.1: (a) Clustering area for the k-means clustering over southeastern Australia in the red box. (b) The results of the calculation of the silhouette coefficient (top) and the dissimilarity index (b) as function of the number of clusters. The final choice of 4 clusters is marked with a vertical line.

## 4.2 Statistical tests about finding the most physically sensible number of clusters

The average silhouette coefficient and the minimum dissimilarity index help determining the optimal number of clusters (see Chapter 3.2.1). For 6 different numbers of cluster, the two indices are calculated and presented as a function of the number of clusters in Figure 4.1(b).

The average silhouette coefficient first increases with a growing amount of clusters, peaks at a number of 4 and decreases afterwards (see Fig. 4.1b, top). Four clusters would therefore be suitable as the distribution of months would represent the respective rainfall anomaly pattern. The dissimilarity index exceeds 1 and indicates anti-correlated vectors when selecting two clusters. With an increasing number of clusters, the dissimilarity index steadily decreases. A noticeable jump in the dissimilarity index occurs when increasing the number of clusters from 4 to 5 (see Fig. 4.1b, bottom). This means that the split of one out of four clusters would lead to two nearly similar rainfall anomaly patterns and would therefore be unnecessary. The interested reader is referred to Figure A.1 and A.2 where we show the resulting rainfall anomaly clusters for different numbers of clusters. The statistical tests demonstrate the most physically sensible number of clusters and therefore we continue to work with the distribution of data into 4 clusters.

## 4.3 Introduction of rainfall anomaly clusters

The resulting four rainfall anomaly clusters over southeastern Australia created by the k-means clustering are described in the following. In each cluster, we average the monthly rainfall anomalies of the respective months (Fig. 4.2). In Cluster 1, rainfall over southeastern Australia is above-average (Fig. 4.2a). The highest rainfall anomalies up to 100mm are located west of the Great Dividing Range. Rainfall in Cluster 2 is anomalous low (below-average) over southeastern Australia (Fig. 4.2b). The rainfall deficits are maximum along the East Coast of New South Wales and parts of Queensland and show averaged anomaly values around  $-100$ mm. Cluster 3 indicates a dipole rainfall anomaly pattern (Fig. 4.2c): eastern parts of New South Wales and Victoria suffer from below-average rainfall with anomalies around  $-100$ mm, whereas the East Coast area get more rainfall with deviations up to 100mm. Cluster 4 shows a reversed pattern compared to Cluster 3 with above-average rainfall along the South Coast areas of Southern Australia and Victoria and negative rainfall anomalies along the East Coast of New South Wales (Fig. 4.2d).

The total number of months and the distribution of the months within a cluster are illustrated in Table 4.1. We also present a short description of the patterns and introduce abbreviation of the rainfall anomaly clusters that we use in the following (Table 4.1). A comparison shows that the number of months within a cluster is highly variable (Table 4.1). The cluster with the least months is wet Cluster 1 that only contains 30 out of 222 available months. This result is not unexpected, as it is well known that the Millennium Drought from 1997 to 2010 in the southern parts of Australia contributed to a statistical long-term decrease in cool-season rainfall (CSIRO, 2010). However, the we did not remove any trends from the monthly time series. The cluster with the highest amount of months is wet South Coast Cluster 4 that contains around 35% of all months

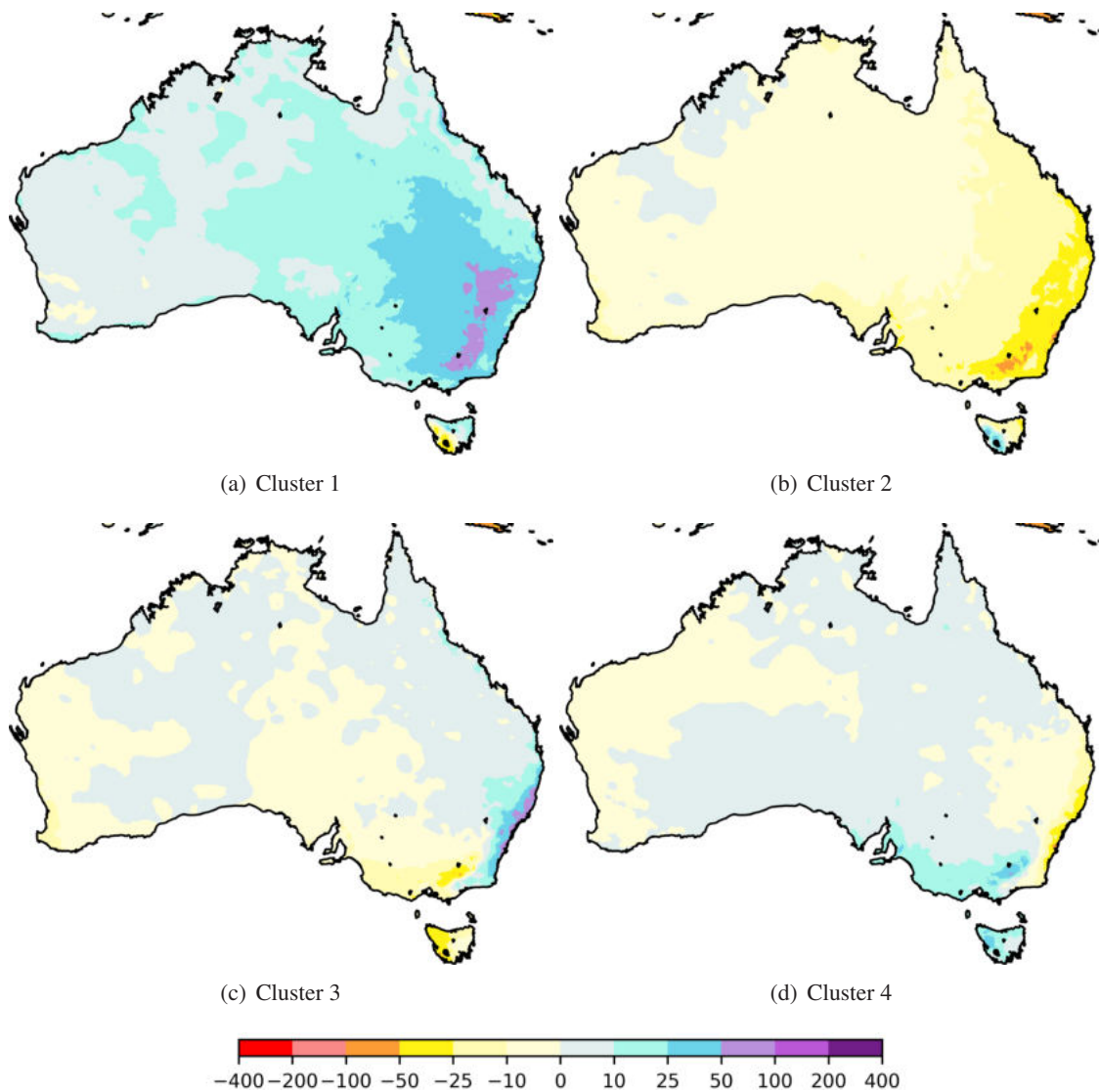


Figure 4.2: Averaged monthly rainfall anomalies (in mm) for each cluster over southeastern Australia: Cluster 1 (a), Cluster 2 (b), Cluster 3 (c) and Cluster 4 (d). The clusters result from the k-means clustering of monthly rainfall anomalies in the winter-spring season between 1979 and 2015.

in this study. The months within the clusters are equally distributed across the season (Table 4.1). Moreover, the clustering results do not point out a clear preference of a specific rainfall anomaly pattern for a month within the winter-spring season between 1979 and 2015.

## 4.4 The El Niño subset of clusters

The clusters that are presented in Chapter 4.3 are based on all months in the winter-spring season between 1979 and 2015. This study identifies and examines influences of El Niño on rainfall variability, so it is of interest to focus on the months during an El Niño phase.

The state of the ENSO in active and inactive periods during 1979 to 2015 is summarized in Table 4.2. The classification for the different ENSO phases is based on the official event classifications of the Bureau of Meteorology (Pepler et al., 2014). Sustained monthly Niño3.4 index

Table 4.1: Main characteristics of each cluster. The description of the rainfall patterns is with regard to the rainfall anomalies. This table shows for each cluster a short description of the rainfall anomaly pattern over southeastern Australia, the number/percentage of months in the cluster and the distribution of the months within the cluster.

	Cluster 1	Cluster 2	Cluster 3	Cluster 4
Description of pattern	wet	dry	wet East Coast	wet South Coast
Number of months	30	62	53	77
	13.51 %	27.93 %	23.87 %	34.69 %
June	5	5	9	18
July	8	10	9	10
August	1	12	8	16
September	4	11	10	12
October	3	15	7	12
November	9	9	10	9

Table 4.2: List of El Niño, La Niña and ENSO neutral years as defined by the Bureau of Meteorology. The data is derived from Pepler et al. (2014), complemented with information of the website of the Bureau of Meteorology and adjusted for the framework of this thesis (Commonwealth of Australia Bureau of Meteorology, 2019[d]). The bold years in the first column are El Niño Modoki years based on the classification of Wang et al. (2018).

El Niño	Neutral	La Niña
1982, <b>1987</b> , <b>1991</b> , 1993, <b>1994</b> , 1997, <b>2002</b> , 2006, <b>2009</b> , 2015	1979, 1980, 1981, 1983, 1984, 1985, 1986, 1989, 1990, 1992, 1995, 1996, 2001, 2003, 2004, 2005, 2012, 2013, 2014	1988, 1998, 1999, 2000, 2007, 2008, 2010, 2011

values above or below one standard deviation from the long-term mean (El Niño: 0.8 °C, La Niña: -0.8 °C) indicate a non-neutral ENSO phase.

In total, 10 El Niño events occurred between 1979 and 2015. Carving out the influences of El Niño, we split the clusters into a subset that only contains the months within an El Niño year. In the following, the subsets are labeled as El Niño clusters. Figure 4.3 presents the average monthly rainfall anomalies for the El Niño clusters. In comparison to the main clusters in Chapter 4.3, the rainfall anomaly patterns do not change a lot. In addition to the mean rainfall anomaly patterns, the Monte Carlo approach is applied on the rainfall anomalies in the clusters to show whether they are statistically significant. All regions that characterize a certain rainfall anomaly pattern (see description in Table 4.3) show statistically significant anomalies (contour lines, Fig. 4.3).

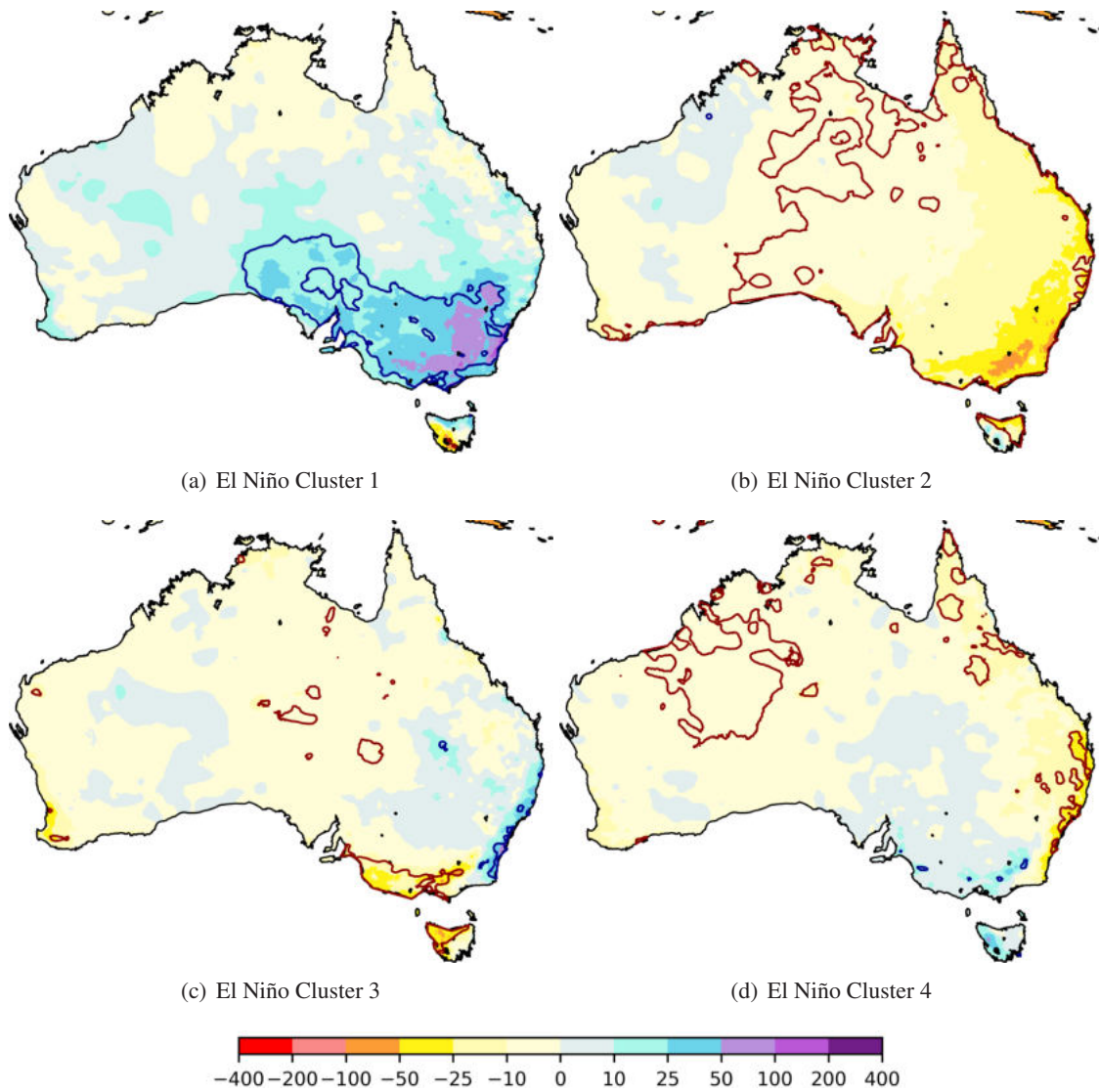


Figure 4.3: Averaged monthly rainfall anomalies (in mm) for each El Niño cluster over southeastern Australia: wet Cluster 1 (a), dry Cluster 2 (b), wet East Coast Cluster 3 (c) and wet South Coast Cluster 4 (d). The contour lines illustrate the results of the Monte Carlo approach. Blue (red) lines show statistical significance where rainfall anomalies exceed (fall below) the upper (lower) 2% percentiles.

Table 4.3: Main characteristics of the El Niño clusters. The description of the rainfall patterns is with regard to rainfall anomalies. This table shows a short description of the rainfall anomaly pattern, the number of months in the cluster, the percentage of El Niño months in the cluster, the percentage of all selected winter-spring months (1979-2015) and the distribution of the months within the cluster.

	El Niño Cluster 1	El Niño Cluster 2	El Niño Cluster 3	El Niño Cluster 4
Description of pattern	wet	dry	wet East Coast	wet South Coast
Number of months	5	29	12	14
Percentage of all El Niño months	8.33 %	48.33 %	20.00 %	23.22 %
Percentage of all months in cluster	16.67 %	46.77 %	22.64 %	18.10 %
June	1	2	3	4
July	1	4	2	3
August	0	7	2	1
September	2	4	2	2
October	1	7	2	0
November	0	5	1	4

The characteristics of the El Niño clusters are presented in Table 4.3. In the following, all months in the winter-spring season within El Niño years are defined as El Niño months. Dry Cluster 2 contains nearly 50% of all regarded El Niño months, which is not an unexpected result since rainfall over southeastern Australia usually is reduced in the cool season during El Niño (Risbey et al., 2009b). Some El Niño events exhibit a weaker rainfall reduction in the cool season tracing back to the fact that there unusually exists near-average or even above-average rainfall months within the season. Nevertheless, above-rainfall over southeastern Australia is rare during El Niño, so the number of months in wet Cluster 1 is small compared to the other clusters. It is of interest to find explanations for this unusual and sporadic incidence. Wet East Coast Cluster 3 and wet South Coast Cluster 4 nearly contain the same number of months (20-24% of all El Niño months). The distribution of months within the main and El Niño clusters highlight that there are no clear preferred months in which a specific rainfall anomaly pattern occurs.

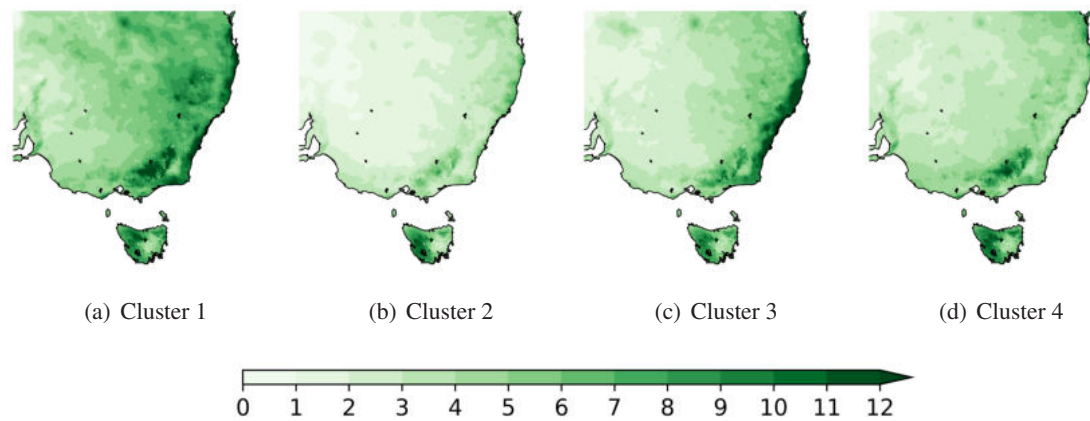


Figure 4.4: Standard deviation of daily rainfall amounts (in mm) within the main clusters over southeastern Australia: wet Cluster 1 (a), dry Cluster 2 (b), wet East Coast Cluster 3 (c) and wet South Coast Cluster 4 (d).

## 4.5 Insights into the cluster sets

After the introduction of the rainfall anomaly clusters and the split of El Niño clusters, it is of further interest to investigate the rainfall variability within the clusters but also the differences between the two cluster sets. In addition, the transition probability from one pattern into the next in the following month is calculated and compared for the two cluster sets. Moreover, we will compare ENSO classification indices with the classification of the ENSO phases by the Bureau of Meteorology and Pepler et al. (2014), that forms the basis for the El Niño clusters.

### Rainfall variability within and between the cluster sets

The clustering of rainfall in southeastern Australia is based on monthly rainfall anomalies. Nevertheless, it is of interest to study the distribution of daily rainfall within the clusters to figure out how tightly the data are clustered around the cluster mean. Figure 4.4 shows the mean standard deviation of daily rainfall for each grid point in the clustering area. The highest values for the mean standard deviation are found in regions of significant positive rainfall anomalies. The standard deviation is low in most of the western half of southeastern Australia. Even in wet Cluster 1, the standard deviation does not exceed values of around 6 mm (Fig. 4.4a). Over east Victoria and along the southern East Coast, the standard deviation is high in particular near and over the Great Dividing Range where the standard deviation shows values above 12 mm. This behavior can be explained by taking into account that orographic rainfall is highly variable in its strength and depends on the large-scale patterns of the atmospheric circulation.

Additionally to the standard deviation of the main set of clusters, the difference of the mean rainfall anomaly from the El Niño cluster and the main cluster is calculated for every cluster to highlight the differences between the two sets (Figure 4.5). The differences between the mean rainfall anomalies are highest in wet Cluster 1 (Fig. 4.5a). The rainfall anomalies are in the mean more negative during El Niño in the southern half and less negative in the northern half of southeastern Australia. Especially the southern East Coast is wetter during the few El Niño months in wet Cluster 1 with a mean difference of around 50 mm. Months in dry Cluster 2 show stronger

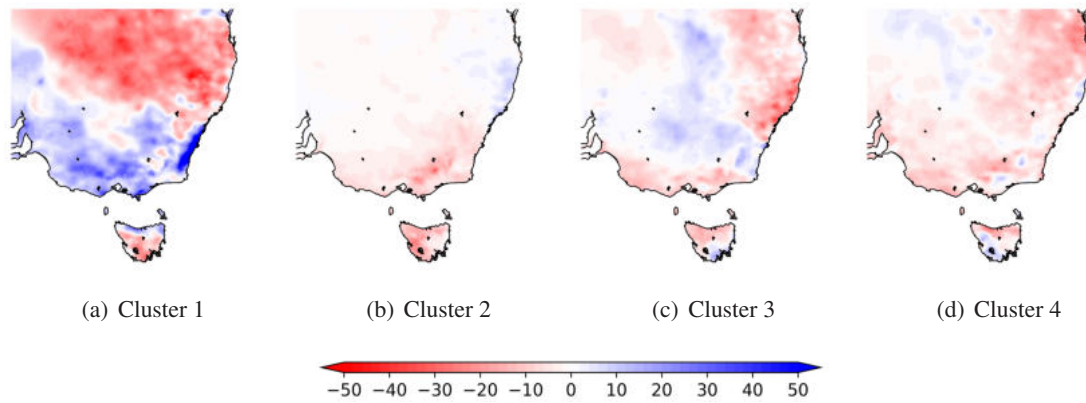


Figure 4.5: Difference of mean rainfall anomalies (in mm) between the El Niño cluster and the main clusters in southeastern Australia for wet Cluster 1 (a), dry Cluster 2 (b), wet East Coast Cluster 3 (c) and wet South Coast Cluster 4 (d).

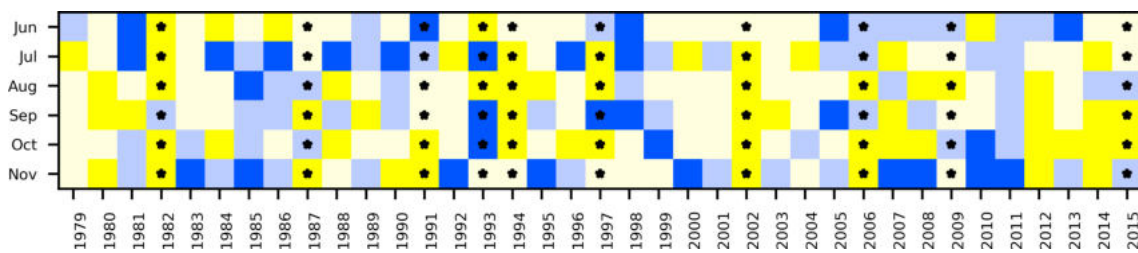


Figure 4.6: The distribution of all months in the winter-spring season between 1979 and 2015 in the 4 clusters: wet Cluster 1 (blue), dry Cluster 2 (yellow), wet East Coast Cluster 3 (light blue) and wet South Coast Cluster 4 (light yellow). El Niño months are marked with a star.

negative rainfall anomalies in the mean over the southern clustering box compared to the main cluster during El Niño (Fig. 4.5b). Only northern East Coast regions seem to get more rainfall during El Niño. Wet East Coast Cluster 3 illustrates the dipole character of the rainfall anomaly pattern and the upcoming differences between the two cluster sets (Fig. 4.5c). During El Niño, the southern regions suffer from stronger below-average rainfall and rainfall along the East Coast is in the mean less intense in New South Wales (up to 30 mm difference) but increased over Victoria. More inland, negative rainfall anomalies are weaker. In wet South Coast Cluster 4, rainfall over southeastern Australia except from some inland regions is lower during El Niño (Fig 4.5d).

### Transitions of clusters

Some characteristics about the two cluster sets are presented in Table 4.1 and Table 4.3. Figure 4.6 shows the exact distribution of months in the clusters. It is now of interest to investigate the transition probability from one cluster in another. The bar plots in Figure 4.7 show the transition probability from each cluster in another for the main clusters and the El Niño clusters.

The transition probability for a winter-spring month in general to a pattern that looks like dry Cluster 2 during El Niño is high (40 to over 60%). Moreover, the transition probability to a dry Cluster 2 pattern is for the first 3 clusters significantly larger compared to the transition probabilities to other clusters. This means that even if unusual monthly above-average rainfall occurs over southeastern Australia, the well-known below-average rainfall pattern is very likely to return

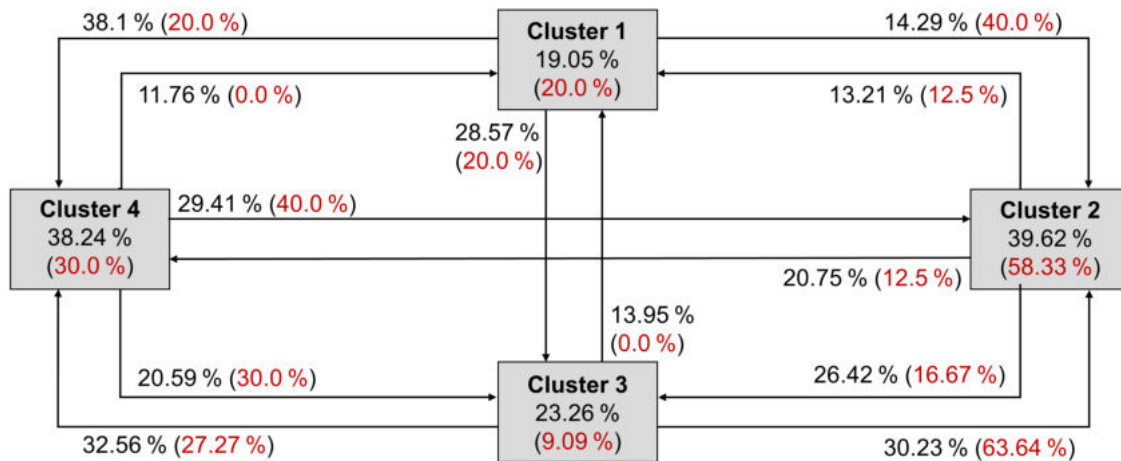


Figure 4.7: Transition probabilities for the main clusters (black) and the El Niño clusters (red) in the winter-spring season. Arrows point to the transition from one cluster into another one.

in the following month during El Niño and tends to more often persist. Taking into account all winter-spring months between 1979 and 2015, the transition probability to a dry Cluster 2 pattern is greatest during a dry Cluster 2 pattern or wet East Coast Cluster 3 pattern. For wet Cluster 1 and wet South Coast Cluster 4 patterns, the transition to a wet South Coast Cluster 4 pattern is the preferred one. Nevertheless, it is interesting that dry Cluster 2 and wet South Coast Cluster 4 patterns generally also in the main clusters tend to persist, whereas others are more variable. The transition probability to a wet Cluster 1 pattern is low for the main clusters and El Niño clusters. Interestingly, the only way to get an above-average rainfall pattern is from a below-average rainfall pattern the months before during El Niño. Nevertheless, the probability that the unusual rainfall anomaly pattern of wet Cluster 1 stays for the following month is with around 20% quite low.

### Consideration of El Niño Modoki and canonical El Niño

We already mentioned in Chapter 2 the different effects of a canonical El Niño event and an El Niño Modoki on rainfall over Australia. We here want to distinguish between the two different types of El Niño as the occurrence frequency of the Modoki event has increased in the past three decades (Wang et al., 2018). El Niño Modoki events are classified by the El Niño Modoki Index, that calculates the SST anomaly differences between the western, central and eastern tropical Pacific (Wang et al., 2018). Following Wang et al. (2018), 50% of the 10 identified El Niño events in the 1979-2015 period are characterized as El Niño Modoki events (see bold years in Table 4.2). The distribution of El Niño Modoki months (short: Modoki months) within a cluster allows us to detect the context between rainfall anomaly patterns and El Niño type.

Wet Cluster 1 shows a low fraction of Modoki months with 25%. In dry Cluster 2 (wet East Coast Cluster 3), the percentage is with 48.3% (41.7%) nearly equally distributed. However, wet South Coast Cluster 4 contains more El Niño Modoki months than canonical El Niño months with a contribution of 71.4%. Wet South Coast Cluster 4 demonstrates a weakened drying effect of the typical dry Cluster 2 El Niño rainfall anomaly pattern in southeastern Australia. In addition, significantly low rainfall is observed over northwestern Australia in wet South Coast Cluster 4 (Fig. 4.3d). This rainfall anomaly pattern fits with the observed impact of El Niño Modoki

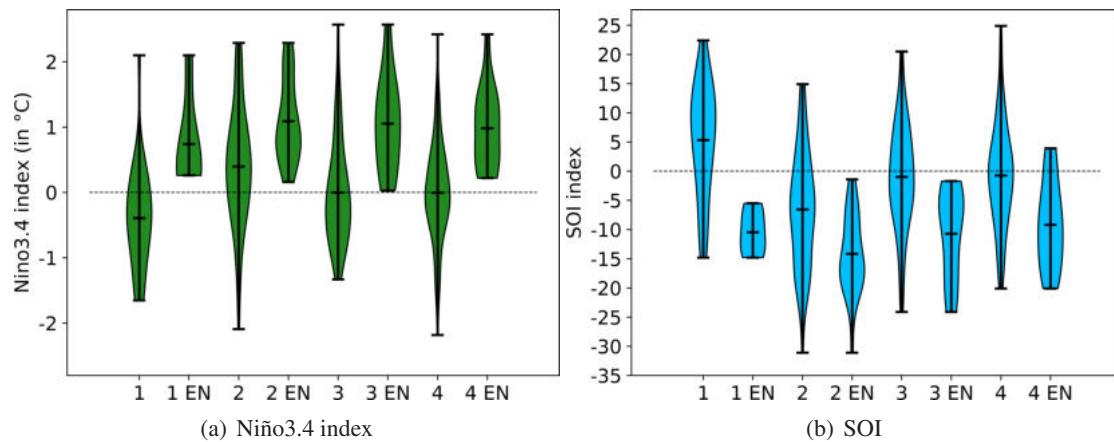


Figure 4.8: Violin plots showing the probability density, the interquartile range and the mean of the data for (a) the Niño3.4 index (in °C) and (b) the SOI for all main clusters and El Niño clusters (labeled with EN): wet Cluster 1, dry Cluster 2, wet East Coast Cluster 3 and wet South Coast Cluster 4. The black dashed line indicates the zero line.

(Taschetto and England, 2009). We will keep the percentages of the different El Niño types in wet Cluster 1 and wet South Coast Cluster 4 in mind for the following investigations. Furthermore, we do not split the El Niño subset into another subset as the sample would be too small.

### The non-linear impact of El Niño

Previous El Niño events showed that the magnitude of SST anomalies in the equatorial Pacific Ocean is a poor guide to forecast the effect on precipitation across the season in Australia (Power et al., 2006; King et al., 2013). We want to examine the distributions of different ENSO indices within our rainfall clusters. It is of interest to proof if specific ENSO modes favor a particular cluster or if we also find inconclusive distributions. Furthermore, we want to investigate the robustness of the classification when different indices are applied. ENSO indices, that are based on SSTs, are often used in combination with measurements of sub-surface ocean temperatures, cloudiness, winds and the SOI (Commonwealth of Australia Bureau of Meteorology, 2019[a]). We will compare a SST-based index with a atmospheric pressure-based index. Our El Niño clusters result from the ENSO classification in Pepler et al. (2014) that is based on the Niño3.4 index and the SOI (Commonwealth of Australia Bureau of Meteorology, 2019[e]).

Violin plots show the distribution of the two different ENSO indices for both cluster sets (Fig. 4.8). With focus on the main clusters, the distributions of the monthly indices in wet Cluster 1 point to a high percentage of La Niña months. This result is not unexpected as the rainfall anomaly pattern of wet Cluster 1 is usually associated with a rainfall anomaly pattern during La Niña. There is a clear opposite behavior in dry main Cluster 2 as most of the months are associated with typical El Niño conditions (negative SOI, positive Niño3.4 index). This fits with below-average rainfall over southeastern Australia in the rainfall anomaly pattern in the main dry Cluster 2. In wet East Coast Cluster 3 and wet South Coast Cluster 4, the mean of both indices is close to zero which indicates an equal distributed mixing of different ENSO states in the main clusters.

Nearly all months within the El Niño clusters show typical negative values of the SOI and positive

values of the Niño3.4 index that usually point to an El Niño event (Fig. 4.8). However, some months within the El Niño clusters are not associated with high positive (negative) El Niño values of the Niño3.4 index (SOI), as the long-term mean is decisive to define an El Niño phase and not a single monthly mean. In contrast to wet El Niño Cluster 1, absolute values observed in dry El Niño Cluster 2 are higher and overlap the range of values of wet El Niño Cluster 1. The overlap is also present in wet East Coast El Niño Cluster 3 and wet South Coast El Niño Cluster 4 but with a weaker mean value compared to dry El Niño Cluster 2.

The differences in the distributions of ENSO indices between the El Niño clusters are small. Nevertheless, it seems that the strength of an event is not decisive for the impact on rainfall in southeastern Australia, as there is a great overlap of the distributions of monthly indices between the clusters.



# 5 Large-scale patterns and influences of climate modes

Multiple modes of the climate system drive rainfall variability in southeastern Australia (Murphy and Timbal, 2008). These climate drivers influence rain-producing processes in this region on intraseasonal and longer timescales. ENSO is the most extensive mode and the leading driver of rainfall in terms of consistency through the season (Risbey et al., 2009b). Further large-scale modes are driven by SST variability in the tropical and extratropical Pacific and the Indian Ocean or by the position of the westerly wind belt (Murphy and Timbal, 2008).

The purpose of this section is two-fold. First, we analyze SST anomaly patterns and the behavior of the climate modes IPO, PDO, IOD and SAM in the rainfall clusters for southeastern Australia. Second, we will investigate how tropical SST anomalies during El Niño modulate the extratropical circulation in the Australian region, and thus affect rainfall variability in southeastern Australia.

## 5.1 SST anomalies and climate modes

The SST anomalies in the tropical Pacific Ocean characterize and define the El Niño phenomenon (Chapter 2.2.1). However, this is not the only SST pattern and mode that drives Australian rainfall variability during El Niño. Apart from the central and eastern tropical Pacific SSTs, there is also a relationship between the SSTs to the West and South of Australia and over the western Indian Ocean with rainfall variability, especially in Victoria (Murphy and Timbal, 2008). Figure 5.1 shows the cluster mean SST anomalies for the El Niño clusters and allows a comparison of different SST patterns in the Pacific Ocean, Indian Ocean, Southern Ocean and the marginal seas east of Australia (e.g., Tasman Sea and Coral Sea).

### 5.1.1 SST anomalies in the Pacific Ocean and the role of PDO and IPO

The traditional El Niño SST anomaly pattern is clearly visible in all El Niño clusters (see Fig. 5.1). Negative SST anomalies prevail in the western equatorial Pacific and extend south-eastward into the South Pacific. Positive SST anomalies in the central and eastern equatorial Pacific Ocean characterize the typical 'warm water tongue' (Allan, 1988). However, a more detailed view indicates slight differences in pattern and strength between the clusters.

Negative SST anomalies are strongest over the maritime continent in wet Cluster 1 with mean deviations up to  $-0.9^{\circ}\text{C}$  (Fig. 5.1a). In dry Cluster 2, the anomalies reach  $-0.5^{\circ}\text{C}$  (Fig. 5.1b). Negative SST anomalies are clearly weaker with a maximum strength in the extratropical Pacific Ocean in wet East Coast Cluster 3 and wet South Coast Cluster 4 (Fig. 5.1c,d). There are also differences in the amplitude of positive SST anomalies over the central and eastern equatorial Pacific

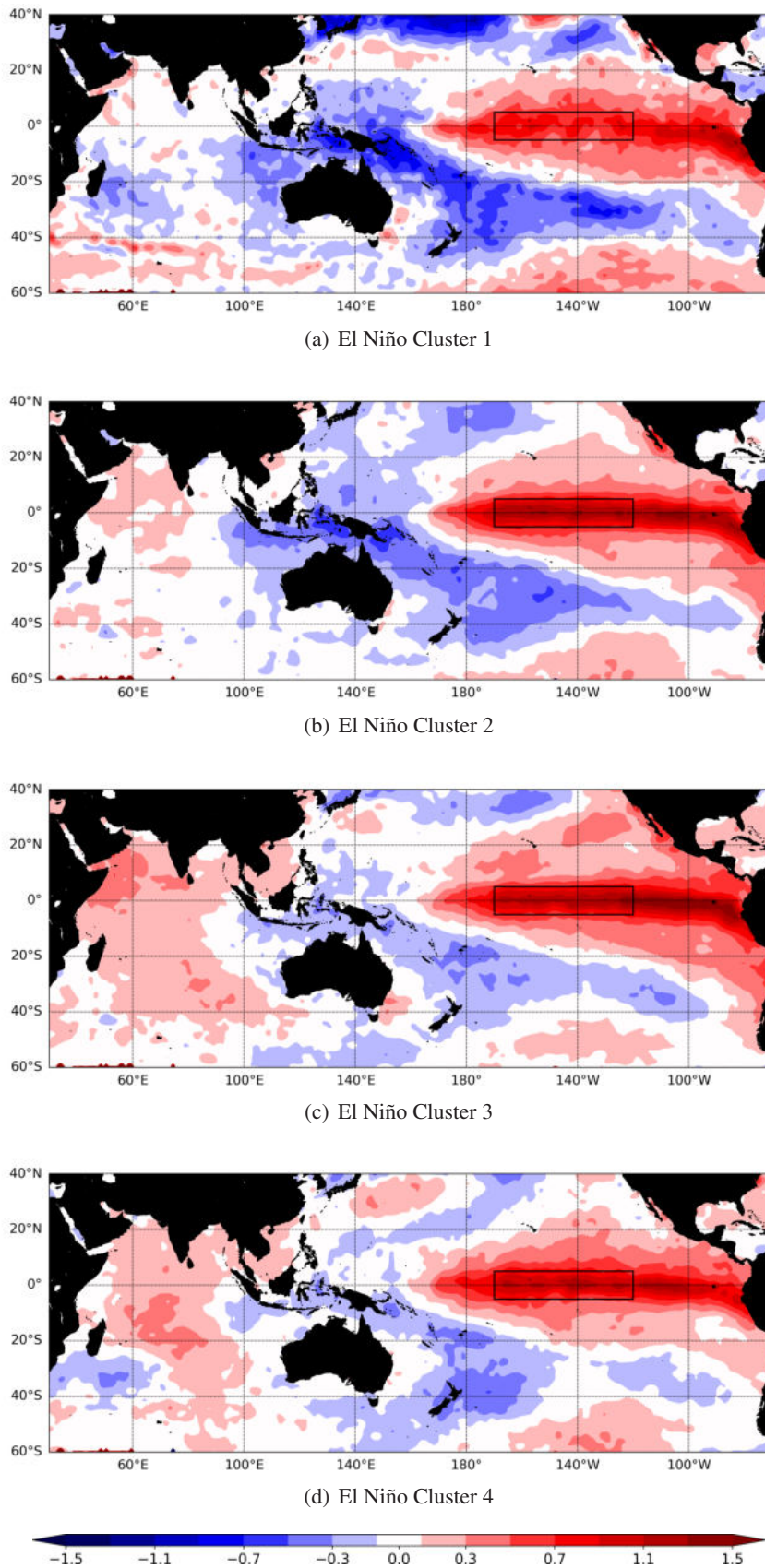


Figure 5.1: Cluster mean SST anomalies (in °C) for the El Niño clusters: wet Cluster 1 (a), dry Cluster 2 (b), wet East Coast Cluster 3 (c) and wet South Coast Cluster 4 (d). Monthly mean SST anomalies are based on the monthly climatological reference period from 1979 to 2015. The black box over the central tropical Pacific marks the Niño3.4 region that is used to measure the state and strength of ENSO.

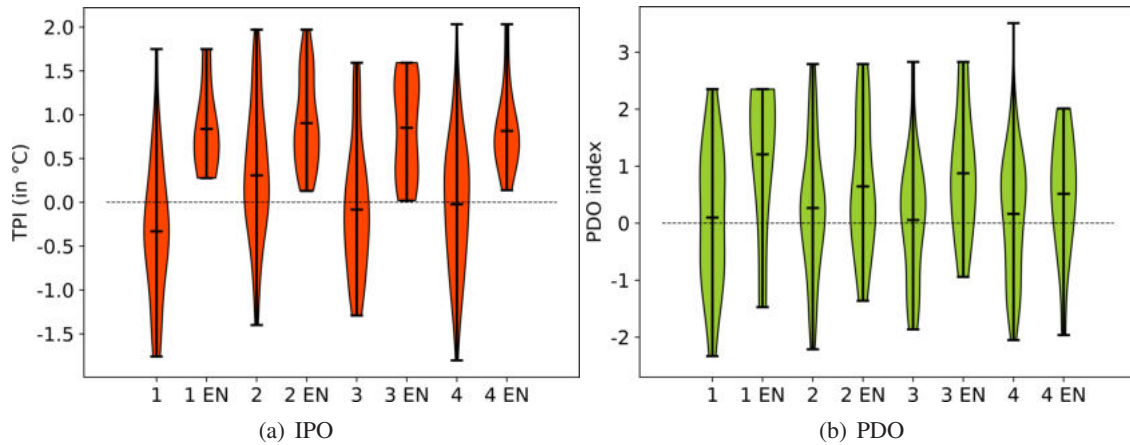


Figure 5.2: Violin plots showing the distribution of monthly values of (a) the TPI (in °C) and (b) the PDO index within the different main clusters and the El Niño clusters (labeled with EN): wet Cluster 1, dry Cluster 2, wet East Coast Cluster 3 and wet South Coast Cluster 4. The dotted line represents the zero line.

Ocean. In wet Cluster 1, the maximum SST anomaly values are concentrated in the far eastern Pacific at 80°W. Wang and Hendon (2007) point out in their study that the rainfall pattern over southeastern Australia is sensitive to the zonal position of maximum SST anomaly values along the tropical Pacific Ocean. They emphasize that maximum SST anomalies in the far east Pacific appear to influence rainfall less over southeastern Australia during an canonical El Niño. The findings are in accordance with the percentage of canonical El Niño months within wet Cluster 1 (75%, Chapter 4.5) and the location of maximum positive SST anomalies (Fig. 5.1a). Wet South Coast Cluster 4 exhibits the weakest SST anomalies along the coast of South America and in the far eastern Pacific. However, maximum SST anomalies are focused near the dateline in wet South Coast Cluster 4 (Fig. 5.1d). This pattern shows similarities with the El Niño Modoki SST pattern that is characterized by maximum positive SST anomalies in the central equatorial Pacific. This is not surprising as the proportion of El Niño Modoki months is 71.4% in wet South Coast Cluster 4 (Chapter 4.5). Following Wang and Hendon (2007), the described pattern tends to have a greater effect on Australian rainfall.

Previous studies showed that PDO and IPO have some modulating effects on rainfall in southeastern Australia during El Niño despite their different time scales (Chapter 2.2.1). It is of interest to examine if the climate modes PDO and IPO can explain the rainfall variability that is observed in the clusters. Clear differences in IPO and PDO distributions between the El Niño clusters could indicate the importance of Pacific oscillations on different rainfall anomaly patterns. According to the results of previous studies, the IPO is highly correlated with ENSO. It is therefore not surprising, that the distributions of the TPI show unexceptional positive values during El Niño in all clusters (Fig. 5.2a). The main clusters additionally include La Niña months and ENSO neutral months. This leads to a larger distribution of the TPI that also covers negative indices. The distributions of the PDO index demonstrate a more unclear picture of the PDO-ENSO relationship (Fig. 5.2b). We expected more clear differences in the distributions, as negative (positive) indices are associated with wet (dry) conditions over eastern Australia. However, the complex phase rela-

tionship between ENSO and PDO and the fact that ENSO, PDO and IPO occur on different time scales point to the unclear signals in the distributions (Kim et al., 2013).

In essence, we find no striking differences in the occurrence of Pacific SSTs anomalies or climate modes such as the PDO and IPO that are related to the rainfall variability in our clusters.

### 5.1.2 SST anomalies in the Indian and Southern Ocean and the role of IOD

In this section, we will discuss the mean SST anomalies in the different clusters with focus on the Indian Ocean and Southern Ocean (Fig. 5.1). For the characterization and definition of IOD phases, we use the DMI that is introduced in Chapter 3.1.5.

The quite similar distributions of DMI values in the main clusters demonstrate that different rainfall anomaly patterns are not associated with a specific IOD phase (Fig. 5.3a). Although negative values point to La Niña or ENSO neutral phases, most of the DMIs are positive in the main clusters. This indicates the dominance of positive IOD phases in the winter-spring seasons of 1979-2015.

During El Niño, all clusters show below-average SSTs at the tropical eastern boarder of the Indian Ocean near Indonesia and near-average or above-average in the tropical western Indian Ocean (Fig. 5.1). This pattern, that defines the positive IOD phase and is associated with decreased rainfall over southeastern Australia, is existent in all El Niño months (Fig. 5.3a). However, the positive IOD pattern fits best with the rainfall anomaly pattern in dry Cluster 2. The mean SST anomalies in the clusters differs in strength as one part of the dipole is more pronounced than the other one (Fig. 5.1). The eastern pole over the maritime continent is stronger in wet Cluster 1 and dry Cluster 2 with SST anomalies up to  $-0.5^{\circ}\text{C}$ . The western pole southwest of India is stronger in wet East Coast Cluster 3 and wet South Coast Cluster 4 with positive SST anomalies that reach  $0.5^{\circ}\text{C}$ . Nevertheless, the resulting DMI indicates a comparable strength of the positive IOD phase between the clusters (Fig. 5.3a). The positive IOD phase is not associated with the well-known drying effect in southeastern Australia in wet Cluster 1. This suggests that there is another process that dominates the rainfall variability or even suppresses the influence of the IOD on rainfall.

During El Niño, SSTs are above-average in the Southern Ocean at Indian Ocean and Pacific Ocean longitudes and below-average in the Southern Ocean at Australian longitudes (Fig. 5.1). With focus on spatial patterns, the signals fluctuate strongly in wet Cluster 1 and dry Cluster 2 but are more developed and clear in wet East Coast Cluster 3 and wet South Coast Cluster 4 where SSTs over the Southern Ocean are warmer than average between  $40^{\circ}\text{E}$  and  $110^{\circ}\text{E}$  and might be related to the strongly developed western pole of the IOD. We will keep the above-average SSTs southwest of Australia in mind as they are correlated with the number of cut-off lows over southern Australia (McIntosh et al., 2007).

The examination of the SSTs in the Indian and Southern Ocean demonstrated that they are not the leading factors of rainfall variability in southeastern Australia during El Niño. The nearly

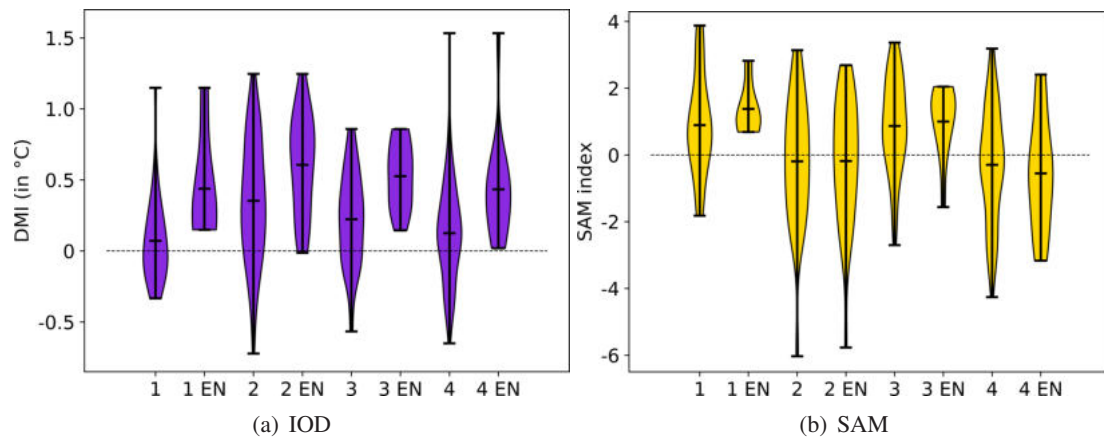


Figure 5.3: Violin plots showing the distribution of monthly values of (a) the DMI (in  $^{\circ}\text{C}$ ) and (b) the SAM index within the different main clusters and El Niño clusters (labeled with EN): wet Cluster 1, dry Cluster 2, wet East Coast Cluster 3 and wet South Coast Cluster 4. The dotted line indicates the zero line.

similar distributions of DMI values of the clusters suggest that the IOD is not the key climate mode for the explanation of rainfall variability in southeastern Australia neither during El Niño nor during the winter-spring season in general.

### 5.1.3 SST anomalies around Australia

Following Allan (1988), SSTs around Australia are typically below-average during El Niño. With focus on Figure 5.1, all El Niño clusters confirm this behavior in general. However, some coastal areas east of Australia tend to have slight above-average SSTs.

In wet Cluster 1 and dry Cluster 2, the strongest mean SST anomalies with over  $-0.5^{\circ}\text{C}$  deviation are located along the north, northeast and west coast of Australia (Fig. 5.1a,b). In comparison, the SSTs are nearly average or weakly deviate from the climatological mean in this regions in wet East Coast Cluster 3 and wet South Coast Cluster 4 (Fig. 5.1c,d). At the southern East Coast of Australia, all clusters except from wet South Coast Cluster 4 show positive SST anomalies especially with values up to  $0.5^{\circ}\text{C}$  in wet Cluster 1 and wet East Coast Cluster 3. At this point, we suggest a connection between the pronounced positive SST anomalies east of Australia and positive rainfall anomalies along the coast. We will come back to a discussion of different SST anomalies around Australia when we examine their possible effect on rainfall over southeastern Australia.

SST anomalies around Australian are not assumed as the main drivers of rainfall variability around Australia. Nevertheless, the more local SST signals off the East Coast of Australia could affect processes on the synoptic-scale and even serve as moisture source of weather systems.

### 5.1.4 The role of SAM

In contrast to the previously discussed climate modes, we want to discuss the distribution of monthly SAM values and the corresponding phases within the El Niño clusters. A first compar-

ison between the El Niño and main clusters illustrates a high degree of consistency within the same rainfall anomaly pattern (Fig. 5.3b). This suggests that the phase of SAM is more related to a specific rainfall anomaly pattern than to a specific ENSO phase. With the focus on El Niño, the differences in the distribution of SAM values between the clusters are distinct in comparison with the SST based climate modes.

During El Niño, wetter-than-average months in southeastern Australia (Cluster 1) are related to positive SAM phases (Fig. 5.3b). Most of the monthly SAM values in wet East Coast Cluster 3 are also positive. During positive SAM, the westerly wind belt is shifted to the south which usually leads to below-average rainfall in southeastern Australia (Chapter 2.2.1). Risbey et al. (2009a) found in their study that cut-off lows are linked to the occurrence of a positive SAM phase as the SAM-associated blocking favors the development of cut-off lows. We proofed this statement with our SAM index and cut-off low frequency data sets (Chapter 3.1.2) and found similar results. During a positive (negative) SAM phase, the cut-off low frequency is increased (decreased) over southeastern Australia (Fig. 5.4). In addition, Risbey et al. (2009b) point to increased rainfall along the East Coast which is in accordance with the rainfall anomaly patterns in wet Cluster 1 and wet East Coast Cluster 3. When southeastern Australia suffers from anomalous dry conditions (Cluster 2), the SAM phase does not seem to play an important role neither in the main cluster nor in the El Niño cluster (Fig. 5.3b). This is quite surprising, as the positive SAM is typically related to suppressed rainfall over southern Australia (Risbey et al., 2009b). In wet South Coast Cluster 4, the occurrence of positive and negative SAM values suggest a minor role of SAM on modulating rainfall during El Niño (Fig. 5.3b). However, the majority of months in wet South Coast Cluster 4 indicates the presence of a negative SAM phase. The well-known impact of a negative SAM phase on rainfall is nearly equal to the observed rainfall anomaly pattern in wet South Coast Cluster 4. During a negative SAM phase, westerlies are shifted equatorward and lead to below-average MSLP over southern Australia. As a consequence, rainfall increases along the South Coast (Risbey et al., 2009a).

The investigation of previous discussed SST-based climate modes demonstrated that neither Pacific climate modes (IPO, PDO) nor the IOD play a key role in driving rainfall variability in southeastern Australia during El Niño. The distribution of SAM values within and between the rainfall clusters suggests that SAM is the primary climate mode on the large-scale that affect rainfall in southeastern Australia as it controls the jet position of the mid-latitudes.

## 5.2 Large-scale atmospheric patterns

We examined the influence of climate modes on different rainfall patterns during El Niño in the previous chapter. Now, we will diagnose tropical and extratropical large-scale circulation anomalies that develop during El Niño.

The direct atmospheric response of El Niño in the Tropics is well known: Subsidence and higher MSLP over the western Pacific that result from diabatic heating anomalies suppresses rainfall in eastern Australia (Cai et al., 2011). As the tropical baroclinic response is equatorially trapped, the impacts are confined to the tropical latitudes of Australia. The same heating anomalies that

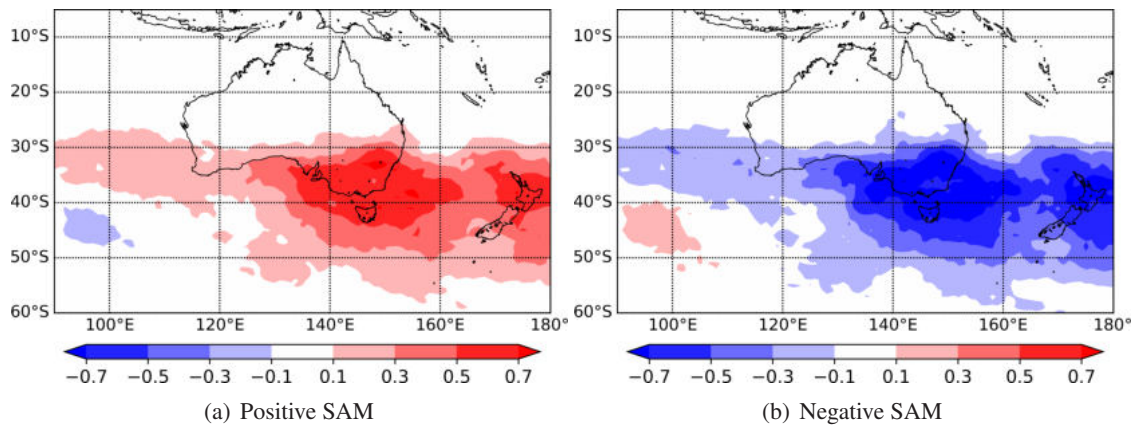


Figure 5.4: Mean monthly cut-off low frequency anomalies (in %) at 315K during positive SAM months (a) and negative SAM months (b) in the winter-spring season from 1979 to 2015.

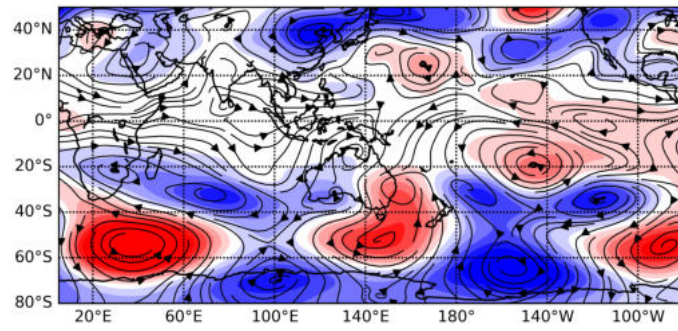
are induced by SST anomalies play also a crucial role in stimulating RWTs that propagate from the Tropics into the Extratropics. The RWTs seem to influence rainfall in southeastern Australia by changing the circulation in Australian latitudes (Cai et al., 2011). We will look at circulation anomalies and RWT responses during El Niño to find pathways of the teleconnections from the equatorial Indian Ocean and Pacific Ocean.

### 5.2.1 Geopotential and streamlines

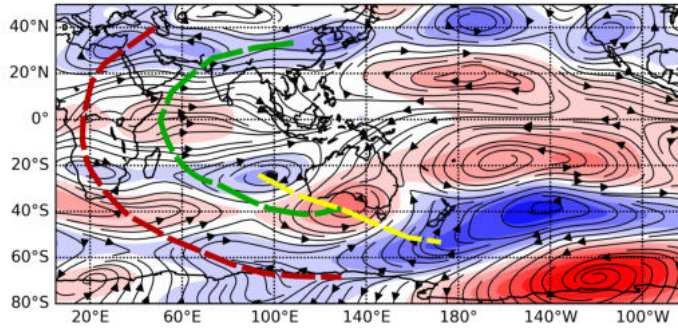
The analysis of the upper-tropospheric large-scale circulation anomalies allows to find teleconnections between convective anomalies in the Tropics and rainfall over extratropical southeastern Australia during El Niño. The monthly circulation anomalies refer to the 1979-2015 climatology. Figure 5.5 shows the cluster mean anomalies for geopotential height and wind as streamlines at 200hPa for the El Niño clusters.

With the focus on equatorial regions, all clusters show a positive geopotential height anomaly over the central and eastern tropical Pacific Ocean during El Niño (Fig. 5.5). This upper-level anticyclonic pair at 200hPa is the response to enhanced diabatic heating (Wang and Hendon, 2007). The strongest mean values of this positive anomaly up to  $35\text{ m}^2\text{ s}^{-2}$  are located around  $5^\circ\text{N/S}$ . The positive geopotential anomalies are stronger in wet East Coast Cluster 3 and wet South Coast Cluster 4 than in wet Cluster 1 and dry Cluster 2. As expected, the wind anomalies in 200hPa match with the geopotential anomalies and indicate the anomalous anticyclonic character that is related to positive geopotential anomalies over the central Pacific. Over the maritime continent, the geopotential is near the climatological mean, especially in wet Cluster 1 and dry Cluster 2 (Fig. 5.5a,b). Nevertheless, there is evidence of confluent anomalous winds over the maritime continent in the upper troposphere in all clusters.

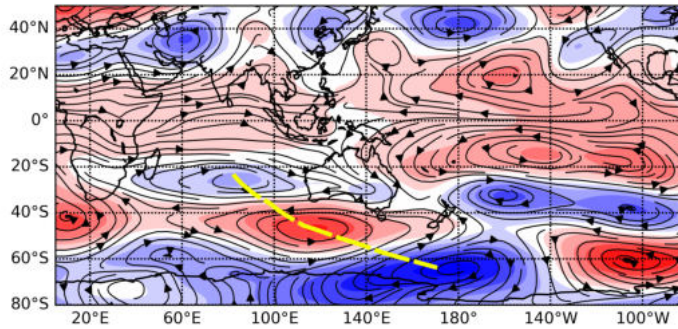
We now focus on the Australian region. In wet Cluster 1, an area of anomalous high geopotential lies with its center at around  $150^\circ\text{E}$  southeast of Australia (Fig. 5.5a). The structure extends from  $60^\circ\text{S}$  south of Australia up to  $20^\circ\text{S}$  into the subtropics and covers the whole clustering area of southeast Australia. Moderate anticyclonic wind anomalies characterize the circulation over the



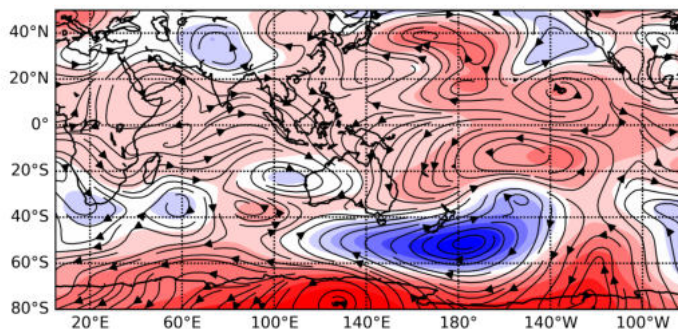
(a) El Niño Cluster 1



(b) El Niño Cluster 2



(c) El Niño Cluster 3



(d) El Niño Cluster 4

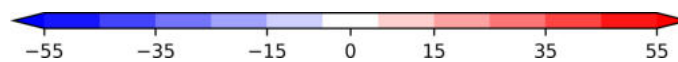


Figure 5.5: Cluster mean geopotential anomalies (shaded, in  $m^2 s^{-2}$ ) and cluster mean wind anomalies (in streamlines) at 200hPa in for the El Niño clusters: wet Cluster 1 (a), dry Cluster 2 (b), wet East Coast Cluster 3 (c) and wet South Coast Cluster 4 (d). The monthly climatological reference period is 1979-2015. Dashed colored lines trace the prominent RWTs that are described in Cai et al. (2011) and introduced in Chapter 2.2.1.

Tasman Sea. A negative geopotential anomaly structure to the west is pushed far into the Subtropics and covers West Australia. Inland of Australia, confluent anticyclonic easterlies and cyclonic westerly winds in central Australia suggest anomalous northerly flow over southeastern Australia. Another area of negative geopotential anomalies is located east of New Zealand that seems to enclose the strong positive geopotential anomaly structure over Australia.

A region of above-average geopotential is located in the Great Australian Bight at  $130^{\circ}\text{E}$  and covers around two third of Australia in dry Cluster 2 (Fig. 5.5b). Anticyclonic wind anomalies are in accordance with the geopotential anomalies and characterize the circulation in the upper troposphere. The area of anomalous high geopotential south of Australia is weaker in dry Cluster 2 and shows a connection with the geopotential anomaly over the tropical central Pacific Ocean. A large area of moderate negative geopotential anomalies lies along  $60^{\circ}\text{S}$  south of Australia and pushes towards lower latitudes at  $160^{\circ}\text{E}$  over New Zealand. ENSO and especially IOD signals can lead to convective variations that in turn force RWTs (McIntosh and Hendon, 2018). RWTs are visible as alternating positive and negative geopotential anomalies in upper levels and 'tele-connect' the effects in higher latitudes (Cai et al., 2011). In spring, Cai et al. (2011) found that decreased tropical convection over the maritime continent seems to excite a RWT, that propagates at  $110^{\circ}\text{E}$  south-eastward to Australia ('eastern Indian Ocean train'). The anomaly pattern in dry Cluster 2 reveals an IOD induced RWT that emanates from the eastern Indian Ocean and results in anomalous high geopotential over southern Australia (yellow dashed line, Fig. 5.5b). Cai et al. (2011) point to another RWT that is excited over the Asian continent and propagates anticlockwise along the western Indian Ocean towards Australia ('West Indian Ocean train'). This RWT is visible in dry Cluster 2 and appears to contribute to the anomalous high geopotential center south of Australia (green dashed line, Fig. 5.5b). Furthermore, Cai et al. (2011) point to a barotropic RWT that emanates from equatorial Africa and results in a negative geopotential anomaly that established around  $60^{\circ}\text{S}$  south of Australia. We can identify the same RWT in dry Cluster 2 (red dashed line, Fig. 5.5b). However, this RWT does not seem impact Australia as it does not produce an anomaly center over the Australian continent (Cai et al., 2011). A RWT that is also known as the Pacific-South American pattern extends into the central and eastern south Pacific and is often stimulated during El Niño over the central equatorial Pacific (Cai et al., 2011). Alternating positive and geopotential anomalies over the Pacific Ocean point to this pattern in dry Cluster 2 that is typical for the winter-spring season during El Niño (Fig. 5.5b).

In comparison with the first two clusters, the region of positive geopotential anomaly sits south of Western Australia with its center at  $120^{\circ}\text{E}$  in wet East Coast Cluster 3 (Fig. 5.5c). A weak negative geopotential anomaly covers the northern part of southeastern Australia. The upper-circulation over southeastern Australia seems to be influenced by two parts: anomalous north-westerlies from the north of Australia that turn cyclonic over southeastern Australia and anomalous easterlies southeast of Australia due to the anomalous anticyclone south of Western Australia. The Eastern Indian Ocean RWT and the Pacific-South American pattern are weakly pronounced, but still present to build up the positive geopotential anomaly south of Western Australia (yellow dashed line, Fig. 5.5).

The circulation anomalies in the Australian sector in wet South Coast Cluster 4 deviate from those in the other clusters during El Niño (Fig. 5.5d). A large area of negative geopotential anomalies resides with its center at the dateline at 50°S and spans from the south of Western Australia to central Pacific longitudes. A positive geopotential anomaly in the tropical Pacific stretches to the east of Australia and leads to weak positive geopotential anomalies over the continent. Both, the anomalous high geopotential to the northeast of Australia and the anomalous low geopotential south of Australia, lead to northwesterly and southwesterly wind anomalies over southeastern Australia in upper levels. In comparison with dry Cluster 2 and wet East Coast Cluster 3, RWT patterns are hard to identify in wet South Coast Cluster 4.

### 5.2.2 Convection and irrotational winds

In addition to the geopotential and wind anomalies in upper levels, we will analyze the OLR (as proxy for convection) and the irrotational wind component anomalies to find areas of increased and decreased convection and the related vertical motions. We vertically average the irrotational wind between 200hPa and 300hPa to capture the signals in the Tropics and Extratropics.

All El Niño clusters represent a typical anomaly pattern for the OLR and irrotational winds during El Niño (Fig. 5.6). Increased convection (negative OLR anomalies) over the central and eastern tropical Pacific occurs with divergent winds in the upper troposphere and indicates above-average ascent in this region. Over the maritime continent, positive OLR anomalies demonstrate reduced or even suppressed tropical convection in connection with anomalous convergent winds. The convergence in this region seems to have its highest contributions from the area between 0° and 20°S. The South Pacific Convergence Zone (SPCZ), that stretches from the maritime continent southeastwards towards the French Polynesia, shows a northeast-shifted position to the equator. Below-average convection at the usual position of the SPCZ is therefore associated with anomalous upper level convergent winds. Cai et al. (2010) examined the anomaly pattern of OLR during El Niño and found the same pattern with a shift of the ITCZ and the SPCZ towards the equator. They also mentioned the migration of the convergence zones to the east during El Niño (Cai et al., 2010). In the following, we will discuss the anomaly patterns over Australia and make first suggestions about the relationship with rainfall.

With focus on Australia, convection over the southern part of Australia is increased with mean values up to  $-14 \text{ W m}^{-2}$  in wet Cluster 1 (Fig. 5.6a). In addition, the irrotational wind shows an anomalous divergent flow pattern over the continent. The anomalies over southeastern Australia suggest increased rainfall over the country and match the rainfall anomaly pattern for wet Cluster 1 with above-average rainfall (Fig. 5.6a). In dry Cluster 2, the irrotational wind anomalies suggest upper-level convergence over central eastern Australia (Fig. 5.6b). A region of anomalous low convection is visible from the eastern part of Australia to the central Pacific at 30°S with strongest decreases over New South Wales and Queensland. Enhanced subsidence over the eastern part of the country points to below-average rainfall anomalies in dry Cluster 2 (Fig. 5.6b). Weak irrotational wind anomalies converge over central and northern parts of Australia in wet East Coast Cluster 3 (Fig. 5.6c). The convergence shows agreement with positive OLR anomalies that indicate

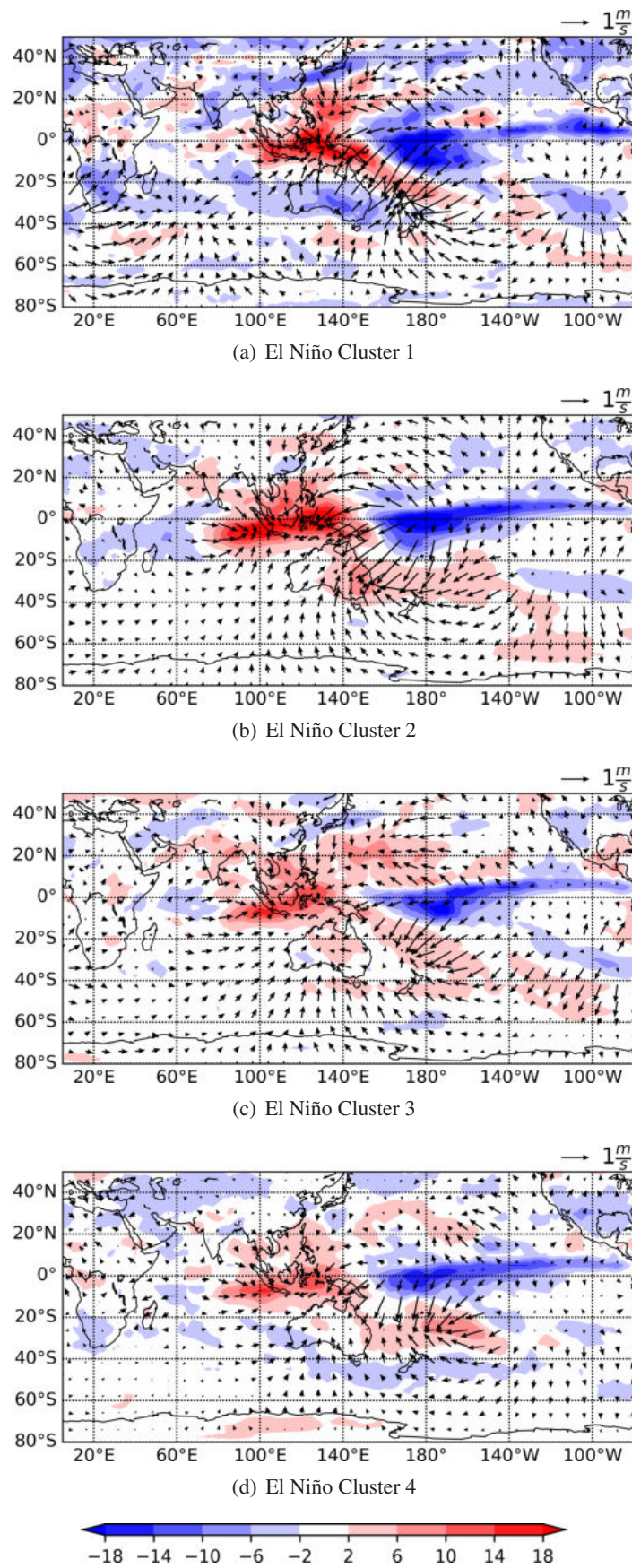


Figure 5.6: Cluster mean OLR anomalies (shaded, in  $\text{W m}^{-2}$ ) and cluster mean irrotational wind anomalies (wind vectors, in  $\text{m s}^{-1}$ ) vertically averaged between 200hPa and 300hPa for the El Niño clusters: wet Cluster 1 (a), dry Cluster 2 (b), wet East Coast Cluster 3 (c) and wet South Coast Cluster 4 (d). The monthly climatological reference period is 1979-2015.

decreased convection. In the mean, OLR anomalies suggest a near-average rainfall pattern due to near-average OLR values. However, rainfall along the East Coast is above average in wet East Coast Cluster 3. The modest negative OLR anomaly at the East Coast can relate to this part of the rainfall anomaly pattern (Fig. 5.6c). In wet South Coast Cluster 4, the irrotational wind anomalies over Australia are weaker in comparison to those in the other three clusters (Fig. 5.6d). Coastal areas in the north and east of Australia show decreased convection (positive OLR anomalies). Above-average convection seems to influence regions in the southwest and south of Australia. Most of southeastern Australia experiences average OLR conditions. Nevertheless, some areas along the East Coast exhibit decreased convection that fits with the negative rainfall anomalies in this area in wet South Coast Cluster 4. Although the South Coast does not show a modified convection pattern, above-average rainfall can be attributed to the negative OLR anomalies along 45°S of Australia (Fig. 5.6d).

The investigation of the large-scale circulation anomaly patterns and the behavior of rainfall related climate modes exhibited first dynamic explanations and assumptions for the specific rainfall anomaly patterns in the El Niño clusters. The predominantly positive IOD seems to force RWTs by convective variations near the tropical Indian Ocean in addition to the pure tropical El Niño signal. In some clusters, RWTs seem to affect and control the anomalous large-scale patterns over Australia. They propagate to extratropical latitudes of Australia, determine the anomalous large-scale pattern and result in anomalous high geopotential southeast of Australia. The shift of the anomalous ridging position between the clusters suggest that the position of anomalous ridging is crucial for a specific rainfall pattern over southeastern Australia. It is now of interest to see which effect a modified upper-level large-scale situation has on local weather systems. We will therefore switch from the large-scale to the synoptic scale in the next chapter.

## 6 Weather system occurrence during El Niño

Previous studies on rainfall variability in southeastern Australia focus predominantly on large-scale climate modes and their influence from a statistical viewpoint. Only a few are occupied with a more dynamic approach and assume the effect of El Niño on local weather systems (e.g., Risbey et al., 2009a; Brown et al., 2009). However, existing studies investigate the causes on seasonal time scales. Here we want to investigate systematic deviations of synoptic activity on monthly time scales from a weather system perspective. Therefore, we focus on the occurrence of various weather systems and other synoptic-scale features around the Australian section during El Niño months. The identification of the teleconnections between large-scale climate modes, circulation and the variability of the contribution of different synoptic weather systems allow to understand how remote climate drivers such as ENSO might affect rainfall patterns over southeastern Australia (Pook et al., 2006).

We will first introduce the climatological occurrence frequency of synoptic-scale features around Australia based on the data set of Sprenger et al. (2017). Afterwards, we investigate the changes in the spatial distribution and occurrence frequency of the features during El Niño in all rainfall anomaly clusters.

### 6.1 A climatology of synoptic activity in the Australian region

We calculate climatologies of flow features from the data set of Sprenger et al. (2017) that is based on a seasonal mean for the period 1979-2015. We focus on the occurrence frequencies of cut-off lows, enhanced moisture flux, cyclones and WCBs. We additionally investigate the frequency of atmospheric blocking that represents the connection between the large scale and the synoptic scale.

During the winter-spring season, cyclones propagate within the westerlies south of Australia with an poleward increasing frequency (orange contour, Fig. 6.1). However, a local maximum exists at 170°E over the Tasman Sea with a higher occurrence frequency in winter which is consistent with the findings of Quinting et al. (2019). In spring, another local maximum of cyclone frequency reflects the occurrence of heat lows over the northern part of the country (roughly 130°E, 20°S) with a mean monthly occurrence frequency of up to 18%. These heat lows develop in late spring and indicate the start of the warm season in the southern hemisphere.

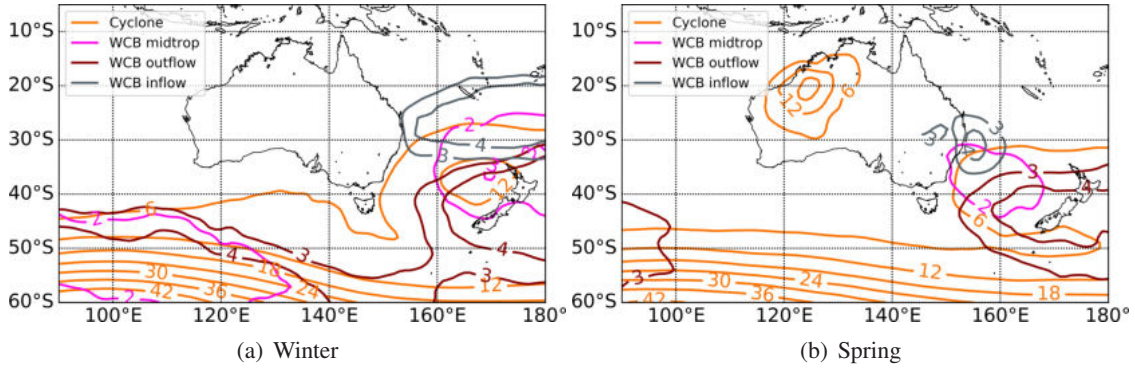


Figure 6.1: (a) Winter and (b) spring frequency climatology of cyclones (orange contour, every 6%), WCB inflow (grey contour, every 1%), mid-tropospheric WCBs (pink contour, every 1%) and WCB outflow (brown contour, every 1%) for the period 1979-2015. The displayed values represent the occurrence percentage of a feature during the considered time range and time steps.

We consider WCB outflow, inflow and mid-tropospheric ascent separately (Chapter 3.1.2). In both seasons, WCB inflow occurs over the Tasman and the Coral Sea with a mean occurrence frequency of up to 4% (grey contour, Fig. 6.1). The WCB ascent is centered in both seasons between 30°S and 40°S (pink contour, Fig. 6.1). In spring, WCB outflow occurs predominantly around New Zealand (brown contour, Fig. 6.1b). In winter, the frequency of WCB outflow is enhanced around New Zealand and also present southwest of Australia (Fig. 6.1a). In accordance with the study of Madonna et al. (2014), WCBs are more frequent during winter due to more cyclone activity.

Atmospheric blocking shows a high occurrence frequency south of 30°S during winter and spring (red contour, Fig. 6.2). The frequencies increase towards the south and show maximum values up to 22% between 50°S and 60°S. However, there is a slight local minimum that covers Tasmania and Victoria in winter that is accompanied by a maximum of cut-off lows north of this minimum.

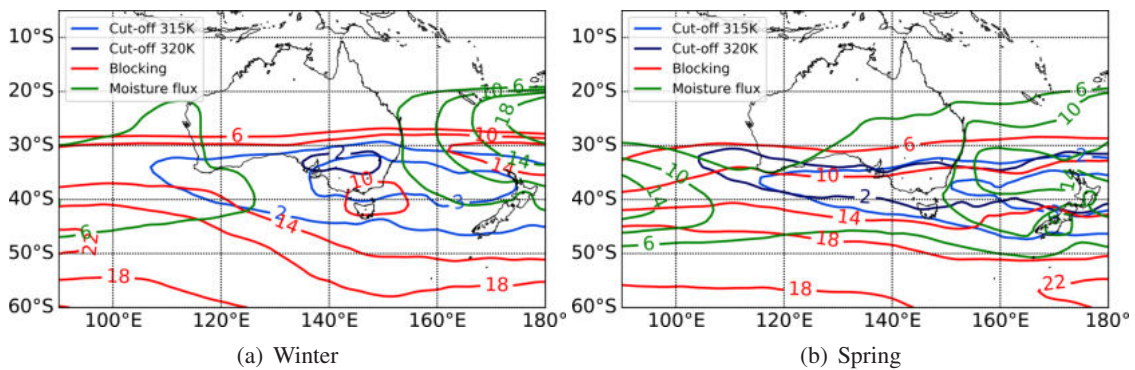


Figure 6.2: (a) Winter and (b) spring frequency climatology of cut-off lows at 315 K (blue contour, every 1%), cut-off lows at 320 K (dark blue contour, every 1%), atmospheric blocking (red contour, every 4%) and moisture flux (green contour, every 4%) for the period 1979-2015. The displayed values represent the occurrence percentage of a feature during the considered time range and time steps.

Cut-off lows around Australia are most frequent along 35°S (blue and dark blue contour, Fig. 6.2) in winter and spring. A maximum is observed between southwestern Australia and New Zealand during winter, similar to the studies of Nieto et al. (2008). Cut-off lows seem to be more present at a higher isentropic level in spring due to the upcoming warm season. A comparison of both seasons indicates a slight shift of the maximum frequency towards the east during spring.

Enhanced moisture fluxes show their strongest occurrence over the open waters east of Australia over the Tasman Sea and southwest of Australia (green contour, Fig. 6.2). In both seasons, the mean frequency per month can reach 18% north of New Zealand. A westward shift of the Tasman Sea signal from winter to spring leads to a higher frequency of moisture fluxes from the Tropics over southeast Australia during spring.

## 6.2 Characteristic weather systems during El Niño

In the following, the weather system occurrence is examined in the different clusters during El Niño. For each cluster, we first calculate the monthly composites for the different flow features and the geopotential height at 500hPa. We average the monthly means within a cluster and apply the Monte Carlo method (Chapter 3.2.2) to carve out the statistically significant anomalies of the flow features. The method is used to achieve a better understanding of the processes that lead to different rainfall patterns over southeastern Australia. In the following, we present the cluster mean characteristic weather system patterns during El Niño and compare the results with previous studies.

### 6.2.1 Wet Cluster 1

An inverted L-structure of positive geopotential anomaly height is located far south and east of Australia in wet Cluster 1 during El Niño (red contour lines, Fig. 6.3). It shows high mean values over  $35 \text{ m}^2 \text{ s}^{-2}$  along 50°S. The structure at 500hPa nearly corresponds to the upper-level circulation anomalies (Fig. 5.5a) and covers parts of southeastern Australia. Negative geopotential anomalies are situated over Western Australia and stretch to parts of Southern Australia (blue dashed contour lines, Fig. 6.3). Significantly enhanced atmospheric blocking within the positive geopotential anomalies south and east of Australia indicates a stationary wave pattern around Australia (yellow shading, Fig. 6.3). In accordance with positive SAM values in wet Cluster 1 (Fig. 5.3), the anomalous circulation pattern illustrates a shift of the main westerlies towards the equator. Nevertheless, the negative geopotential anomalies over western Australia suggest a shift of a branch of the westerly wind belt towards the equator. Negative anomalies in cyclone frequency far south and southeast of Australia seem to occur due to the shift of the main westerly wind belt (orange shading, Fig. 6.4). By contrast, enhanced cyclone activity is observed along the western South Coast (orange shading, Fig. 6.3). The anomalous anticyclone seems to 'block' the further eastward movement of weather systems near 140°E. Blocking is often accompanied by cut-off lows at its flanks and on its equatorward side. Consistently above-average frequency of cut-off lows occurs along the South Coast of Australia (blue shading, Fig. 6.3). In fact, the frequency of cut-off lows is more than double of the climatological mean reaching up to 5.5% along the South

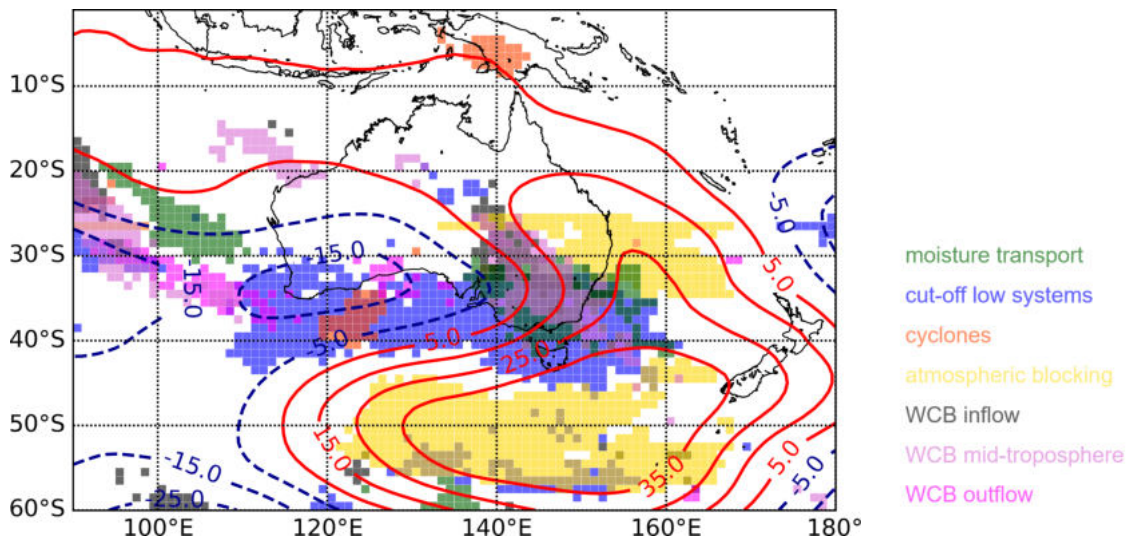


Figure 6.3: Positive frequency anomalies of weather systems and mean geopotential anomalies at 500hPa for wet El Niño Cluster 1. Only significant positive frequency anomalies in the upper 98% percentiles of the Monte Carlo composites are displayed in the specific color: moisture transport (green), cut-off lows (blue), cyclones (orange), atmospheric blocking (yellow), WCB inflow (grey), mid-tropospheric WCB (light pink) and WCB outflow (deep pink). The contour lines indicate the geopotential anomalies in  $\text{m}^2 \text{s}^{-2}$  at 500hPa: positive (negative) anomalies in solid red (dashed blue) lines.

Coast in wet Cluster 1 (Fig. 6.5a). This suggests that a strengthened frequency of cut-off lows due to a blocking anticyclone led to enhanced rainfall during El Niño especially along the south coastal areas. Over southeastern Australia and further into the continent, the cut-off low frequency is accompanied by enhanced frequencies of WCB ascent and moisture flux indicating that WCBs are associated with cut-off lows that strongly contribute to the positive rainfall anomalies in the region (green, blue and pink shading in Fig. 6.3). Enhanced moisture fluxes over southeastern Australia and parts of the Tasman Sea may have played a role in the intensification of the systems. The above-average rainfall anomaly pattern in sum can be related to an enhanced frequency of cut-off lows but also to an increased occurrence of WCBs that are related to extratropical cyclones and also cut-off lows (Fig. 6.5).

A comparison with existing studies shows that it is of interest to find the causes of unusual wet months in the winter-spring season during El Niño. In accordance with our results, Risbey et al. (2009a) found a 'wet Australia' pattern in the cool season with the presence of a positive SAM-like pattern and enhanced blocking southeast of Australia (at around  $160^\circ\text{E}$ ). This situation promotes cut-off lows which in turn efficiently produce rainfall (Risbey et al., 2009a). Brown et al. (2009) investigated the causes of the rainfall variability during El Niño in the Mallee region. With regard to the near-average cool-season rainfall amounts during the El Niño of 1997, they highlight that it is the rainfall amount per cut-off low and not the frequency of events that led to the unusual rainfall anomalies. In contrast to Brown et al. (2009), we found positive frequency anomalies of cut-off lows along the South Coast in wet Cluster 1. Nevertheless, this can point to an enhanced number of cut-off low events but also to few events with longer lifetimes. Furthermore, Brown et al. (2009) indicate that moisture availability plays an important role in the intensification of

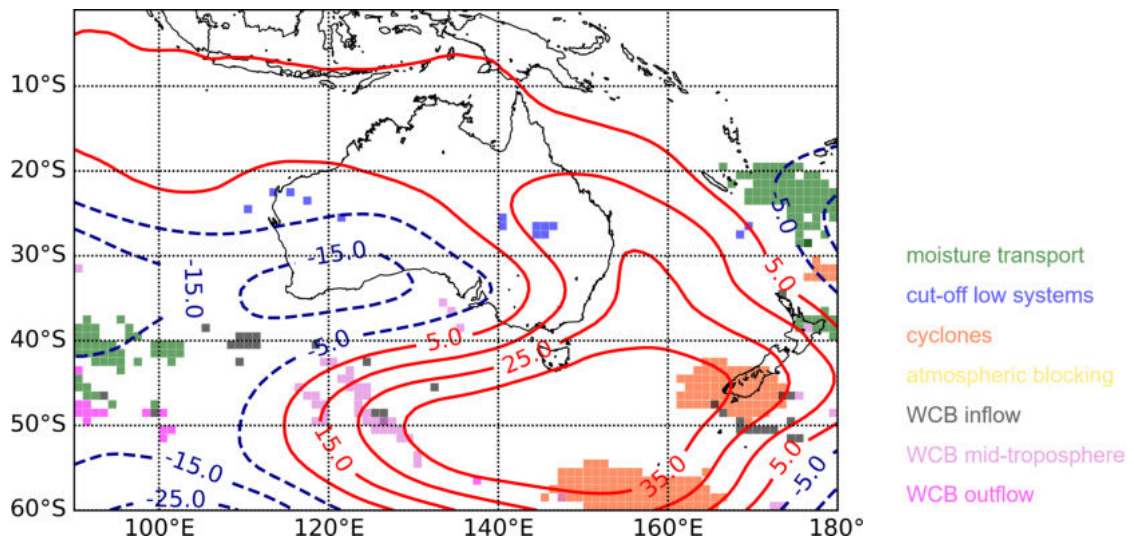


Figure 6.4: Negative frequency anomalies of weather systems and mean geopotential anomalies at 500hPa for wet El Niño Cluster 1. Only significant negative frequency anomalies in the lower 2% percentiles of the Monte Carlo composites are displayed in the specific color: moisture transport (green), cut-off lows (blue), cyclones (orange), atmospheric blocking (yellow), WCB inflow (grey), mid-tropospheric WCB (light pink) and WCB outflow (deep pink). The contour lines indicate the geopotential anomalies in  $\text{m}^2 \text{s}^{-2}$  at 500hPa: positive (negative) anomalies in solid red (dashed blue) lines.

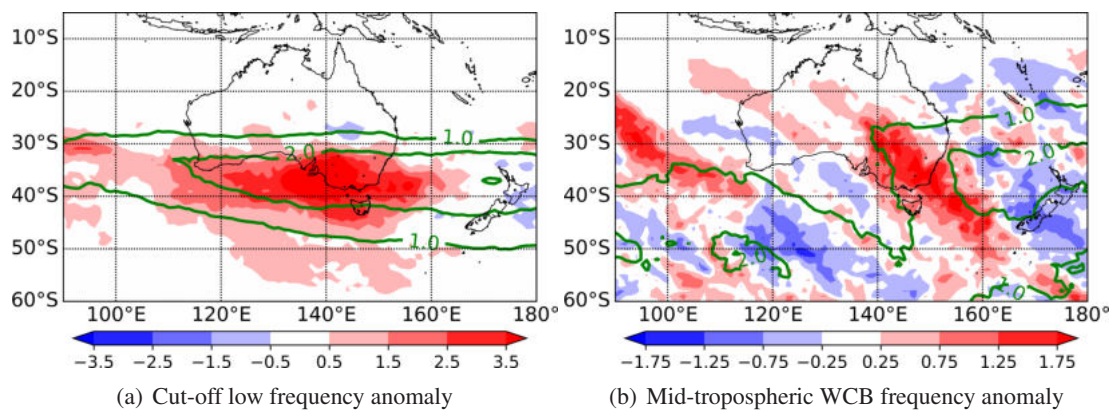


Figure 6.5: (a) Cluster mean anomaly of cut-off low frequency averaged between 315K and 320K in wet Cluster 1. (b) Cluster mean anomaly of mid-tropospheric WCB frequency in wet Cluster 1. The climatological reference period is 1979-2015 and the displayed values represent the occurrence percentage of a feature during the considered time range and time steps.

cut-off low rainfall. The significant increase of moisture fluxes over Australia might contribute to enhanced rainfall of cut-off lows but we should also keep in mind that the increase of moisture may actually be due to the circulation induced by the cut-off lows (Fig. 6.3).

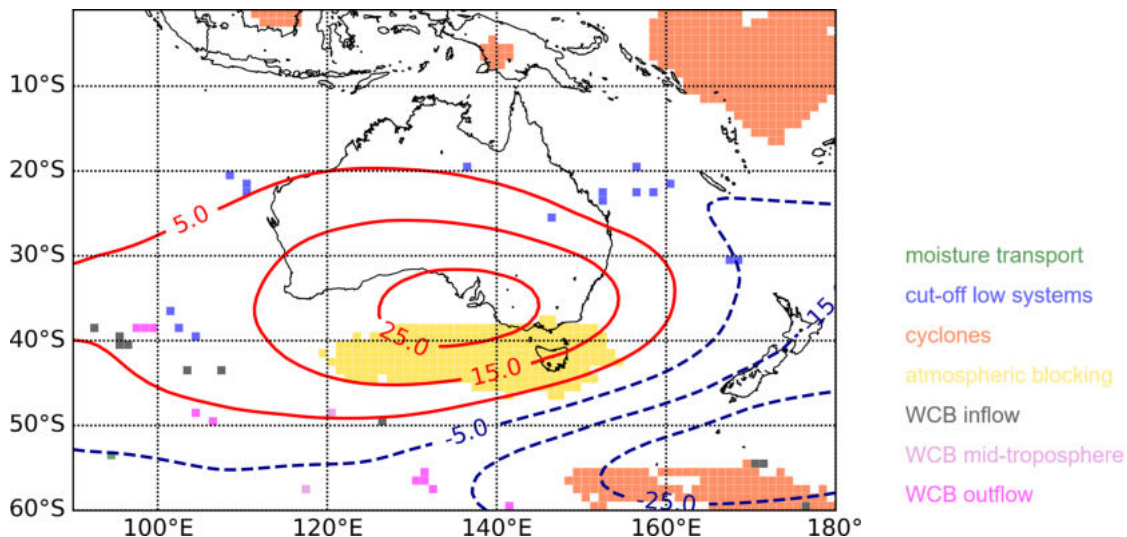


Figure 6.6: Positive frequency anomalies of weather systems and mean geopotential anomalies at 500hPa for dry El Niño Cluster 2. Only significant positive frequency anomalies in the upper 98% percentiles of the Monte Carlo composites are displayed in the specific color: moisture transport (green), cut-off lows (blue), cyclones (orange), atmospheric blocking (yellow), WCB inflow (grey), mid-tropospheric WCB (light pink) and WCB outflow (deep pink). The contour lines indicate the geopotential anomalies in  $\text{m}^2 \text{s}^{-2}$  at 500hPa: positive (negative) anomalies in solid red (dashed blue) lines.

## 6.2.2 Dry Cluster 2

An anomalous anticyclone covers most parts of Australia in dry Cluster 2 (red contour lines, Fig. 6.6). In comparison with wet Cluster 1, the anomalous anticyclone is shifted  $15^\circ$  towards the equator and is more centered at Australian longitudes. The structure with its center over the Great Australian Bight shows mean deviations with over  $25 \text{ m}^2 \text{ s}^{-2}$  from the climatological mean. An enhanced frequency of blocking is observed near the center of the anomalous anticyclone between  $120^\circ \text{E}$  and  $155^\circ \text{E}$  and indicates the stationarity of the illustrated wave pattern (yellow shading). Figure 6.8a demonstrates the enhanced blocking signal south of the continent and gives the impression of an anomalous zonal shift to the west. This matches with the average neutral SAM conditions in dry Cluster 2 (Fig. 5.3b). Negative geopotential anomalies are situated over the eastern part of the Tasman Sea (blue dashed contour lines, Fig. 6.6). They cover New Zealand and extend into the subtropics at New Zealand longitudes. In comparison with wet Cluster 1, the two major geopotential anomaly regions are comparable in strength in dry Cluster 2. The absence of positive frequency anomalies of weather systems around Australia confirms the assumption that an anomalous anticyclone over the continent suppresses the rain-producing synoptic activity in particular in the eastern half of Australia. In addition, the signal of increased cyclone frequency at  $55^\circ \text{S}$  indicates a shift of the main westerly wind belt to the south (orange shading). A large area of enhanced occurrence frequency of cyclones in the tropical West Pacific suggests the co-occurrence of tropical cyclones within dry months in southeastern Australia in dry Cluster 2 (Fig. 6.6). Whether tropical cyclones are associated with the absence of precipitation over southeastern Australia is not further investigated here. The signals of negative frequency anomalies of flow features are large in particular east of  $130^\circ \text{E}$  (Fig. 6.7). All considered rain-bringing flow features occur significantly less often over the eastern half of Australia and over the Tasman Sea in

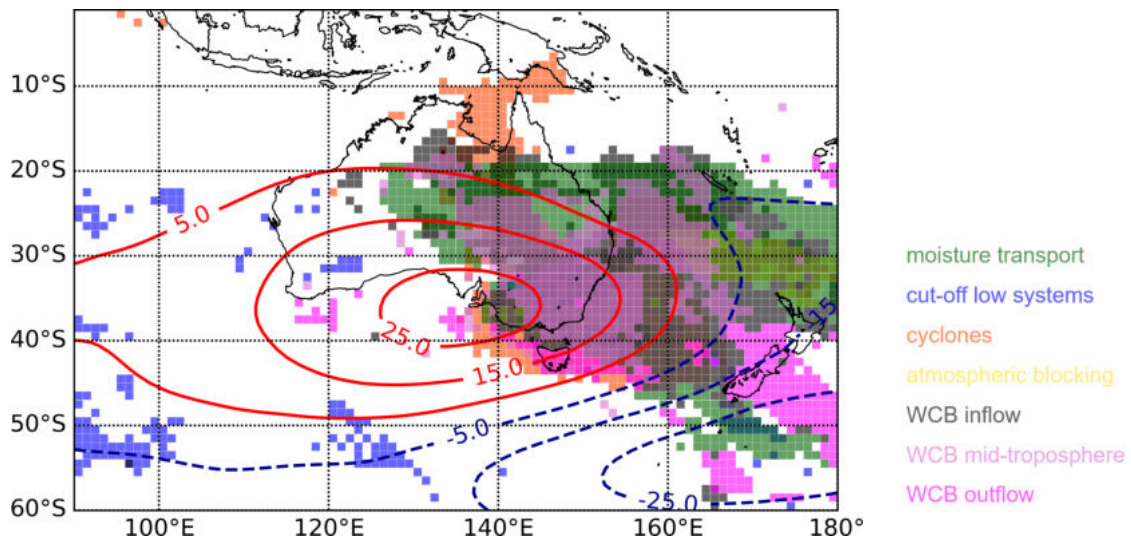


Figure 6.7: Negative frequency anomalies of weather systems and mean geopotential anomalies at 500hPa for dry El Niño Cluster 2. Only significant negative frequency anomalies in the lower 2% percentiles of the Monte Carlo composites are displayed in the specific color: moisture transport (green), cut-off lows (blue), cyclones (orange), atmospheric blocking (yellow), WCB inflow (grey), mid-tropospheric WCB (light pink) and WCB outflow (deep pink). The contour lines indicate the geopotential anomalies in  $\text{m}^2 \text{s}^{-2}$  at 500hPa: positive (negative) anomalies in solid red (dashed blue) lines.

dry months during El Niño. It's not primarily the cut-off lows, but also the suppression of moisture fluxes, extratropical cyclones and their associated WCB ascent that lead to dry conditions over southeastern Australia (Fig. 6.7, Fig. 6.8b).

Brown et al. (2009) highlighted that it is the rainfall amount per cut-off low that changes during different El Niño events over southeastern Australia and not the frequency of cut-off lows. According to their study, we suggest that cut-off lows that developed through the blocking situation over Australia however produced less rainfall than average in the months in dry Cluster 2. Cowan et al. (2013) discuss the position of blocking around Australia and link it to precipitation patterns over Australia. They highlight that blocking at different meridians leads to different rainfall patterns. Following Risbey et al. (2009a), unusual low blocking activity over the Tasman Sea can be related to below-average rainfall in Australia and therefore reduces the incidence of cut-off lows and their associated rainfall amounts. This seems to be consistent with our findings, although the reduced frequency of cut-off lows is not statistically significant (Fig. 6.8b). Van Rensch et al. (2019) found similar connections in their comparison of three different El Niño events. They also note the importance of the downstream trough and its relationship with MSLP anomalies near New Zealand for rainfall patterns over Australia.

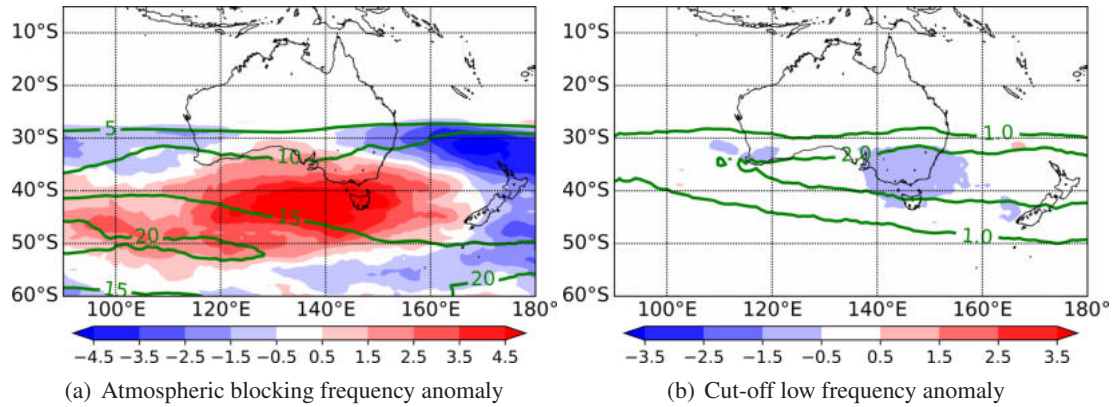


Figure 6.8: (a) Cluster mean anomaly of atmospheric blocking frequency in dry Cluster 2. (b) Cluster mean anomaly of cut-off low frequency averaged between 315 K and 320 K in dry Cluster 2. The climatological reference period is 1979-2015 and the displayed values represent the occurrence percentage of a feature during the considered time range and time steps.

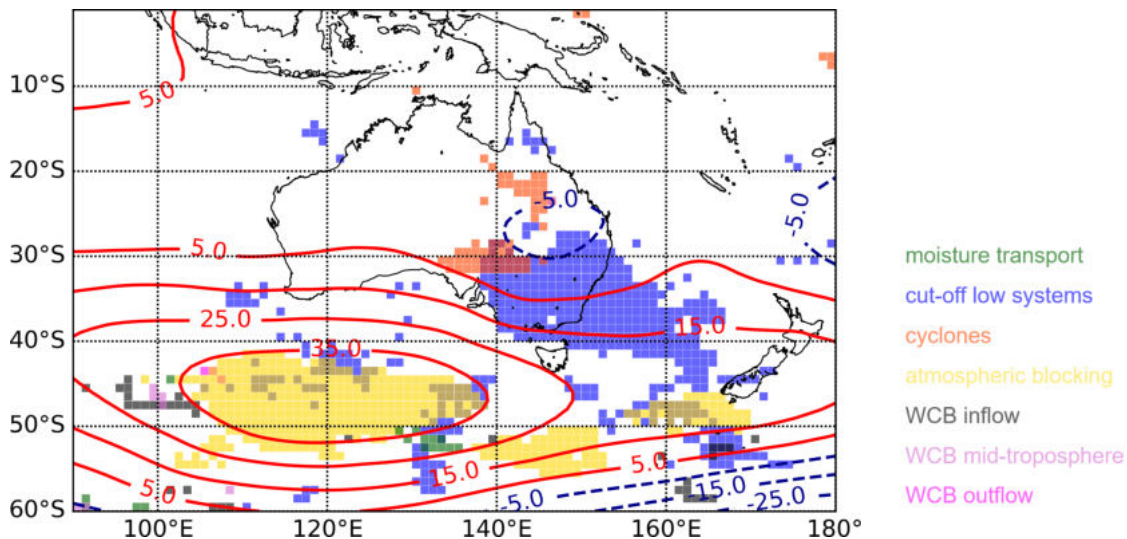


Figure 6.9: Positive frequency anomalies of weather systems and mean geopotential anomalies at 500hPa for wet East Coast El Niño Cluster 3. Only significant positive frequency anomalies in the upper 98% percentiles of the Monte Carlo composites are displayed in the specific color: moisture transport (green), cut-off lows (blue), cyclones (orange), atmospheric blocking (yellow), WCB inflow (grey), mid-tropospheric WCB (light pink) and WCB outflow (deep pink). The contour lines indicate the geopotential anomalies in  $\text{m}^2 \text{s}^{-2}$  at 500hPa: positive (negative) anomalies in solid red (dashed blue) lines.

### 6.2.3 Wet East Coast Cluster 3

Above-average rainfall along the East Coast and below-average rainfall along the South Coast and more inland of Australia characterize the rainfall anomaly pattern of wet East Coast Cluster 3 (Fig. 4.3c). Strong positive geopotential anomalies up to  $35 \text{ m}^2 \text{ s}^{-2}$  with a broadly pronounced shape lie south of Australia with the center at  $120^\circ \text{E}$  (red contour lines, Fig. 6.9). The main signal of enhanced blocking within the geopotential anomaly center (yellow shading roughly between  $105^\circ \text{E}$  and  $135^\circ \text{E}$ ) indicates the stationarity of this pattern. However, there are further significant blocking signals further east (roughly  $145^\circ \text{E}$  and  $165^\circ \text{E}$ ). Negative frequency anomalies of blocking over the Tasman Sea along  $35^\circ \text{S}$  suggest an anomalous poleward shift of blocking

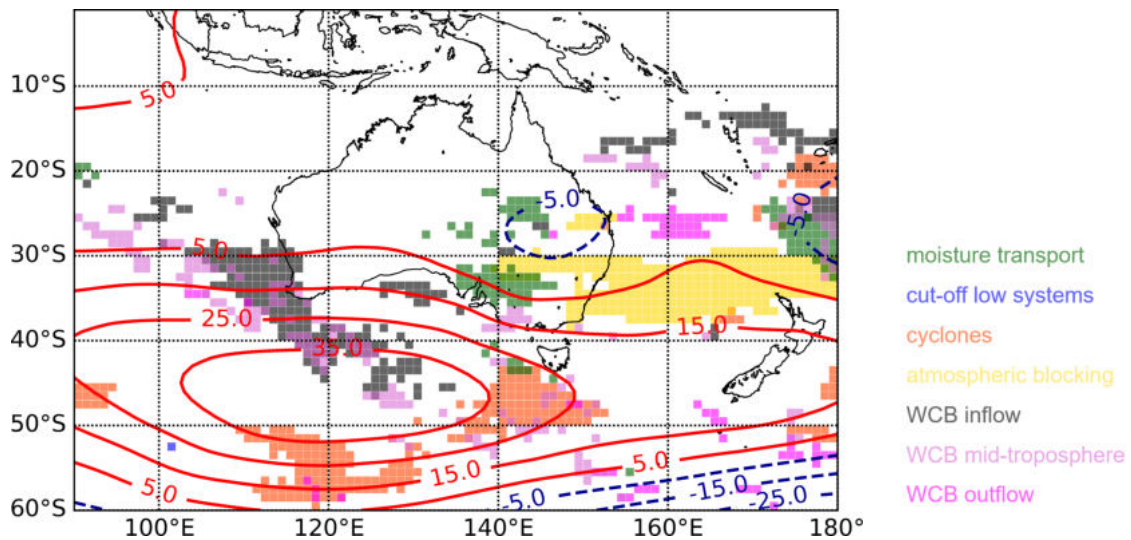


Figure 6.10: Negative frequency anomalies of weather systems and mean geopotential anomalies at 500hPa for wet East Coast El Niño Cluster 3. Only significant negative frequency anomalies in the lower 2% percentiles of the Monte Carlo composites are displayed in the specific color: moisture transport (green), cut-off lows (blue), cyclones (orange), atmospheric blocking (yellow), WCB inflow (grey), mid-tropospheric WCB (light pink) and WCB outflow (deep pink). The contour lines indicate the geopotential anomalies in  $\text{m}^2\text{s}^{-2}$  at 500hPa: positive (negative) anomalies in solid red (dashed blue) lines.

during El Niño in wet East Coast Cluster 3 (yellow shading, Fig. 6.10). This meridional shift is in accordance with the shape of positive and negative blocking frequency anomalies (Fig. 6.11a). With the predominant observed positive SAM values in wet East Coast Cluster 3, this indicates a shift of the main westerly wind belt to the south (Fig. 5.3b). However, the cyclone frequency over southeastern Australia is near-average but suppressed to the south of Australia (orange shading, Fig. 6.10). A region of weak negative geopotential anomaly is located over southern Queensland (blue dashed contour lines, Fig. 6.9). In wet East Coast Cluster 3, cut-off lows predominantly occur more frequently over southeastern Australia and over the Tasman Sea and suggest a high contribution to above-average rainfall along the East Coast (blue shading, Fig. 6.9). A more detailed view indicates that the frequency of cut-off lows is even more than double around 35°S during El Niño in wet East Coast Cluster 3 (Fig. 6.11b). There is enhanced cyclone activity near 30°S and over Queensland but we suggest that their contribution to above-average rainfall along the East Coast is small (orange shading, Fig. 6.9). The anomalous circulation situation points to the favored development of cut-off lows at the northern flank due to the anomalous anticyclone south of Australia. Furthermore, the extension of enhanced cut-off low frequencies might imply that cut-off lows propagated within the anomalous upper-level easterlies towards the East Coast of Australia. It further indicates their role as primary contributor to rainfall along the East Coast due to orographic effects at the windward side of the Great Dividing Range. In contrast, rainfall west of the Great Dividing Range might receive below-average rainfall due to the lack of moisture fluxes and extratropical cyclones and their associated rain-producing fronts (green and orange shading, Fig. 6.10).

In their model study, Pepler et al. (2016) point to the existence of a strong negative correla-

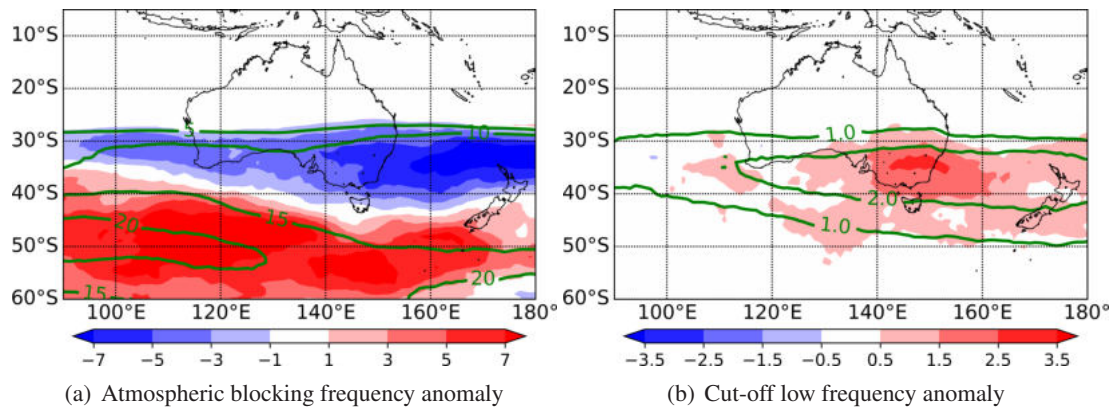


Figure 6.11: (a) Cluster mean anomaly of atmospheric blocking frequency in wet East Coast Cluster 3. (b) Cluster mean anomaly of cut-off low frequency averaged between 315 K and 320 K in wet East Coast Cluster 3. The climatological reference period is 1979-2015 and the displayed values represent the occurrence percentage of a feature during the considered time range and time steps.

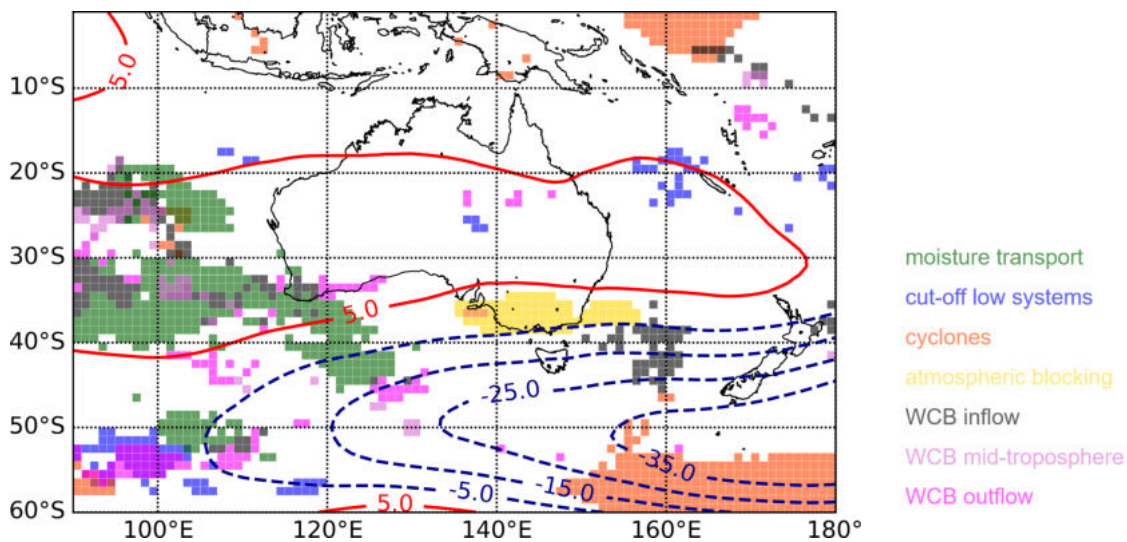


Figure 6.12: Positive frequency anomalies of weather systems and mean geopotential anomalies at 500hPa for wet South Coast El Niño Cluster 4. Only significant positive frequency anomalies in the upper 98% percentiles of the Monte Carlo composites are displayed in the specific color: moisture transport (green), cut-off lows (blue), cyclones (orange), atmospheric blocking (yellow), WCB inflow (grey), mid-tropospheric WCB (light pink) and WCB outflow (deep pink). The contour lines indicate the geopotential anomalies in  $\text{m}^2 \text{s}^{-2}$  at 500hPa: positive (negative) anomalies in solid red (dashed blue) lines.

tion between zonal wind at 850hPa between 25°S and 35°S and rainfall along the East Coast of Australia. In accordance with our results, onshore easterly flow seems to remain the main source of rainfall in this area. In contrast, a positive correlation between zonal wind and rainfall in the southwest of southeastern Australia (Pepler et al., 2016) fits with the below-average rainfall in this region in wet East Coast Cluster 3. Risbey et al. (2009a) observed in their 'wet Australia' cluster that rainfall along the East Coast of Australia is associated with blocking east of Australia and the related tendency for the development of cut-off lows. We can confirm this although our blocking signal is more dominant to the southwest of southeastern Australia (Fig. 6.9).

### 6.2.4 Wet South Coast Cluster 4

Wet South Coast Cluster 4 reflects a reversed rainfall pattern of wet East Coast Cluster 3 with positive rainfall anomalies over most of Victoria and negative rainfall anomalies most notably along the East Coast (Fig. 4.3d). The anomalous circulation over Australia strongly differs from the patterns in the other clusters. An anomalous anticyclone is situated over central Australia with only weak deviations from the climatology up to  $5 \text{ m}^2 \text{ s}^{-2}$  (red contour lines, Fig. 6.12). However, well-pronounced negative geopotential anomalies over  $-35 \text{ m}^2 \text{ s}^{-2}$  south of Australia might play a major role during El Niño in wet South Coast Cluster 4 (blue dashed contour lines). The strong negative geopotential anomalies suggest a more frequent progress of cold air masses from higher latitudes towards Australia. The majority of negative SAM values also points to an equatorward shift of the mean westerly wind belt which suggest enhanced westerlies in upper levels (Fig. 5.3b). The anomalies of cyclone frequency reflect the enhanced extratropical cyclone frequency south of Australia within the negative geopotential anomaly (Fig. 6.14b). However, the positive frequency anomalies between  $35^\circ\text{S}$  and  $50^\circ\text{S}$ , that also cover Victoria, are not statistically significant. We further suggest that increased moisture fluxes southwest of Australia might intensify rainfall contributions of weather systems along the South Coast of Australia during El Niño in wet South Coast Cluster 4 (green shading, Fig. 6.12). An area of enhanced blocking is centered at  $38^\circ\text{S}$  and indicates the high monthly variability within the cluster as the cyclone frequency is also enhanced in this region (Fig. 6.12). This might point to an anomalous fast or quite slow sequence of blocking ridges and troughs with embedded extratropical cyclones. Decreased frequency of blocking is located south of New Zealand (Fig. 6.13). Cut-off lows, that usually develop during blocking over the Tasman Sea, show a general decline in frequency along the South Coast of Australia and in particular over southeastern Australia (Fig. 6.14a). Over the Tasman Sea, negative frequency anomalies of cut-off lows are statistically significant (Fig. 6.13). In addition, cyclones and WCBs occur significant less often east of Australia (Fig. 6.14b, Fig. 6.13). The lack of important rain-bringing weather systems east of Australia implies that in particular blocking is less frequent over southern Australia which usually favors the development of cut-off lows that produce rainfall along the East Coast and more inland.

Pepler et al. (2016) examined the relationship of zonal wind anomalies and rainfall at the East Coast of Australia. They found that enhanced westerly flow across southern Australia is associated with increased rainfall over the southern part of southeastern Australia but decreased rainfall along the East Coast. This reflects the observed anomaly pattern in wet South Coast Cluster 4. Risbey et al. (2009a) highlight that 'wet south' rainfall patterns are dominated by enhanced frontal rain due to an equatorward shift of the westerlies. These results fit with our findings in wet South Coast Cluster 4. Ashok et al. (2009) examined the impact of El Niño Modoki events on rainfall in Australia. They found that anomalous blocking over the Australian continent leads to the suppression of extratropical cyclone activity over parts of southeastern Australia. Around 71 % of the months in wet South Coast Cluster 4 are from El Niño Modoki events but the results of Ashok et al. (2009) are reflected only in parts of our findings (Chapter 4.5). A reason for this deviation might be due to the fact that the maximum impact of El Niño Modoki on Australian rainfall occurs prior to our focused winter-spring season (Taschetto and England, 2009).

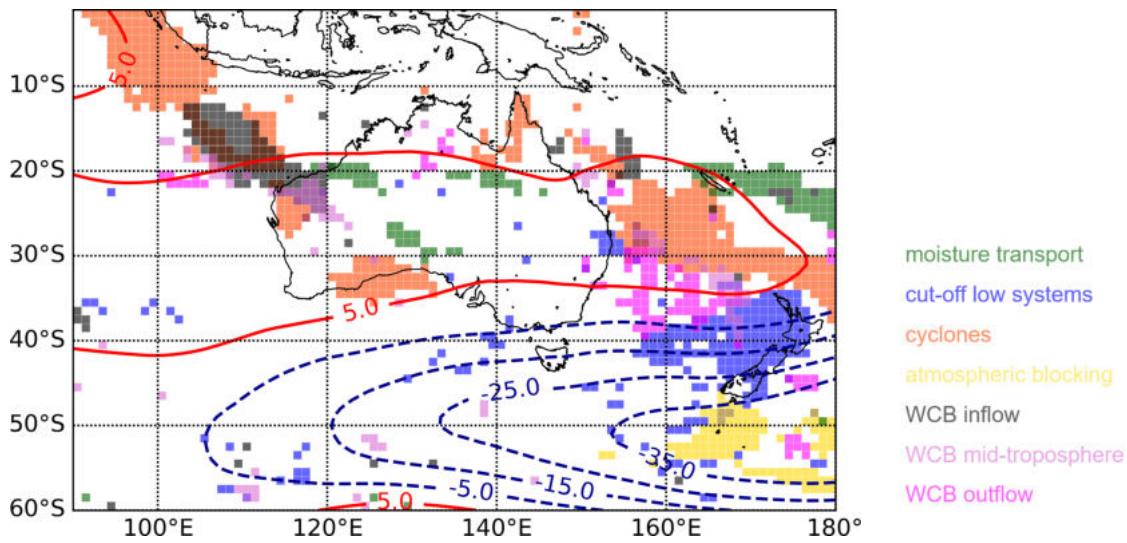


Figure 6.13: Negative frequency anomalies of weather systems and mean geopotential anomalies at 500hPa for wet South Coast El Niño Cluster 4. Only significant negative frequency anomalies in the lower 2% percentiles of the Monte Carlo composites are displayed in the specific color: moisture transport (green), cut-off lows (blue), cyclones (orange), atmospheric blocking (yellow), WCB inflow (grey), mid-tropospheric WCB (light pink) and WCB outflow (deep pink). The contour lines indicate the geopotential anomalies in  $\text{m}^2\text{s}^{-2}$  at 500hPa: positive (negative) anomalies in solid red (dashed blue) lines.

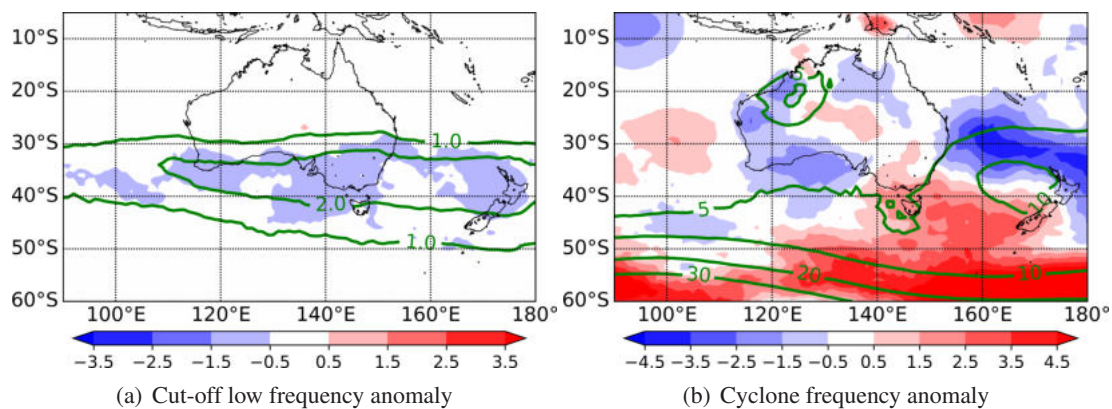


Figure 6.14: (a) Cluster mean anomaly of cut-off low frequency averaged between 315K and 320K in wet South Coast Cluster 4. (b) Cluster mean anomaly of cyclone frequency in wet South Coast Cluster 4. The climatological reference period is 1979-2015 and the displayed values represent the occurrence percentage of a feature during the considered time range and time steps.

We investigated the changes in weather system frequency for different rainfall anomaly patterns during El Niño. Atmospheric blocking seems to own the leading role in controlling the propagation of weather systems around southeastern Australia, except in wet South Coast Cluster 4. Furthermore, the examination showed that the strongest rainfall anomalies might be related to the changes in cut-off low frequency. Nevertheless, it remains unclear which weather systems produces the different rainfall anomalies in the El Niño cluster. In the following, we investigate the origin of rainfall during El Niño by performing a transition from monthly time scales to daily time scales.



# 7 The origin of rainfall during El Niño

In the previous chapter, we found that El Niño affects the frequency of weather systems around Australia. As this might change the contributions of weather systems to rainfall in the winter-spring season, we identify the rain-producing weather systems and associated features for southeastern Australia in this chapter. Furthermore, we investigate surface synoptic patterns during rainfall events within the clusters. Finally, backward trajectories of rainfall events will shed light on the origin and character of air parcels that result in rainfall over southeastern Australia during El Niño.

## 7.1 Contribution of weather systems to rainfall

In the winter-spring season, cut-off lows and extratropical cyclones are the main contributors to rainfall over southeastern Australia (Chapter 2.2.2). Positive rainfall anomalies are related to an increased frequency of these weather systems around Australia (Chapter 6). However, we still have no insights into the moisture origin of rainfall in particular for individual rainfall events. Therefore, we now attribute individual rainfall events to cut-off lows and WCBs and assess the percentage contribution of these weather systems to the overall rainfall in the El Niño clusters. We use WCBs as a proxy of extratropical cyclones, as WCBs show a strong relationship with cold and warm fronts (Catto et al., 2015).

### Method

We match the accumulated daily rainfall with cut-off lows and WCBs. We perform the following steps to cope with the different spatial and temporal resolutions of the two data sets (weather systems:  $1^\circ$ , 6 h; rainfall:  $0.05^\circ$ , daily):

- For the matching, we choose the following weather system features: mid-tropospheric WCBs between 400 and 800 hPa and cut-off lows at two isentropic levels (315 K and 320 K).
- We selected to downscale and interpolate the coarse weather system data to the  $0.05^\circ$  rainfall grid to account for the spatially more variable rainfall patterns on smaller scales.
- A radius  $R$  is defined to capture remote effects of cut-off lows and WCBs apart from their spatial extension identified by the algorithm (Fig. 7.1B,C). The cut-off low and WCB mask are inflated to a selected radius before the matching process. The choice of  $R = 500$  km is inspired by Catto et al. (2012) and justified by considerations of the typical Rossby Radius of deformation for these weather systems.

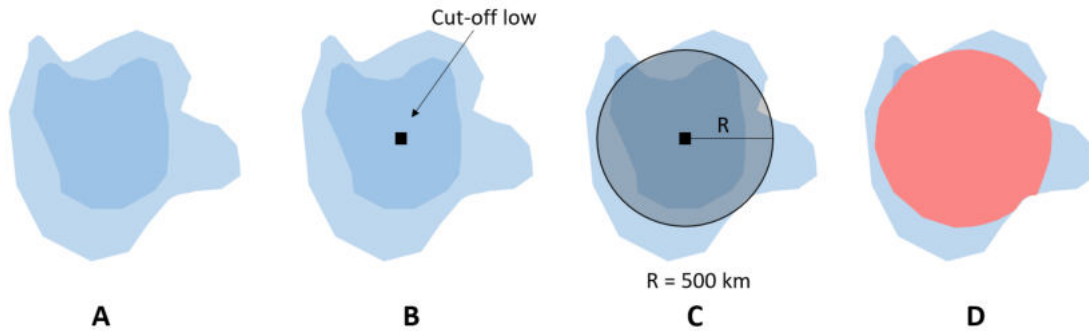


Figure 7.1: Sketch to explain the method of matching daily accumulated rainfall data with mid-tropospheric WCBs and cut-off low systems (from left to right). In this demonstration example the blue area indicates a field with rainfall. The black box symbolizes an identified cut-off low or WCB signal. The black circle shows the influence area of a selected weather system with an influence radius  $R$ . On the right part of the sketch, rainfall in the red area is assumed to be generated by the weather system in the black box.

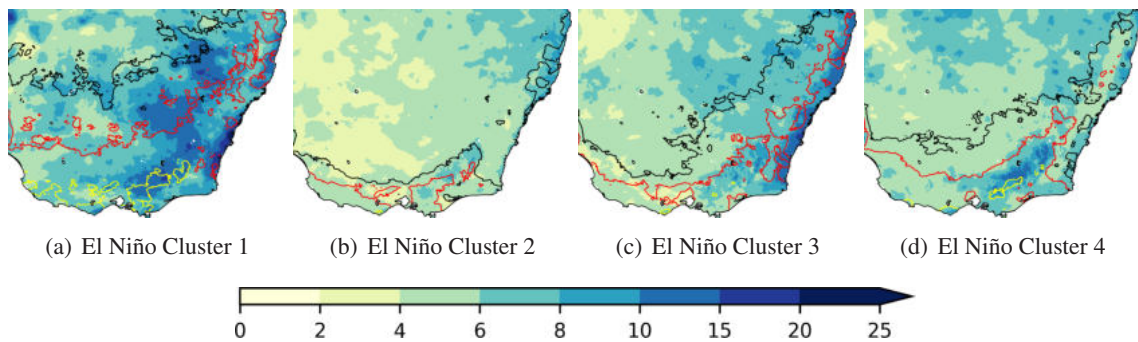


Figure 7.2: Mean daily rainfall sum (shading, in mm) during rainy days ( $> 0.2$  mm) and percentage frequency of rainy days (contour lines; black: 20%, red: 30%, yellow: 50%) within the days in the El Niño clusters: wet Cluster 1 (a), dry Cluster 2 (b), wet East Coast Cluster 3 (c) and wet South Coast Cluster 4 (d).

- Only grid points that show a daily rainfall sum of at least 0.2 mm are taken into account for the matching with the weather systems. Rainfall at a grid point is attributed to a WCB (cut-off low) when at least one temporal term out of 4 (0, 6, 12, 18 UTC) shows the presence of a WCB (cut-off low at 315 or 320 K) within a selected day (Fig. 7.1D).

After inflating the mask of WCBs and cut-off lows, we downscale the data from the  $1^\circ$  grid to the  $0.05^\circ$  grid. The algorithm will then check for every day and every grid point if there is (1) a cut-off low or (2) a WCB present at the same grid point during rainfall. However, the inflated masks of the two weather systems can overlap at certain grid points. We also identify (3) rainfall with the presence of both a WCB and a cut-off low. The final category (4) contains all rainfall events, that cannot be matched with neither cut-off lows nor WCBs.

Remote inland parts of southeastern Australia show low rainfall and a high rainfall variability (Pook et al., 2014). Great distances between the few separated stations in this region can lead to errors in the interpolation (Chapter 3.1.3, Fig. 3.1). Some areas inland might receive a large proportion of their winter-spring rainfall amount due to one event resulting in a very high percentage contribution of one matching case to rainfall. Figure 7.2 illustrates the characteristics of

days with rainfall within the El Niño clusters. In accordance with Pook et al. (2014), the remote inland regions show a low frequency of rainy days (<20%) and also low mean rainfall per rainy day in all clusters. Towards the coasts, the frequency of rainy days increases. In wet Cluster 1, the rainfall per rainy day is high with up to 15 mm east and west of the Great Dividing Range (Fig. 7.2a). The rainfall frequency demonstrates that half of the days in the cluster were rainy days in parts of Victoria. In contrast, the mean rainfall per rainy day is clearly lower in dry Cluster 2 with around a third of the area showing mean values of just 2-4 mm (Fig. 7.2b). The low frequency of rainy days and the small rainfall amounts per rainy day suggest low rainfall in dry Cluster 2. In wet East Coast Cluster 3, mean rainfall sums are highest with 10-15 mm along the East Coast where the rainfall anomalies are strongest (Fig. 4.3c, Fig. 7.2c). However, high rainfall sums during rainy days occur in the south of southeastern Australia in combination with a high frequency of rainy days up to 50% in wet South Coast Cluster 4 (Fig. 7.2d). Along the East Coast and more inland, the rainfall amount is still moderate, but the frequency is noticeably lower than in the south.

The characterization of rainy days within the clusters during El Niño demonstrates that the amount of rainy days and also the mean rainfall sum per rainy day strongly vary between the clusters.

## Results

The main contributors of rainfall in wet Cluster 1 are WCBs who bring around 50% of the rainfall to most of the remote inland areas (Fig. 7.3e). This might be likely due to significant positive frequency anomalies of WCBs over southeastern Australia (Fig. 6.3). Cut-off lows contribute only 10-30% along the South and East Coast, where we also found positive frequency anomalies (Fig. 7.3a). Furthermore, a high percentage of rainfall towards the areas around the Great Dividing Range (black contour lines, Fig. 7.3) and towards coastal areas in the southwest are associated with a combination of cut-off lows and WCBs (Fig. 7.3i). The results of the matching point to a high contribution of cut-off lows and WCBs of around 80% to rainfall over southeastern Australia. We suggest that the small percentage of non-matching rainfall results from the many assumption in the matching, further weather features or small-scale convection. However, rainfall in the northwestern corner of southeastern Australia do not receive rainfall from cut-off lows or WCBs (Fig. 7.3m). This suggests that convective systems are responsible for the rainfall in the remote subtropical inland.

In dry Cluster 2, cut-off lows bring around 30-40% of rainfall to the east of the Great Dividing Range (Fig. 7.3b). WCBs contribute up to 40% to rainfall in the eastern half of southeastern Australia (Fig. 7.3f). Although there is a high contribution from the combination of cut-off lows and WCBs in Southern Australia and New South Wales, a high amount of rainfall cannot be explained by one of the two weather systems (Fig. 7.3j,n). WCBs are often related to strong extratropical cyclones and in particular to strong precipitation events along fronts (Catto et al., 2015). However, the frequency and rainfall per rainy day are quite low in dry Cluster 2 (Fig. 7.2b). This leads to the assumption that the low rainfall over Victoria might be due to a front that is not connected with WCBs. A high fraction of rainfall in the north of southeastern Australia is associated with neither WCBs nor cut-off lows and suggests a contribution from convective systems (Fig. 7.3n).

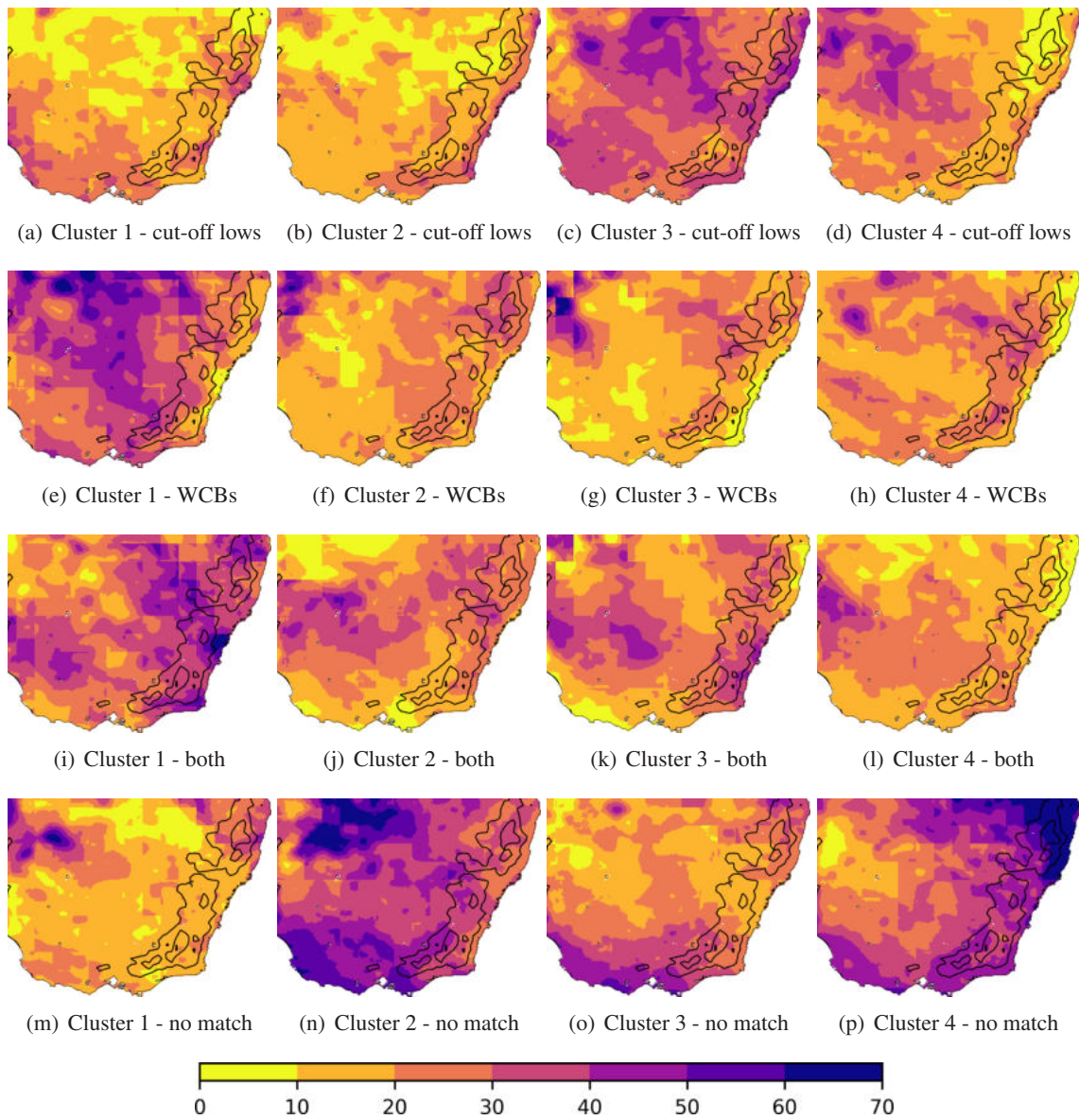


Figure 7.3: The results of matching rainfall with cut-off lows and WCBs in southeastern Australia in the El Niño clusters: wet Cluster 1, dry Cluster 2, wet East Coast Cluster 3 and wet South Coast Cluster 4. The shading indicates the percentage of rainfall that is explained in the cluster by (a)-(d) cut-off lows, (e)-(h) WCBs, (i)-(l) both and (m)-(p) none of them. The black contour lines illustrates the topography (levels: 500 and 1000m).

The main contributor in terms of spatial coverage and high percentage is the cut-off low in wet East Coast Cluster 3 (Fig. 7.3c). This weather system can explain up to 60% of rainfall in the remote inland region but also along southwestern and eastern coastal areas. This fits with the significant increase of cut-off low frequency over the Tasman Sea documented in Chapter 6. Rainfall due to WCBs is moderate around the Great Dividing Range but relatively rare elsewhere. A combination of both weather systems brings around 40% of the observed rainfall to the inland regions and to the southern East Coast in wet East Coast Cluster 3. However, most of the rainfall over Victoria cannot be explained by cut-off lows or WCBs and might result from fronts in wet East Coast Cluster 3 (Fig. 7.3o).

In wet South Coast Cluster 4, cut-off lows bring about 20-50% of the rainfall to central southeastern Australia (Fig. 7.3d). WCBs contribute 30-40% to rainfall around the Great Dividing Range and in areas more inland (Fig. 7.3h). A combination of both weather systems illustrates its contribution to rainfall especially in the west of southeastern Australia with values up to 50% (Fig. 7.3l). Nevertheless, a huge amount of rainfall along the coasts is unexplained by one of the two weather systems (Fig. 7.3p). As there is an enhanced westerly wind zone over the south of southeastern Australia in wet South Coast Cluster 4 (Fig. 6.12), the unmatched rainfall along the South Coast might be related to extratropical cyclones. The rainfall at the northern East Coast seems to result from convective systems in the Subtropics.

The attribution of rainy days in southeastern Australia to either WCBs or cut-off lows or both reveals that the different rainfall patterns during El Niño are related to the modulated occurrence of weather systems. Above-average rainfall in wet Cluster 1 is primarily generated by WCBs partly in combination with cut-off lows. In dry Cluster 2, convective systems in the north and extratropical cyclones in the south produce most of the rainfall in southeastern Australia. Enhanced rainfall along the East Coast shows a dominant contribution from cut-off lows in wet East Coast Cluster 3. In Cluster 4, the above-average rainfall over Victoria is likely a result of frontal rain, that is not captured by one of the selected weather systems.

## 7.2 Synoptic patterns of rainfall during El Niño

The analyses of the upper-level circulation (Chapter 5) and the weather system frequency (Chapter 6) for the clusters, are complemented by an analysis of surface patterns. The focus is on synoptic patterns during rainy days in southeastern Australia. As this investigation cannot be made for every grid point, we have to form a criterion that covers most of the rainfall situations in southeastern Australia.

### Method

For the selection of rainy days, we use daily rainfall data on every grid point in the clustering region over southeastern Australia (29°S to 40°S, 140°E to 154°E). The focus is on rainfall over land, so grid points over the ocean are ignored. We define two criteria within our algorithm for the selection of rainy days:

1. Daily rainfall amount: a threshold is defined (in mm) to decide whether a grid point shows rain or not.
2. Coverage of (1) in southeastern Australia: a threshold that shows the spatial percentage coverage of grid points that fulfill criterion (1) in proportion to all points in the clustering region over land.

We tested the algorithm with different criteria and combinations and compared the percentage of rainy days in southeastern Australia within the clusters (Table 7.1). The focus is on surface patterns, so we select the MSLP and winds at 850 hPa for further investigations. Figure 7.4 illustrates exemplary the cluster-mean MSLP anomalies for different criteria and combinations in wet Cluster 1. The increase of the threshold for daily rainfall amounts leads to more pronounced patterns which is in accordance with the other clusters (not shown). Although the number of rainy days decreases while increasing the threshold, we decide to further work with the 5 % spatial coverage and 5 mm rainfall criteria as more than 20 % of the days in dry Cluster 2 fulfill the criteria.

### Results

Anomalous high MSLP to the southeast of Australia dominates the circulation pattern in the lower troposphere during rainfall in wet Cluster 1 (Fig. 7.5a,b). The positive MSLP anomaly extends from the south of Australia over the Tasman Sea to the Coral Sea. Below normal MSLP over southeastern Australia is associated with anomalous cyclonic winds at 850 hPa that result in a deflection of the westerlies over Australia and to the south over the Tasman Sea where the winds turn anticyclonic due to anomalous high MSLP. Northerlies and north-westerlies over the region indicate north-south oriented WCBs during rainfall that bring most of the rainfall to the inland regions of southeastern Australia in wet Cluster 1 (Fig. 7.5a,b).

In dry Cluster 2, the typical rainfall situation shows anomalous low MSLP that extends from high latitudes into the subtropics of Australia at around 150°E (Fig. 7.5c,d). With positive MSLP anomalies to the west (around 120°E), confluent south-westerlies dominate over western south-eastern Australia and turn cyclonic towards the east. Although this synoptic pattern seems to be

Table 7.1: Results of the algorithm for different threshold values for the daily rainfall amount per grid point (1 mm, 3 mm, 5 mm) and for the percentage coverage in the southeastern Australian clustering region (2%, 3%, 5%). The number shows the percentage of days within a cluster that fulfill both conditions.

Cluster 1 (Cluster 2)	1 mm	3 mm	5 mm
2%	93.42 (76.13)	76.32 (52.03)	65.13 (37.39)
3%	88.16 (68.69)	71.71 (44.37)	57.90 (30.18)
5%	80.26 (59.35)	63.82 (33.67)	51.32 (21.96)
Cluster 3 (Cluster 4)	1 mm	3 mm	5 mm
2%	85.52 (87.97)	68.03 (65.80)	56.56 (53.30)
3%	81.42 (82.78)	62.30 (59.43)	48.63 (46.93)
5%	72.95 (73.59)	52.73 (50.24)	40.98 (40.09)

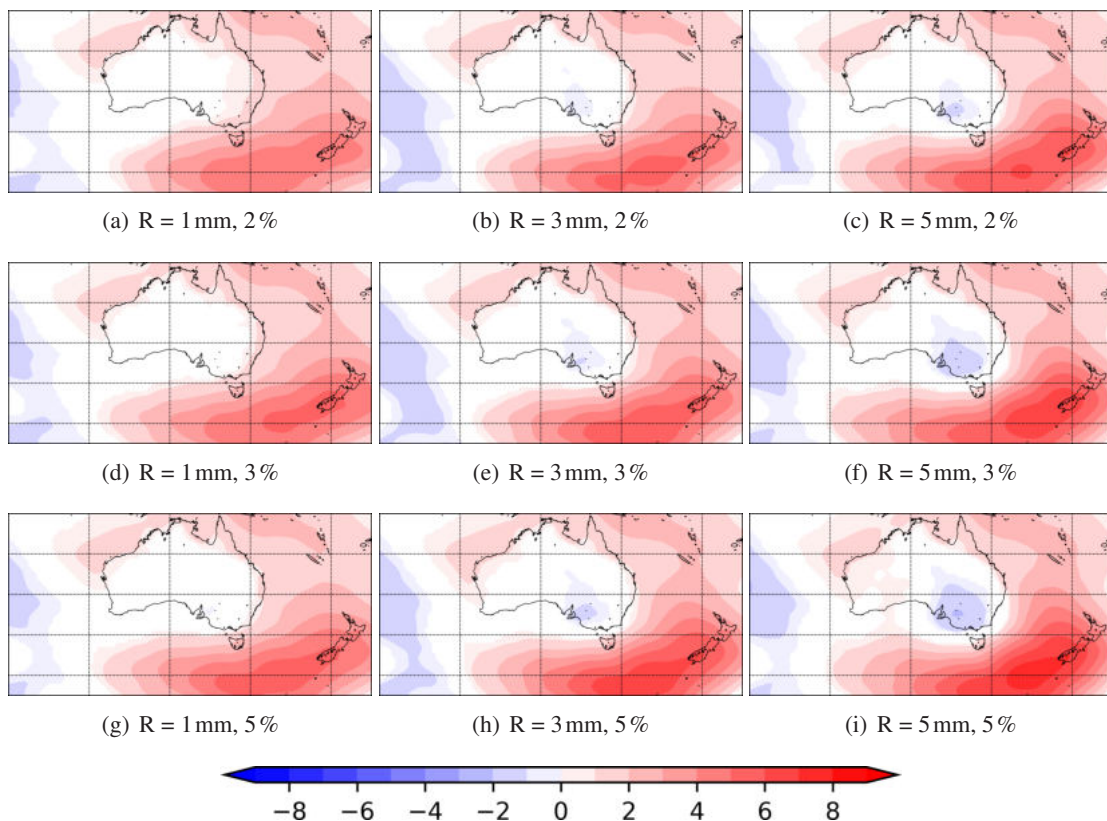


Figure 7.4: Exemplary MSLP anomalies (in hPa) during rainy days for different thresholds and combinations in wet El Niño Cluster 1: percentage coverage of rainfall grid points (2%, 3% and 5%) and the daily rainfall amount criteria (1 mm, 3 mm, 5 mm). For each identified rainy day, we take the MSLP field for the middle of the 24h rainfall period and calculate the anomalies based on the monthly reference period 1979-2015. The anomaly patterns here represent the cluster mean of all rainy days. Latitudes in  $10^\circ$  steps and longitudes in  $20^\circ$  steps beginning with  $10^\circ\text{S}$  and  $90^\circ\text{E}$  in the upper left corner.

quite rare in dry Cluster 2 (20% of days, Tab. 7.1), rain-producing systems within the westerlies are suggested to reach the continent from the southwest of southeastern Australia.

The rainfall situation in wet East Coast Cluster 3 is characterized by broad high MSLP anomalies south of Australia, that stretch from the south of Western Australia to the dateline, and by slight negative MSLP anomalies over the southeast (Fig. 7.5e,f). The mean winds at 850hPa illustrate a shift of the westerlies towards the south due to the anomalous high MSLP. A further part of the westerlies turn anticyclonic toward the inland of Australia at 140°E. With focus on the East Coast, the mean wind is nearly zero and indicates anomalous easterlies over the Tasman Sea. This is in accordance with our results in Chapter 6 where we suggested that cut-off lows develop over the Tasman Sea and move to the west accompanied by weak anomalous easterly onshore flow.

The synoptic pattern of wet South Coast Cluster 4 shows similarities with the pattern in dry Cluster 2 (Fig. 7.5g,h). However, the area of anomalous low MSLP that stretches from higher latitudes to southeastern Australia is more pronounced and the high positive MSLP anomaly to the west is weaker compared to dry Cluster 2. Accordingly, the wind anomalies at 850hPa are stronger over the southeast of Australia. This indicates a more intensified character during rainfall and a faster movement of rain-producing systems over southeastern Australia.

The examination of the synoptic situation during rainfall demonstrates that the mean surface circulation patterns differ between the El Niño clusters. Rainfall events in dry Cluster 2 and wet South Coast Cluster 4 are associated with pronounced anomalous low MSLP at 150°E over southeastern Australia that reaches from higher latitudes into the Subtropics. Anomalous south-westerlies and westerlies in the west of southeastern Australia are connected with high MSLP between 100°E and 130°E. In contrast, strong positive MSLP anomalies to the south and southeast of Australia characterize the surface patterns during rainfall in wet Cluster 1 and wet East Coast Cluster 3. The high MSLP anomaly is centered southeast of the Australian coast and anomalous north-westerlies are observed during rainfall in wet Cluster 1. A broad MSLP anomaly with two maxima to the south of Australia points to the rainfall situation with anomalous north-easterlies along the East Coast in wet East Coast Cluster 3.

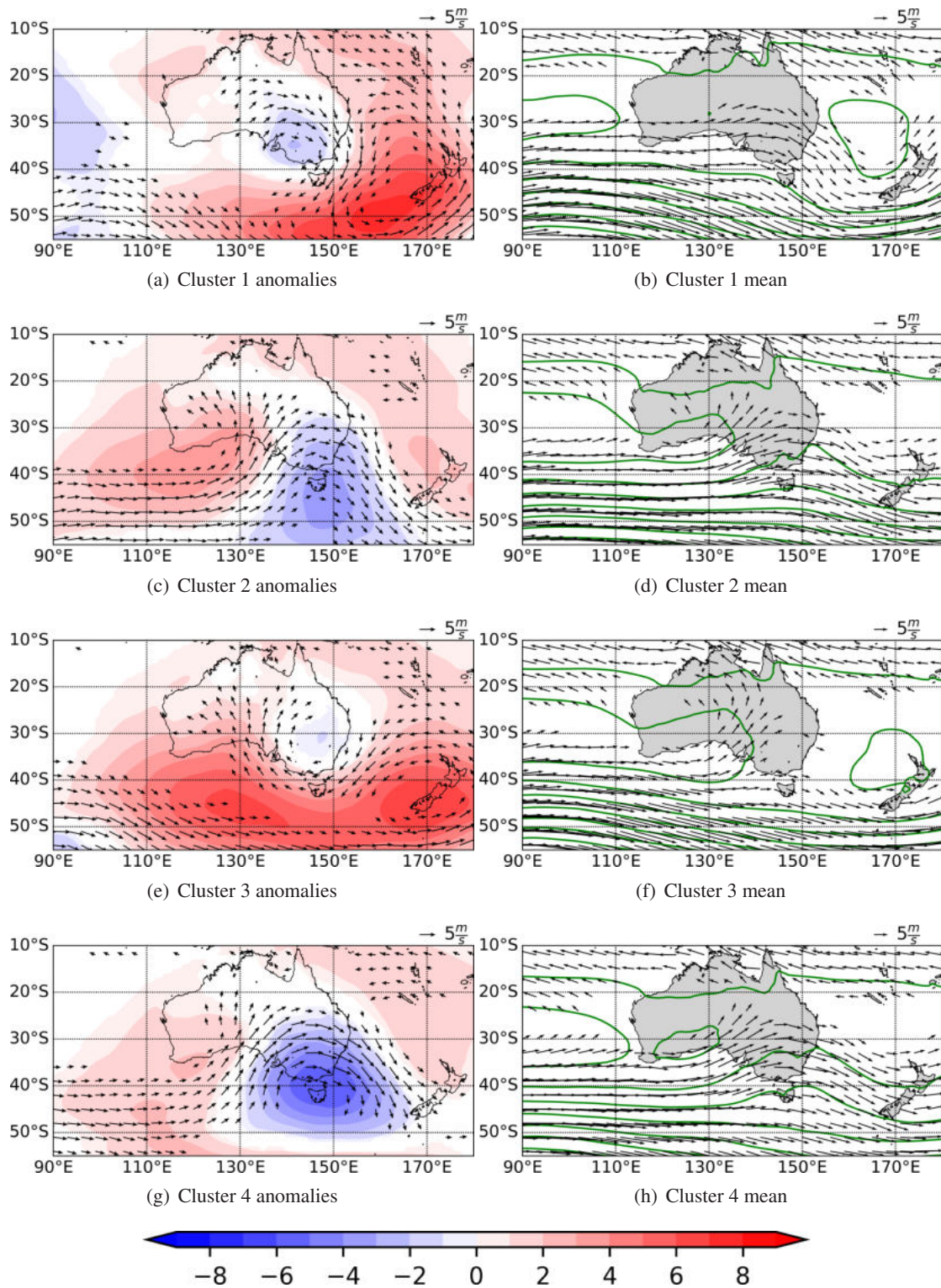


Figure 7.5: Synoptic fields for rainy days in southeastern Australia in the different El Niño Clusters. The left panels show the MSLP anomalies (in hPa) and wind anomalies at 850hPa. Only wind anomalies that exceed  $2 \text{ m s}^{-1}$  are shown. The right panels show the MSLP (green contours) and the mean wind at 850hPa. Only mean winds that exceed  $3 \text{ m s}^{-1}$  are shown.

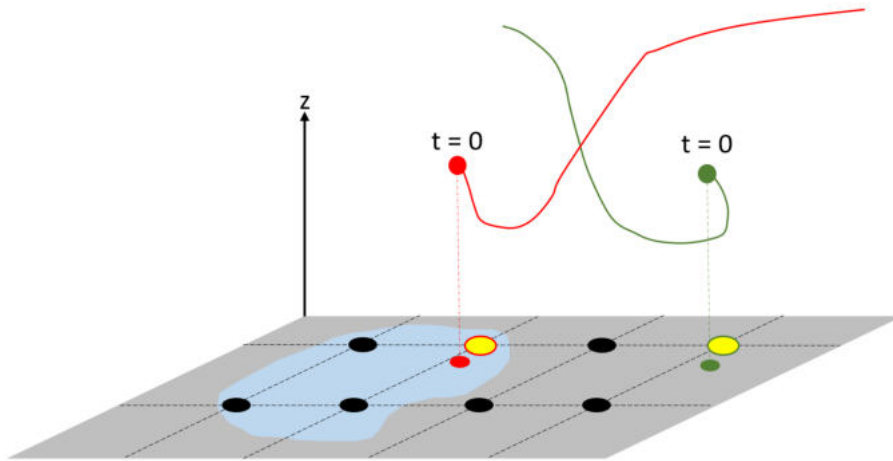


Figure 7.6: A schematic overview of using the result from the matching of rainfall with weather systems to select cut-off low trajectories and WCB trajectories. The black dots represent grid points of the  $0.05^\circ$  matching grid. An area of rainfall is displayed in blue. This area is exemplary associated with a cut-off low. Backward trajectories with their starting points ( $t = 0$ h) are colored in red and green. The yellow dots are the nearest grid points of the respective trajectory. In this example, we would use the red trajectory for further calculations. The green trajectory is ignored as it does not match with rainfall on the ground.

### 7.3 Backward trajectories for rainfall events

We already discussed the different occurrence of weather systems and showed that the mean daily rainfall amount strongly varies between the El Niño clusters. The section aims for a more detailed understanding of physical and dynamical processes and explores the moisture sources for the synoptic systems. We therefore examine the pathways of air masses that are related to rainfall events during El Niño over southeastern Australia by calculating backward trajectories with LAGRANTO (Chapter 3.2.3).

#### Method

Following Sodemann et al. (2008), we only want to consider precipitating air parcels so that air parcels need to exceed 80% relative humidity. We calculate backward trajectories starting at an equidistant grid of  $60\text{km} \times 60\text{km}$  and between 970 and 490hPa at intervals of 30hPa over the clustering region in southeastern Australia when this rainfall criteria is fulfilled at that level and grid point. Additionally, the matching results from Chapter 7.1 are consulted to distinguish between the trajectories of WCB and cut-off low rainfall.

The schematic sketch in Figure 7.6 demonstrates how we choose the trajectories for the two cases. For every trajectory within a cluster, we search for the nearest grid point on our  $0.05^\circ$  matching grid. If the nearest grid point shows rainfall at the same time as the trajectory starts and if it matches with only one of the weather systems (cut-off low or WCB), we take the trajectory for the respective case (red trajectory, Fig. 7.6). We ignore trajectories for further calculations when the conditions at the nearest grid point are not fulfilled (green trajectory, Fig. 7.6). Finally, the trajectory density is calculated for different time steps and brought back to a latitude-longitude grid with a spatial resolution of  $1^\circ$ .

Traced variables along the trajectories help to get a better physical understanding of the processes along the trajectories. We therefore calculated for each cluster a mean trajectory that shows the temporal progression of specific humidity, potential temperature and pressure.

## Results

The discussion of the trajectories for each weather system is divided in two parts. We will first describe the pathways of air parcels that reach the respective rain-producing weather systems. In the second part, we present physical characteristics and in particular the thermodynamic history of air parcels.

### Cut-off low trajectories

In all El Niño clusters, backward trajectories that are calculated for cut-off low rainfall show a consistent pathway. At  $t = -120\text{h}$ , most of the trajectories are distributed between  $140^\circ\text{E}$  and  $160^\circ\text{E}$  south of Australia, and over the Tasman Sea (Fig. 7.7q-t). Air parcels of cut-off low rainfall move northeastward nearly parallel to the East Coast of Australia towards lower latitudes (Fig. 7.7m-p). Two days prior to rainfall, the trajectory density is highest close to the East Coast between  $20^\circ\text{S}$  and  $40^\circ\text{S}$  (Fig. 7.7i-l). At  $t = -24\text{h}$ , most of the air parcels have already reached the north of the target area (Fig. 7.7e-h). In the last 24 hours, the trajectories move southward towards the coastal areas where most of the backward trajectories are located at  $t = 0\text{h}$  (Fig. 7.7a-d). This anticyclonic propagation of air parcels that originate from the south of Australia is consistent in all clusters. Air parcels spend most of their time over the maritime regions and reach the cut-off low at its north-eastern flank, where they are effectively lifted further up. Previous studies assume that rain-bringing northwest cloudbands typically extending from the Indian Ocean northwest of Australia towards southeastern Australia indicate the transport of moisture between the two regions (McIntosh et al., 2012). However, air parcels reach the north-eastern flank of the cut-off low from the northern inner continent and not as one would intuitively expect from the Indian Ocean or the Southern Ocean. This is consistent with previous trajectory studies on cut-off low events in southeastern Australia highlighting the value of the Lagrangian perspective compared to the Eulerian view point (McIntosh et al., 2007; Brown et al., 2009; McIntosh et al., 2012).

In the following, we point to differences between the clusters by discussing the pathways for each cluster separately. In contrast to the general pathway described above, the pathway and in particular the propagation speed of air parcels that end in cut-off low rainfall differs in wet Cluster 1 (Fig. 7.7m,q). Most of the trajectories move relatively slowly from the South Coast along the East Coast and anticyclonically towards southeastern Australia. However, multiple density maxima indicate that a few air parcels also originate from the northwest and far east of Australia (Fig. 7.7i,m). In combination with the synoptic pattern during rainfall in wet Cluster 1, the pathway from far east is connected to anomalous easterlies between  $30^\circ\text{S}$  and  $40^\circ\text{S}$  due to above-average MSLP over the Tasman Sea (Fig. 7.5a,b). Anomalous MSLP over southeastern Australia causes unusual cyclonic winds that point to another pathway from the northwest (Fig. 7.7e,i,m). Multiple density maxima in dry Cluster 2 suggest additional pathways to the general pathway of

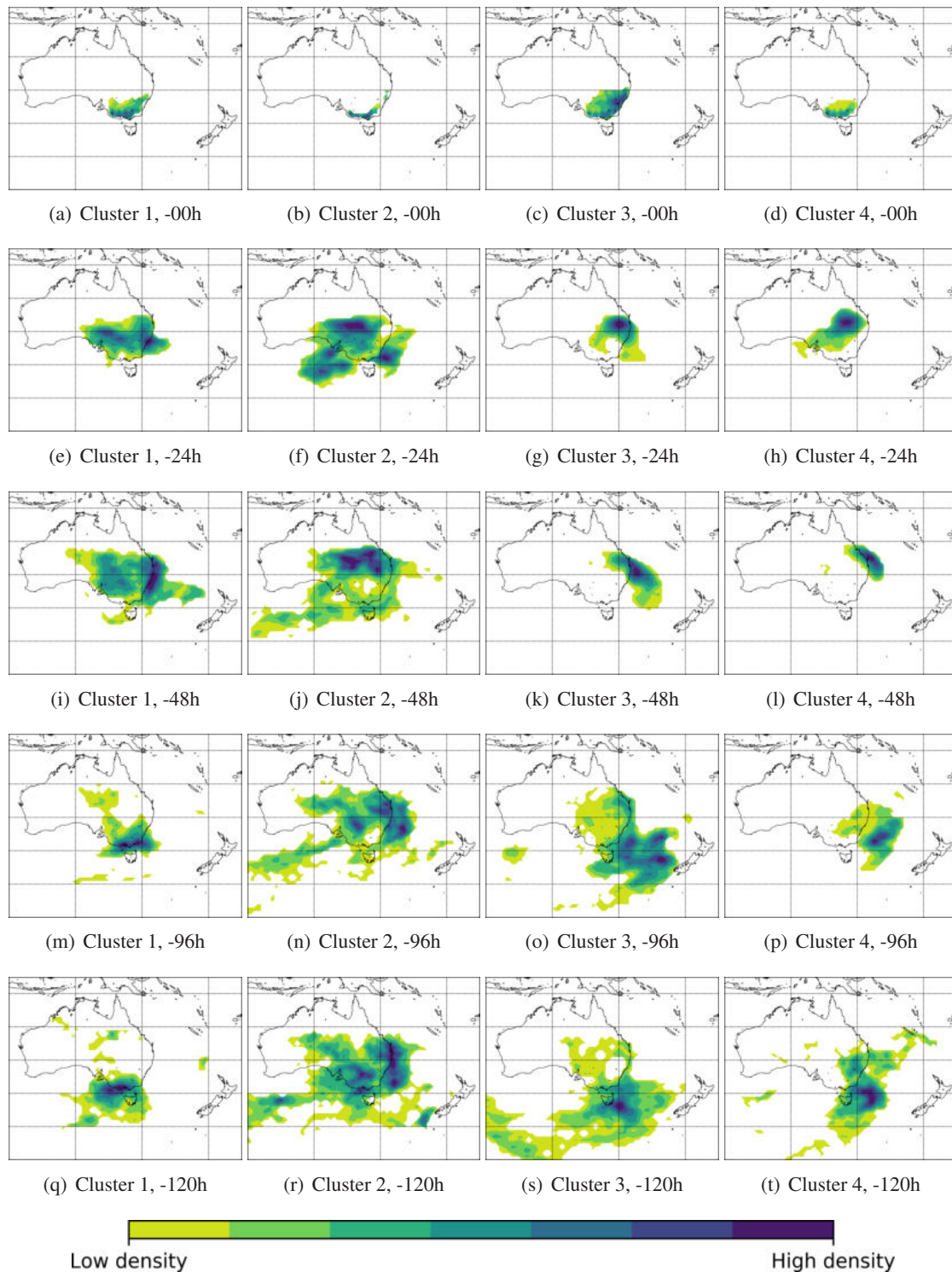


Figure 7.7: Density of cut-off low rainfall backward trajectories in southeastern Australia during El Niño for wet Cluster 1 (a,e,i,m,q), dry Cluster 2 (b,f,j,n,r), wet East Coast Cluster 3 (c,g,k,o,s) and wet South Coast Cluster 4 (d,h,l,p,t). Density plots are shown for 0, -24, -48, -96 and -120h time steps. The trajectory densities are normalized and only normalized densities between 0.3 and 1.0 are shown in 0.1 steps. Latitudes in 10° steps and longitudes in 20° steps begin with 40°S and 110°E in the lower left corner.

cut-off lows (Fig. 7.7r). A further pathway is visible to the south of Western Australia that is related to the synoptic patterns in dry Cluster 2 (Fig. 7.5c,d). Anomalous low MSLP during rainfall extends south of Australia and leads to a northward deflection of the mean westerlies (Fig. 7.5c,d). Trajectories indicate an upstream origin from the Southern Ocean and air parcels follow the enhanced westerly winds. The pathway from the southwest has already been observed during less precipitating cut-off low events during El Niño (Brown et al., 2009; McIntosh et al., 2012). This is in accordance with the low daily mean rainfall in dry Cluster 2 in our study (Fig. 7.2b). Another pathway suggests an origin of air parcels over central Australia between 120°E and 140°E (Fig. 7.7n,r). At  $t = -24$ h, three density maxima indicate the flow into the cut-off low from the north, northwest, southeast and southwest (Fig. 7.7f). In wet East Coast Cluster 3, the pathway of cut-off low rainfall backward trajectories follows the general pathway from the Tasman Sea that is described above (Fig. 7.7c,g,k,o,s). Trajectories that end in cut-off low rainfall at  $t = 0$ h are located also along the East Coast and more inland (Fig. 7.7c). A curved density pattern of trajectories between 40°S and 60°S can be related to the synoptic pattern during rainfall. Positive MSLP anomalies south of Australia are connected with anomalous anticyclonic flow in lower levels which result in enhanced westerlies far south of Australia (Fig. 7.7s; Fig. 7.5e,f). Air parcels of cut-off low rainfall travel within enhanced westerly winds around the anomalous high MSLP area. In wet South Coast Cluster 4, the trajectory density pattern for the different time steps follows the pattern in wet East Coast Cluster 3 (Fig. 7.7h,l,p,t). Although the synoptic patterns show enhanced westerlies over southeastern Australia, there is no pathway from the Southern Ocean that reaches southeastern Australia at  $t = 0$ h directly from the southwest (Fig. 7.5g,h). The low contribution of cut-off lows to rainfall in wet South Coast Cluster 4 explains why the pathway does not show an agreement with the synoptic patterns (Fig. 7.3d).

We now investigate the physical properties of cut-off low backward trajectories. In all El Niño clusters, backward trajectories start at a mean height of around 700hPa ten days prior to the rainfall event ( $t = -240$ h) and slowly descend until  $t = -36$ h (Fig. 7.8a). On their way to southeastern Australia, the air parcels continuously pick up moisture and experience slight adiabatic cooling as indicated by a specific humidity increase and a potential temperature decrease, respectively (Fig. 7.8b,c). SSTs to the east of Australia are positively correlated with the rainfall amount of cut-off lows over southeastern Australia (McIntosh et al., 2007). In addition, sensitivity studies revealed that SSTs northeast of Australia contribute around a fifth to rainfall change during strong El Niño events (Van Rensch et al., 2019). In accordance with Van Rensch et al. (2019), we suggest that average and in particular above-average SSTs along the East Coast of Australia favor the moisture collection of air parcels and therefore indirectly influence the rainfall in southeastern Australia (Fig. 5.1). Around 1-2 days prior to rainfall, the trajectories reach their lowest level with a pressure of around 880hPa (Fig. 7.8). However, they seem to reach the northeastern flank of the cut-off low and start to ascend quickly while they further pick up moisture. One assumption is that some trajectories already produce precipitation in higher layers, which evaporates and is thus collected by trajectories from lower levels. After the specific humidity reaches maxima values between  $5.1 \text{ g kg}^{-1}$  and  $5.5 \text{ g kg}^{-1}$ , an abrupt increase of potential temperature indicates saturation, the condensation of water vapor and latent heat release. At the same time, the specific humidity of the parcel decreases as clouds start to form. The parcels ascend in the mean by 100hPa within the

last two days prior to rainfall.

We will discuss the physical properties of cut-off low rainfall trajectories for each cluster separately to highlight differences to the other clusters. In wet Cluster 1, backward trajectories of cut-off low rainfall start at a lower height and with a considerably higher amount of specific humidity at  $t = -240\text{h}$  (Fig. 7.8a,c). They cover a smaller distance which indicates a slower propagation speed. Therefore, air parcels are raised at an earlier stage due to their vicinity of the region where backward trajectories are started at  $t = 0\text{h}$ . In dry Cluster 2, air parcels start at higher levels with a lower amount of moisture compared to the air parcels in wet Cluster 1 (Fig. 7.8a,c). However, they pick up most of their moisture during their descent along the East Coast and over the Tasman Sea. In wet East Coast Cluster 3 and wet South Coast Cluster 4, the thermodynamic history of trajectories is similar (Fig. 7.8a,c). The general pathway is in accordance with the findings of previous studies that investigated the backward trajectories of cut-off low rainfall over southeastern Australia. In accordance with their results, air parcels pick up most of the moisture between  $t = -72\text{h}$  and  $t = -24\text{h}$  when the air parcels are distributed close to the East Coast and reach the continent. This pathway indicates that air parcels traveled over the marine boundary layer off northwestern Australia where they became wetter by diffusive processes (Brown et al., 2009; McIntosh et al., 2012).

We investigated the pathway of air parcels that end in cut-off low rainfall over southeastern Australia. The general pathway originates from the south of Australia and air parcels move anticyclonically over the Tasman Sea towards southeastern Australia. On their way over the Tasman Sea they continuously pick up moisture pointing to the importance of anomalous SSTs east of Australia. During anomalous warm SSTs, trajectories potentially pick up more moisture which would result in increased rainfall in southeastern Australia. This supports sensitivity studies showing that SSTs northwest of Australia influence rainfall in eastern Australia through the process of moisture availability rather than through changes in the atmospheric circulation (Van Rensch et al., 2019). Northwest cloudbands, the well-known effect of IOD to rainfall in the southeast of Australia and the eastward movement of cut-off lows imply the Indian Ocean as main source of moisture (McIntosh et al., 2012). However, a key finding is that trajectories reach the southeastern Australian region from the inner continent and not as one would intuitively expect from the Indian or Southern Ocean.

### **WCB trajectories**

In all El Niño clusters, backward trajectories of WCB rainfall show a similar pathway for the different rainfall anomaly clusters in the last 48 hours before rainfall (Fig. 7.9). At  $t = -48\text{h}$ , most of the air parcels that feed into the WCB are located north and northwest of southeastern Australia. One day prior to rainfall, the air parcels have moved further south towards southeastern Australia with the highest density of trajectories at around  $140^\circ\text{E}$  and  $25^\circ\text{S}$  (Fig. 7.9e,f,g,h). Air parcels that end up in WCB rainfall over southeastern Australia reach the rainfall region from the north in all El Niño clusters. However, the source regions of backward trajectories before  $t = -48\text{h}$  are different between the clusters.

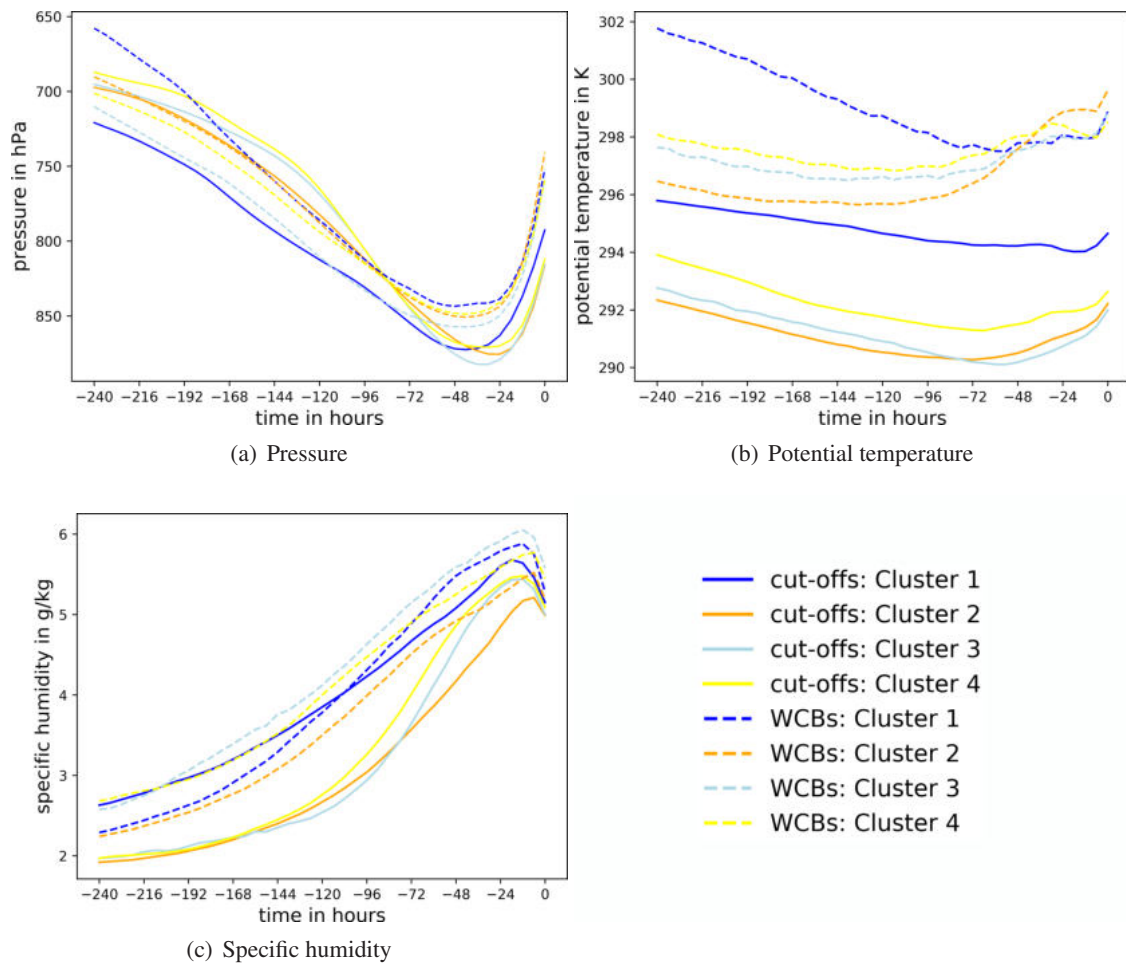


Figure 7.8: Time evolution of physical characteristics and thermodynamical properties for the 10 day (240h) backward trajectories for each weather system (cut-off low, WCB) and each cluster: wet Cluster 1, dry Cluster 2, wet East Coast Cluster 3 and wet South Coast Cluster 4. Mean trajectories show the changes of pressure (a), potential temperature (b) and specific humidity (c).

In the following, we discuss the pathways of WCB trajectories for each cluster separately. Two pathways of backward trajectories point to different sources for WCB rainfall in wet Cluster 1. At  $t = -120\text{h}$ , most of the trajectories are located over the Coral Sea (Fig. 7.9q). A further but less pronounced pathway is implied over the continent and indicates the contribution of air parcels to WCB rainfall from Northern and Central Australia. Air parcels over the Coral Sea move towards the East Coast, reach the continent and merge with the eastward propagating air parcels from continental Australia at  $t = -48\text{h}$  (Fig. 7.9i,m). With focus on the synoptic patterns during rainfall in wet Cluster 1, the air parcels turn within anomalous north-westerlies to the south and bring rainfall in particular to the coastal areas but also to the inland regions of southeastern Australia (Fig 7.5a,b; Fig. 7.9a,e). In dry Cluster 2, the dominant pathway originates from the Tasman Sea (Fig. 7.9r). Further areas of high trajectory density point to more pathways from the northwest of Australia and central Australia. Most of the backward trajectories are associated with an anticyclonic movement from the Tasman Sea to the north up to  $20^\circ\text{S}$  where they turn west and reach the continent (Fig. 7.9n,r). At  $t = -48\text{h}$ , they merge with air parcels from the northwest and with

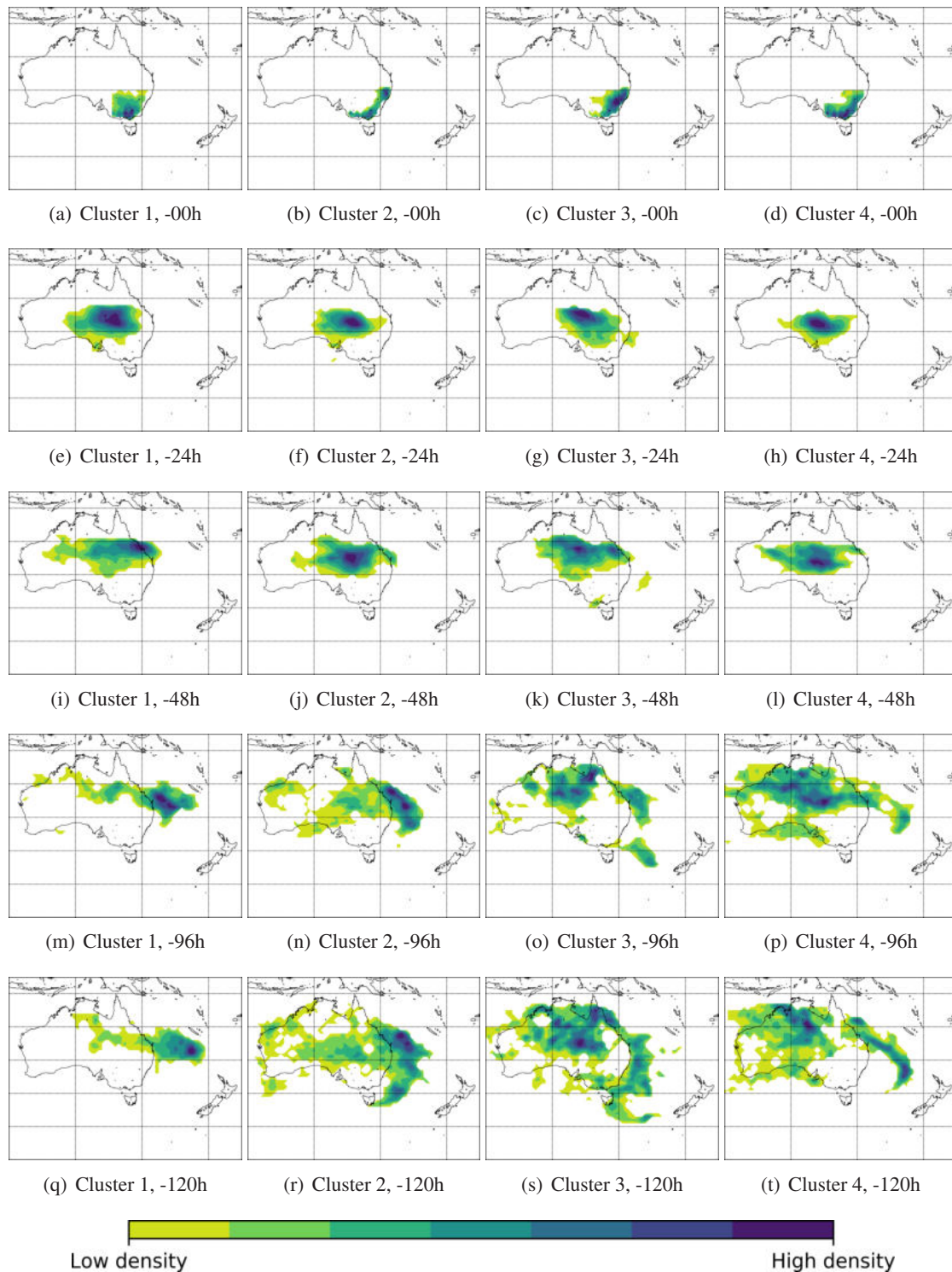


Figure 7.9: Density of WCB rainfall backward trajectories in southeastern Australia during El Niño for wet Cluster 1 (a,e,i,m,q), dry Cluster 2 (b,f,j,n,r), wet East Coast Cluster 3 (c,g,k,o,s) and wet South Coast Cluster 4 (d,h,l,p,t). Density plots are shown for 0, -24, -48, -96 and -120h time steps. The trajectory densities are normalized and only normalized densities between 0.3 and 1.0 are shown in 0.1 steps. Latitudes in  $10^\circ$  steps and longitudes in  $20^\circ$  steps begin with  $40^\circ\text{S}$  and  $110^\circ\text{E}$  in the lower left corner.

air parcels from the south of Australia that move northeastward (Fig. 7.9j,n,r). In the last 2 days prior to rainfall, the trajectories reach southeastern Australia from the northwest and bring rainfall to the East Coast (Fig. 7.9b,f). The pathway from the Tasman Sea in dry Cluster 2 is also visible in wet East Coast Cluster 3 (Fig. 7.9o,s). However, there is a second pathway that indicates the origin of air parcels from the northern part of Australia. At  $t = -120\text{h}$ , air parcels that result in WCB rainfall over southeastern Australia are located along the East Coast and over tropical North Australia (Fig. 7.9s). Air parcels from the north of Australia move southeastward, merge with the trajectories from the Tasman Sea at  $t = -48\text{h}$  around  $140^\circ\text{E}$  and bring rainfall to the East Coast of Australia (Fig. 7.9c,g,k). In wet South Coast Cluster 4, two trajectory density maxima point to multiple pathways of WCB rainfall backward trajectories (Fig. 7.9t). A pathway from the north of Australia is similar to the pathway in wet East Coast Cluster 3. In addition, a large fraction of air parcels originate over the Tasman Sea and travel from around  $160^\circ\text{E}$  northwestward towards Australia and reach the continent at around  $20^\circ\text{S}$ . The two pathways merge together with another pathway from the south of Australia (Fig. 7.9l,p,t). In accordance with the other clusters, the air parcels reach southeastern Australia from the northwest and bring rainfall to coastal regions of southeastern Australia (Fig. 7.9d,h,l).

We now investigate the physical properties of WCB rainfall backward trajectories. In all clusters, air parcels are located between 660 and 700hPa at  $t = -216\text{h}$  (Fig. 7.8a). They steadily descend, pick up moisture on their way and experience slight diabatic cooling as indicated by an increase in specific humidity and a slight decrease in potential temperature, respectively (Fig. 7.8). Around 2 days prior to rainfall, the trajectories reach their lowest level of 850hPa when they are all located north of southeastern Australia and finally start to rise. Although most of the air parcels are already located over the inner continent, the air parcels still pick up moisture until they reach maxima values of up to  $6\text{ g kg}^{-1}$  at  $t = -24\text{h}$  (Fig. 7.8c). This is not intuitive as one would expect that trajectories collect moisture from the ocean and not from the dry subtropical inland region of Australia. The abrupt increase of potential temperature indicates saturation, the condensation of water vapor and latent heat release. As clouds start to form, the specific humidity within the air parcels start to decrease quickly. In the following, we will discuss striking signals in the individual clusters to mark the differences.

We will discuss the physical properties of WCB rainfall trajectories for each cluster separately to highlight differences to the other clusters. In wet Cluster 1, air parcels strongly descend and strongly adiabatically cool ( $-4\text{K}$ ) on their way from the Coral Sea to Australia (Fig. 7.8a,b). They pick up most of their moisture over the Coral Sea (Fig. 7.8c). This is in accordance with the fact that the Coral Sea and the Tasman Sea region are the prominent moisture sources of WCBs around Australia (Pfahl et al., 2014). In contrast to the other clusters, the potential temperature increase starts much earlier at  $t = -96\text{h}$  in dry Cluster 2 (Fig. 7.8b). The sharp increase of the potential temperature ( $4\text{K}$ ) suggests an impact of enhanced sensible heat fluxes at the ground that comes from anomalous dry conditions in dry Cluster 2. Air parcels in wet East Coast Cluster 3 show the highest amount of moisture on their way to southeastern Australia. This points to the dominance of the pathway from the humid areas north of Australia (Fig. 7.8c). As there is also a pathway from the north of Australia in wet South Coast Cluster 4, the temporal evolution of specific humidity is

nearly similar to the one in wet East Coast Cluster 3.

We investigated the backward trajectories of WCB rainfall events in southeastern Australia for each of the four rainfall anomaly clusters. In all El Niño clusters, backward trajectories continuously pick up moisture and finally reach southeastern Australia from the north. In comparison with cut-off low pathways, air parcels of WCB rainfall additionally originate from the north of Australia indicating the importance of tropical air masses. Contrary to what might be expected, the trajectories also collect a considerable amount of moisture over the dry interior of Australia. A further key finding is the lack of an active transport of air masses from the eastern Indian Ocean towards southeastern Australia leading to the assumption that SSTs northwest of Australia influence rainfall in southeastern Australia mainly by changes in the atmospheric circulation rather than via moisture availability processes.

## 8 Conclusions and outlook

Southeastern Australia receives most of its annual rainfall during the austral winter-spring season between June and November. The major rain-producing processes include extratropical cyclones and their associated fronts and cut-off low pressure systems (cut-off lows). However, the processes are thought to be influenced by modes of climate variability on intraseasonal or longer time scales: the El Niño-Southern Oscillation (ENSO), the Indian Ocean Dipole (IOD) and the Southern Annular Mode (SAM). ENSO is the dominant climate mode with the largest effect on rainfall variability in southeastern Australia. The relationship of rainfall over southeastern Australia and the strength of a specific ENSO phase is linear during La Niña but asymmetric during El Niño.

This thesis investigates the rainfall variability in southeastern Australia during the winter-spring seasons of the last 10 El Niño events from a weather system perspective. We apply a clustering algorithm on monthly rainfall anomalies in the winter-spring season for the 1979-2015 period with a particular interest on El Niño years. We then focus on the distribution of large-scale climate modes and upper-level circulation anomalies. Furthermore, we investigate significant changes of the characteristic weather system patterns in the winter-spring season and identify the origin of rainfall during El Niño. We now briefly answer the research questions that are raised in the introduction (Chapter 1):

### **1. What characterizes the monthly rainfall anomaly patterns in southeastern Australia?**

Four different spatial rainfall anomaly patterns dominate the rainfall variability in the winter-spring season and separate roughly wet, dry, East Coast wet and South Coast wet months in southeastern Australia.

### **2. Which effect do large-scale climate modes (ENSO, IOD, SAM) and blocking have on rainfall in southeastern Australia? Is there evidence of teleconnection patterns between the tropical ENSO and IOD signals and the large-scale circulation in higher latitudes of southeastern Australia?**

The phase of IOD and the strength of El Niño is not decisive for a specific rainfall anomaly pattern. However, there is evidence for enhanced cut-off low frequency during positive SAM leading to anomalous high rainfall. Depending on the rainfall anomaly pattern, upper-level geopotential anomalies point to Rossby wave trains (RWTs) that are excited in the tropical Indian Ocean and might affect the midlatitude large-scale Rossby wave pattern over Australia. The observed RWTs are in high agreement with the RWTs that were identified during El Niño and positive IOD events by Cai et al. (2011).

### 3. How do the weather system patterns over Australia change during El Niño?

Changes of weather system frequencies occur during El Niño over southeastern Australia and highly depend on the respective monthly rainfall anomaly pattern. The most prominent changes are observed in the atmospheric blocking and cut-off low frequencies in all clusters.

### 4. Which weather systems produce rainfall in southeastern Australia during El Niño and what characterizes the synoptic surface patterns during rainfall?

Most of the rainfall in southeastern Australia is produced by cut-off lows and warm conveyor belts (WCBs) in the winter-spring season. However, the contributions strongly vary between the different clusters. There are also clear differences in mean sea level pressure (MSLP) and wind fields during rainfall.

### 5. Where is the origin of air masses during rainfall events? Are there specific pathways that determine the strength of rainfall?

Pathways of cut-off low rainfall show an origin of air masses over the Tasman Sea and the Southern Ocean. This is consistent with previous trajectory studies in southeastern Australia (McIntosh et al., 2007; Brown et al., 2009; McIntosh et al., 2012). However, the backward trajectories of WCB rainfall point to different source regions between different rainfall anomaly patterns. A key finding is that trajectories reach southeastern Australia from the inner continent, where they continuously pick up moisture, and not as one would intuitively expect from the Indian or Southern Ocean.

As the answers to the research questions highly depend on the rainfall anomaly pattern in southeastern Australia, we will summarize the results of this thesis for each pattern separately by also referring back to the research questions.

Wet Cluster 1 is characterized by above-average rainfall in southeastern Australia in particular west of the Great Dividing Range. The dominant positive phase of SAM points to anomalous high geopotential and to an increased frequency of blocking southeast of Australia (roughly 150°E) that is connected with increased cut-off low activity along the South Coast of Australia (Fig. 8.1a). This link between blocking and enhanced rainfall due to cut-off lows is in accordance with the findings of Risbey et al. (2009a). Cut-off lows contribute around 40% to rainfall along the South Coast of southeastern Australia and backward trajectories indicate the Southern Ocean as the origin of moisture. Air parcels move close to the coast lines to the East Coast of Australia and reach the continent from the South and East. In accordance with the result of Van Rensch et al. (2019), warm SSTs to the east of Australia potentially influence rainfall through the availability of moisture. The occurrence frequency of WCBs is significantly enhanced inland of southeastern Australia. Backward trajectories of WCB rainfall point to an origin of air parcels from the Coral Sea that reach southeastern Australia from the North. This is in accordance with the fact that the Coral Sea is the prominent moisture source of WCBs around Australia (Pfahl et al., 2014). WCBs contribute up to 50% to rainfall inland and in combination with cut-off lows they contribute be-

---

tween 40 % and 70 % to rainfall around the Great Dividing Range. The daily mean rainfall during rainy days reaches 15 mm and the frequency of rainy days is between 30 % and 50 %. During rainfall, anomalous high MSLP south and east of southeastern Australia characterize the synoptic situation leading to anomalous northwesterly winds.

Below-average rainfall in southeastern Australia defines the anomaly pattern in dry Cluster 2. Neither SAM nor IOD have an effect on rainfall but several RWTs are excited by tropical convection in the tropical Indian Ocean resulting in anomalous high geopotential that is associated with an increased frequency of blocking over the southern half of Australia (Fig. 8.1b). The observed RWTs in Cluster 2 are in agreement with the identified RWTs during El Niño in the study of Cai et al. (2011). From a weather system perspective, below-average rainfall results from negative frequency anomalies of rain-bringing weather systems over the eastern half of Australia. Rainy days in dry Cluster 2 are rare with an occurrence frequency of 20 % and daily rainfall amounts do not exceed 8 mm. Anomalous low MSLP that stretches far south and anomalous westerlies over southeastern Australia characterize the synoptic pattern during rainfall. Nevertheless, WCBs and cut-off lows are responsible for 40-60 % of rainfall in southeastern Australia. Their corresponding air masses originate from the Tasman Sea and the Southern Ocean and air parcels move anticyclonically along the East Coast towards southeastern Australia. An additional pathway of cut-off low trajectories from the southwest is associated with less precipitating cut-off low events and agrees with the results of the backward trajectory studies of Brown et al. (2009) and McIntosh et al. (2012).

In wet East Coast Cluster 3, positive rainfall anomalies are observed along the East Coast and negative rainfall anomalies characterize the rainfall anomaly pattern to the south and inland of southeastern Australia. A broad pronounced anomalous anticyclone that is connected with a RWT from the eastern Indian Ocean is observed south of Australia and indicates a shift of the westerly wind belt to the south in accordance with positive SAM values (Fig. 8.1c). The enhanced occurrence of cut-off lows over the Tasman Sea and southeastern Australia suggests the development of cut-off lows at the northeastern flank of a blocking anticyclone. Anomalous easterlies over the Tasman Sea push the cut-off lows to the west where they bring a high percentage of rainfall to the windward side of the Great Dividing Range. The positive correlation between zonal wind and rainfall in the southwest of southeastern Australia fits with the below-average rainfall anomalies in this region (Pepler et al., 2016). Cut-off lows contribute up to 70 % to rainfall along the East Coast and more inland. Backward trajectories reveal the origin of air masses from the Southern Ocean. From a weather system perspective, below-average rainfall along the South Coast results from the decreased frequency of extratropical cyclones south of Australia. Rainy days occur with a frequency of over 30 % and daily rainfall amounts are in particular high along the East Coast with up to 15 mm. During rainfall, two anticyclones are located southeast and southwest of Australia and anomalous cyclonic winds occur over southeastern Australia due to anomalous low MSLP. WCBs in combination with cut-off lows contribute between 20 % and 50 % to rainfall inland and along the East Coast. Air parcels of WCB rainfall originate from the north of Australia and the Tasman Sea.

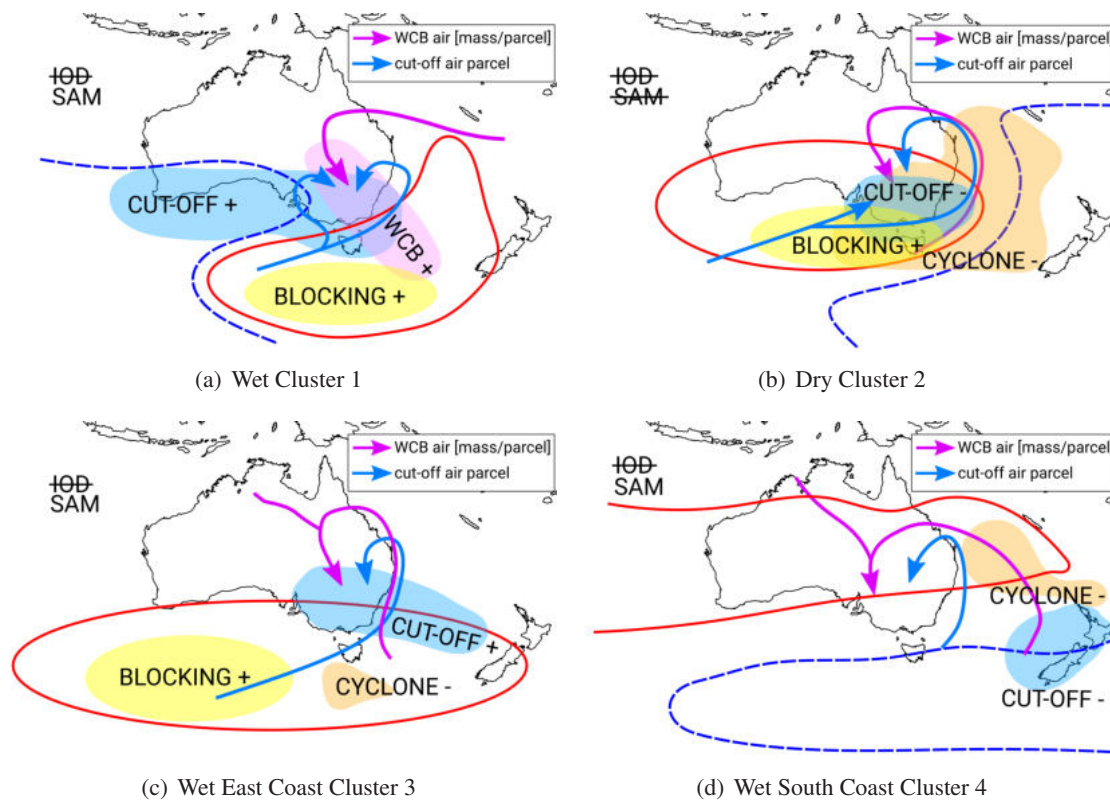


Figure 8.1: Schematic summary of important processes and patterns during El Niño for different rainfall anomaly patterns over southeastern Australia. Red (blue dashed) contour lines point to positive (negative) geopotential anomalies. The shaded regions show positive (+) and negative (-) significant frequency anomalies of cut-off lows (blue), extratropical cyclones (orange), mid-tropospheric WCBs (pink) and blocking (yellow). Pink (blue) arrows indicate the mean pathway of backward trajectories and point to the moisture origin during WCB (cut-off low) rainfall. Climate modes that do not seem to drive rainfall variability in southeastern Australia are crossed out.

Negative rainfall anomalies along the East Coast and positive rainfall anomalies along the South Coast mark the rainfall anomaly pattern in wet South Coast Cluster 4. A negative geopotential anomaly south of southeastern Australia points to enhanced westerlies and suggests an increased frequency of extratropical cyclones in accordance with the dominant occurrence of negative SAM (Fig. 8.1d). This reflects the results of Risbey et al. (2009a) that point to an equatorward shift of the main westerlies during 'wet south' rainfall patterns. With a daily mean rainfall during rainy days of up to 10mm and a frequency of rainy days above 30% along the South Coast, anomalous low MSLP south of Australia is associated with enhanced westerlies over southeastern Australia during rainfall. From a weather system perspective, the lack of weather systems over the east of Australia contributes to below-average rainfall along the East Coast. Cut-off lows and WCB bring around 10-50% of rainfall in particular to the inland area of southeastern Australia. Most of the rainfall along the South Coast (up to 70%) is not explained by cut-off lows and WCBs and suggests a contribution from convective systems or fronts. Backward trajectories of cut-off low rainfall originate from the Tasman Sea and air parcels of WCB rainfall travel from the north of Australia and also from New Zealand to southeastern Australia.

---

This master thesis contributes to a better understanding of physical processes on the synoptic scale during El Niño. In particular, the investigation of weather system frequencies in combination with further synoptic-scale diagnostics opened up a new way to look at rainfall variability. However, the origin of rainfall variability is still not completely understood as it remains a complex interaction between large-scale drivers and synoptic systems. Further research is required to gain a more detailed understanding in the dynamic link of multiple rainfall drivers.

A different clustering method, the application of total rainfall for clustering and variations in the size of the clustering area could be of interest to examine the robustness of our results. Furthermore, an additional consideration of fronts that are also detected by Sprenger et al. (2017) might contribute to a better understanding of rainfall origin during El Niño in particular for the matching of rainfall. A more detailed approach on the backward trajectories during rainfall and especially the use of a Lagrangian moisture diagnostic by Sodemann et al. (2008) could provide more explicit insights into the sources of water vapor. Lastly, it is of high interest to apply our methods to La Niña events to also advance the dynamic understanding of the drivers leading to above-average rainfall in southeastern Australia.



# A Appendix

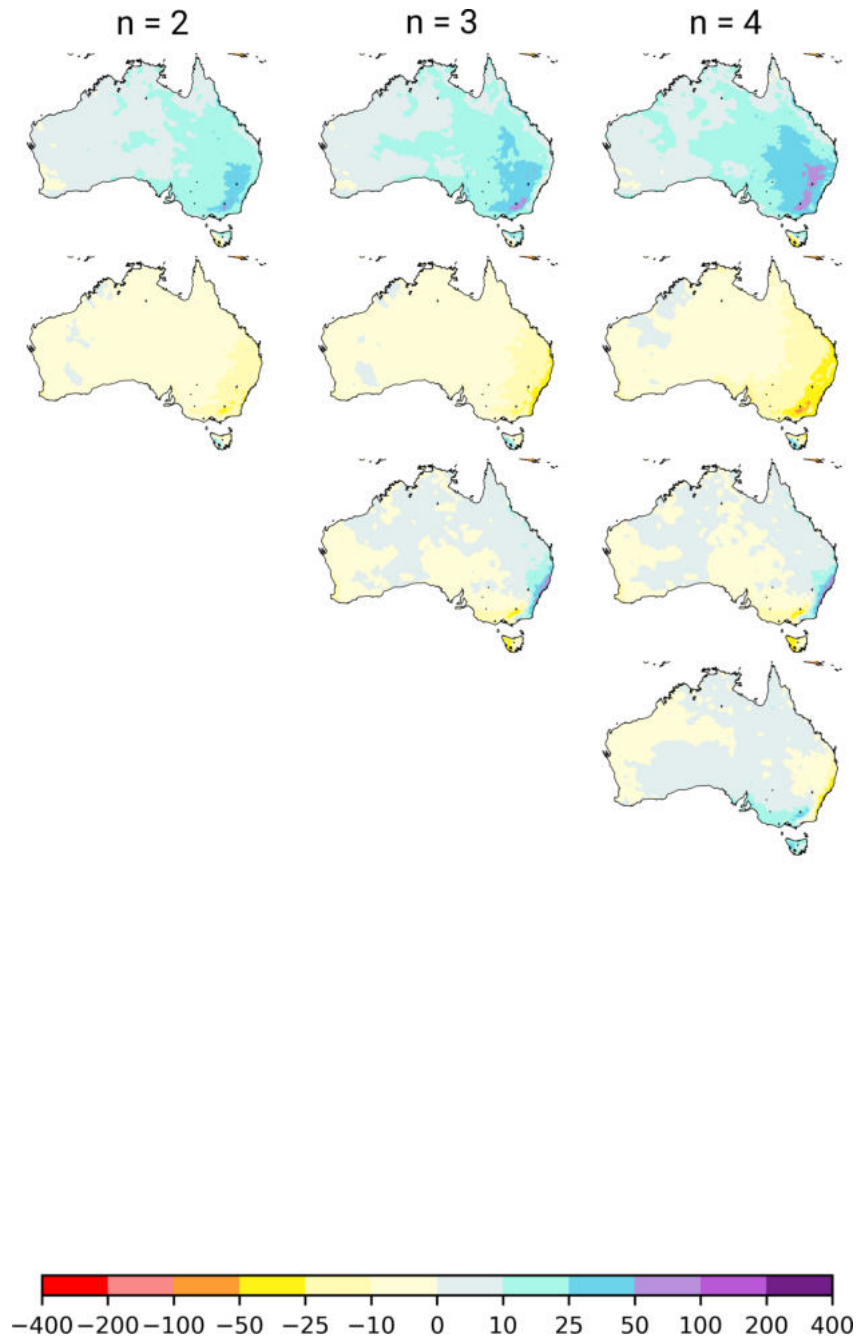


Figure A.1: Resulting clusters of the k-means clustering algorithm with different numbers of clusters (n) over southeastern Australia (29°S to 40°S, 140°E to 154°E) that is applied for the monthly rainfall anomalies in the winter-spring season months of 1979-2015. The shading shows the mean rainfall anomalies for each cluster (in mm).

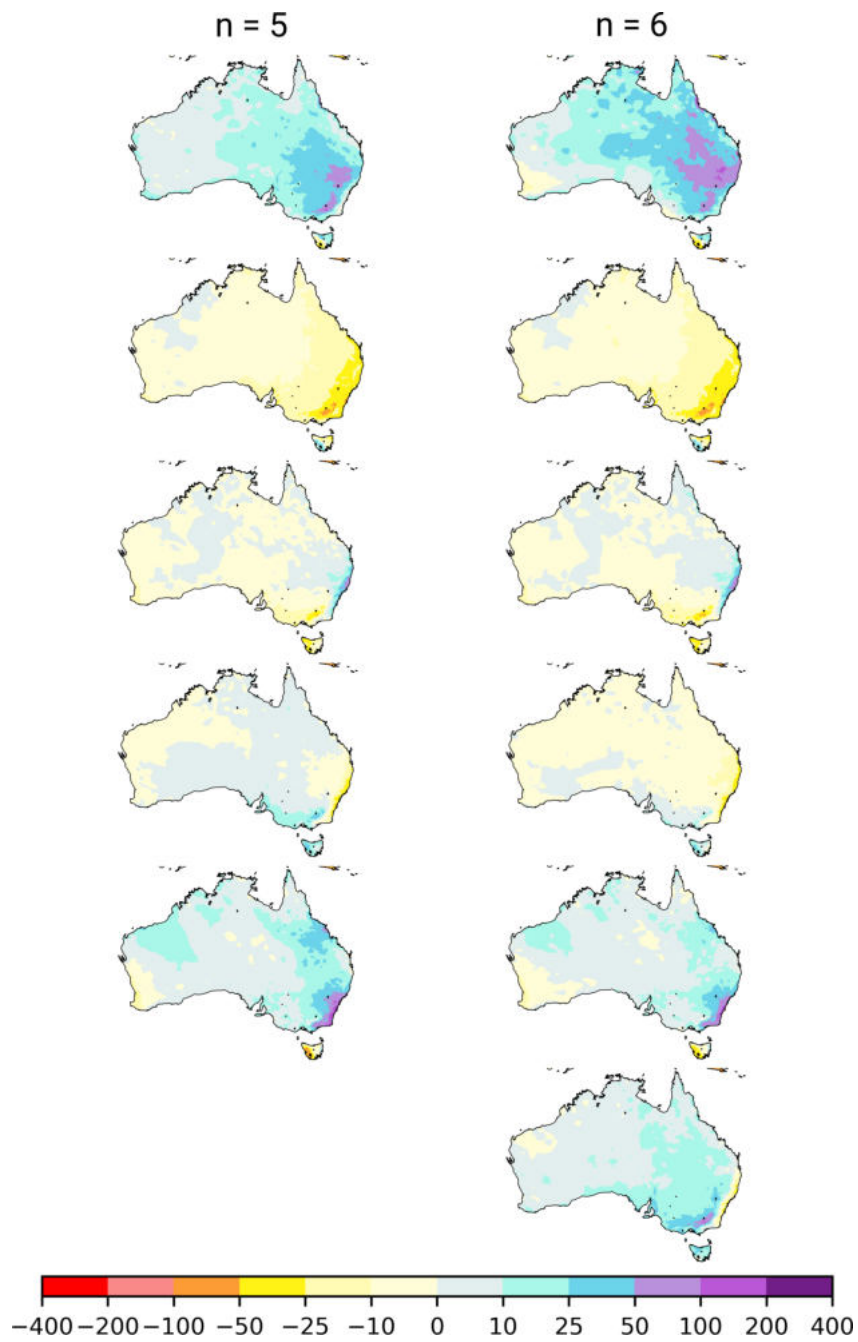


Figure A.2: Resulting clusters of the k-means clustering algorithm with different numbers of clusters ( $n$ ) over southeastern Australia ( $29^{\circ}\text{S}$  to  $40^{\circ}\text{S}$ ,  $140^{\circ}\text{E}$  to  $154^{\circ}\text{E}$ ) that is applied for the monthly rainfall anomalies in the winter-spring season months of 1979-2015. The shading shows the mean rainfall anomalies for each cluster (in mm).

# Bibliography

- Agriculture Victoria, ed. (2019). The Climatedogs: Sam. Accessed: 2019-06-13. URL: <http://agriculture.vic.gov.au/agriculture/weather-and-climate/understanding-weather-and-climate/climatedogs/sam>.
- Allan, R. J., 1988: El Niño Southern Oscillation influences in the Australasian region. *Progress in Physical Geography: Earth and Environment*, **12(3)**, pp. 313–348.
- Ashcroft, L., J. Gergis, and D. J. Karoly, 2016: Long-term stationarity of El Niño–Southern Oscillation teleconnections in southeastern Australia. *Climate Dynamics*, **46(9-10)**, pp. 2991–3006.
- Ashok, K., Z. Guan, and T. Yamagata, 2003: Influence of the Indian Ocean Dipole on the Australian winter rainfall. *Geophysical Research Letters*, **30(15)**.
- Ashok, K., C.-Y. Tam, and W.-J. Lee, 2009: ENSO Modoki impact on the Southern Hemisphere storm track activity during extended austral winter. *Geophysical Research Letters*, **36(12)**.
- Beale, B., 2009. Indian Ocean causes big dry: drought mystery solved. Ed. by University of New South Wales. Accessed: 2019-06-13. URL: <http://www.connectedwaters.unsw.edu.au/news/2009/02/indian-ocean-causes-big-dry-drought-mystery-solved>.
- Berrisford, P., D. Dee, P. Poli, R. Brugge, K. Fielding, M. Fuentes, P. Kållberg, S. Kobayashi, S. Uppala, and A. Simmons, 2009. *The ERA-interim archive - version 2.0*. Tech. rep. 1. Reading: European Centre for Medium Range Weather Forecasts.
- Brown, J. N., P. C. McIntosh, M. J. Pook, and J. S. Risbey, 2009: An investigation of the links between ENSO flavors and rainfall processes in southeastern Australia. *Monthly Weather Review*, **137(11)**, pp. 3786–3795.
- Cai, W., P. van Rensch, T. Cowan, and A. Sullivan, 2010: Asymmetry in ENSO teleconnection with regional rainfall, its multidecadal variability, and impact. *Journal of Climate*, **23(18)**, pp. 4944–4955.
- Cai, W., P. van Rensch, T. Cowan, and H. H. Hendon, 2011: Teleconnection pathways of ENSO and the IOD and the mechanisms for impacts on Australian rainfall. *Journal of Climate*, **24(15)**, pp. 3910–3923.

- Catto, J. L., C. Jakob, G. Berry, and N. Nicholls, 2012: Relating global precipitation to atmospheric fronts. *Geophysical Research Letters*, **39**(10).
- Catto, J. L., E. Madonna, H. Joos, I. Rudeva, and I. Simmonds, 2015: Global relationship between fronts and warm conveyor belts and the impact on extreme precipitation. *Journal of Climate*, **28**(21), pp. 8411–8429.
- Chung, C. and S. Power, 2017: The non-linear impact of El Niño, La Niña and the Southern Oscillation on seasonal and regional Australian precipitation. *Journal of Southern Hemisphere Earth System Science*, **67**(1), pp. 25–45.
- Clark, S., M. J. Reeder, and C. Jakob, 2018: Rainfall regimes over northwestern Australia. *Quarterly Journal of the Royal Meteorological Society*, **144**(711), pp. 458–467.
- Commonwealth of Australia Bureau of Meteorology, ed. (2019[a]). About ENSO and IOD indices. Accessed: 2019-06-13. URL: <http://www.bom.gov.au/climate/enso/indices/about.shtml>.
- Commonwealth of Australia Bureau of Meteorology, ed. (2019[b]). Australian rainfall patterns during El Niño. Accessed: 2019-06-13. URL: <http://www.bom.gov.au/climate/enso/ninocomp.shtml>.
- Commonwealth of Australia Bureau of Meteorology, ed. (2019[c]). El Niño Southern Oscillation (ENSO). Accessed: 2019-06-13. URL: <http://www.bom.gov.au/watl/about-weather-and-climate/australian-climate-influences.shtml?bookmark=enso>.
- Commonwealth of Australia Bureau of Meteorology, ed. (2019[d]). El Niño - Detailed Australian Analysis. Accessed: 2019-06-13. URL: <http://www.bom.gov.au/climate/enso/enlist/index.shtml>.
- Commonwealth of Australia Bureau of Meteorology, ed. (2019[e]). ENSO Outlook - An alert system for the El Niño Southern Oscillation. Accessed: 2019-06-13. URL: <http://www.bom.gov.au/climate/enso/outlook/#tabs=Criteria>.
- Cowan, T., P. van Rensch, A. Purich, and W. Cai, 2013: The association of tropical and extratropical climate modes to atmospheric blocking across southeastern Australia. *Journal of Climate*, **26**(19), pp. 7555–7569.
- CSIRO, 2010. *Climate variability and change in south-eastern Australia - A synthesis of findings from Phase 1 of the South Eastern Australian Climate Initiative (SEACI)*. Tech. rep. Canberra: CSIRO.

- Dee, D. P., S. M. Uppala, A. J. Simmons, P. Berrisford, P. Poli, S. Kobayashi, U. Andrae, M. A. Balmaseda, G. Balsamo, P. Bauer, P. Bechtold, A. C. Beljaars, L. van de Berg, J. Bidlot, N. Bormann, C. Delsol, R. Dragani, M. Fuentes, A. J. Geer, L. Haimberger, S. B. Healy, H. Hersbach, E. V. Hólm, L. Isaksen, P. Kållberg, M. Köhler, M. Matricardi, A. P. McNally, B. M. Monge-Sanz, J. J. Morcrette, B. K. Park, C. Peubey, P. de Rosnay, C. Tavolato, J. N. Thépaut, and F. Vitart, 2011: The ERA-Interim reanalysis: Configuration and performance of the data assimilation system. *Quarterly Journal of the Royal Meteorological Society*, **137(656)**, pp. 553–597.
- Dewitte, S. and N. Clerbaux, 2018: Decadal changes of earth's outgoing longwave radiation. *Remote Sensing*, **10(10)**.
- Fuenzalida, H. A., R. Sánchez, and R. D. Garreaud, 2005: A climatology of cutoff lows in the Southern Hemisphere. *Journal of Geophysical Research*, **110(18)**.
- Gong, D. and S. Wang, 1999: Definition of Antarctic oscillation index. *Geophysical Research Letters*, **26(4)**, pp. 459–462.
- Hartigan, J. A. and M. A. Wong, 1979: Algorithm AS 136: A k-means clustering algorithm. *Journal of the Royal Statistical Society. Series C (Applied Statistics)*, **28(1)**, pp. 100–108.
- Henley, B. J., J. Gergis, D. J. Karoly, S. Power, J. Kennedy, and C. K. Folland, 2015: A Tripole Index for the Interdecadal Pacific Oscillation. *Climate Dynamics*, **45(11-12)**, pp. 3077–3090.
- Jones, D, W Wang, and R Fawcett, 2009: High-quality spatial climate data-sets for Australia. *Australian Meteorological and Oceanographic Journal*, **58(4)**, pp. 233–248.
- Kiladis, G. N. and C. M. Kingtse, 1998: Interannual and Intraseasonal Variability in the Southern Hemisphere. In: *Meteorology of the Southern Hemisphere*, Eds. Koroly, D. J. and D. G. Vincent. vol. 27, 1st ed. American Meteorological Society, Boston, pp. 307–336.
- Kim, J.-W., S.-W. Yeh, and E.-C. Chang, 2013: Combined effect of El Niño-Southern Oscillation and Pacific Decadal Oscillation on the East Asian winter monsoon. *Climate Dynamics*, **42**.
- King, A. D., L. V. Alexander, and M. G. Donat, 2013: Asymmetry in the response of eastern Australia extreme rainfall to low-frequency Pacific variability. *Geophysical Research Letters*, **40(10)**, pp. 2271–2277.
- Liebmann, B. and C. A. Smith, 1996: Description of a complete (interpolated) outgoing longwave radiation dataset. *Bulletin of the American Meteorological Society*, **77(6)**, pp. 1275–1277.
- Lim, E. P. and H. H. Hendon, 2015: Understanding the contrast of Australian springtime rainfall of 1997 and 2002 in the frame of two flavors of El Niño. *Journal of Climate*, **28(7)**, pp. 2804–2822.

- Madonna, E., H. Wernli, H. Joos, and O. Martius, 2014: Warm conveyor belts in the ERA-Interim Dataset (1979-2010). Part I: Climatology and potential vorticity evolution. *Journal of Climate*, **27**(1), pp. 3–26.
- Mantua, N. J. and S. R. Hare, 2002: The Pacific Decadal Oscillation. *Journal of Oceanography*, **58**(1), pp. 35–44.
- Martius, O., C. Schwierz, and H. C. Davies, 2008: Far-upstream precursors of heavy precipitation events on the Alpine south-side. *Quarterly Journal of the Royal Meteorological Society*, **134**, pp. 417–428.
- McIntosh, P. C. and H. H. Hendon, 2018: Understanding Rossby wave trains forced by the Indian Ocean Dipole. *Climate Dynamics*, **50**(7-8), pp. 2783–2798.
- McIntosh, P. C., M. J. Pook, J. S. Risbey, S. N. Lisson, and M. Rebbeck, 2007: Seasonal climate forecasts for agriculture: Towards better understanding and value. *Field Crops Research*, **104**(1-3), pp. 130–138.
- McIntosh, P. C., J. S. Risbey, J. N. Brown, and M. J. Pook, 2012: Apparent and real sources of rainfall associated with a cutoff low in southeast Australia. *CAWCR Research Letters Issue 8, August 2012*, (8), pp. 4–9.
- Murphy, B. F. and B. Timbal, 2008: A review of recent climate variability and climate change in southeastern Australia. *International Journal of Climatology*, **28**(7), pp. 859–879.
- National Center for Atmospheric Research, ed. (2014). Elevation data in netCDF. Accessed: 2019-06-13. URL: [http://research.jisao.washington.edu/data\\_sets/elevation/](http://research.jisao.washington.edu/data_sets/elevation/).
- Nicholls, N, W Drosowsky, and B Lavery, 1997: Australian rainfall variability and change. *Weather*, **52**(3), pp. 66–72.
- Nicholls, N., 2010: Local and remote causes of the southern Australian autumn-winter rainfall decline, 1958-2007. *Climate Dynamics*, **34**(6), pp. 835–845.
- Nieto, R., M. Sprenger, H. Wernli, R. M. Trigo, and L. Gimeno, 2008: Identification and climatology of cut-off lows near the tropopause. *Annals of the New York Academy of Sciences*, **1146**(1), pp. 256–290.
- NOAA Physical Sciences Division, ed. (2019[a]). 20CR Climate Indices: Southern Annular Mode (SAM). Accessed: 2019-06-13. URL: [https://www.esrl.noaa.gov/psd/data/20thC\\_Rean/timeseries/monthly/SAM/](https://www.esrl.noaa.gov/psd/data/20thC_Rean/timeseries/monthly/SAM/).

- NOAA Physical Sciences Division, ed. (2019[b]). Climate Timeseries - Dipole Mode Index (DMI). Accessed: 2019-06-13. URL: [https://www.esrl.noaa.gov/psd/gcos\\_wgsp/Timeseries/DMI/](https://www.esrl.noaa.gov/psd/gcos_wgsp/Timeseries/DMI/).
- NOAA Physical Sciences Division, ed. (2019[c]). Climate Timeseries - TPI (IPO) Tripole Index for the Interdecadal Pacific Oscillation. Accessed: 2019-06-13. URL: <https://www.esrl.noaa.gov/psd/data/timeseries/IPOTPI/>.
- NOAA Physical Sciences Division, ed. (2019[d]). Download Climate Timeseries - Niño 3.4 SST Index. Accessed: 2019-06-13. URL: [https://www.esrl.noaa.gov/psd/gcos\\_wgsp/Timeseries/Nino34/](https://www.esrl.noaa.gov/psd/gcos_wgsp/Timeseries/Nino34/).
- NOAA Physical Sciences Division, ed. (2019[e]). Download Climate Timeseries - Pacific Decadal Oscillation (PDO). Accessed: 2019-06-13. URL: [https://www.esrl.noaa.gov/psd/gcos\\_wgsp/Timeseries/PDO/](https://www.esrl.noaa.gov/psd/gcos_wgsp/Timeseries/PDO/).
- NOAA Physical Sciences Division, ed. (2019[f]). Download Climate Timeseries - Southern Oscillation Index (SOI). Accessed: 2019-06-13. URL: [https://www.esrl.noaa.gov/psd/gcos\\_wgsp/Timeseries/SOI/](https://www.esrl.noaa.gov/psd/gcos_wgsp/Timeseries/SOI/).
- NOAA Physical Sciences Division, ed. (2019[g]). NOAA Interpolated Outgoing Longwave Radiation (OLR). Accessed: 2019-06-13. URL: [https://www.esrl.noaa.gov/psd/data/gridded/data.interp\\_OLR.html](https://www.esrl.noaa.gov/psd/data/gridded/data.interp_OLR.html).
- Parker, W. S., 2016: Reanalyses and observations: what's the difference?. *Bulletin of the American Meteorological Society*, **97(9)**, pp. 1565–1572.
- Pepler, A., A. Coutts-Smith, and B. Timbal, 2014: The role of east coast lows on rainfall patterns and inter-annual variability across the east coast of Australia. *International Journal of Climatology*, **34(4)**, pp. 1011–1021.
- Pepler, A. S., L. V. Alexander, J. P. Evans, and S. C. Sherwood, 2016: Zonal winds and southeast Australian rainfall in global and regional climate models. *Climate Dynamics*, **46(1-2)**, pp. 123–133.
- Pfahl, S., C. Schwierz, M. Croci-Maspoli, C. M. Grams, and H. Wernli, 2015: Importance of latent heat release in ascending air streams for atmospheric blocking. *Nature Geoscience*, **8(8)**, pp. 610–614.
- Pfahl, S., E. Madonna, M. Boettcher, H. Joos, and H. Wernli, 2014: Warm conveyor belts in the ERA-Interim Dataset (1979-2010). Part II: Moisture origin and relevance for precipitation. *Journal of Climate*, **27(1)**, pp. 27–40.

- Philander, S. G. H., 1983: El Niño Southern Oscillation phenomena. *Nature*, **302**, pp. 295–301.
- Pook, M. J., 1994. “Atmospheric blocking in the Australasian region in the Southern Hemisphere winter”. Dissertation. University of Tasmania.
- Pook, M. J., P. C. McIntosh, and G. A. Meyers, 2006: The synoptic decomposition of cool-season rainfall in the southeastern Australian cropping region. *Journal of Applied Meteorology and Climatology*, **45(8)**, pp. 1156–1170.
- Pook, M. J., J. S. Risbey, and P. C. McIntosh, 2014: A comparative synoptic climatology of cool-season rainfall in major grain-growing regions of southern Australia. *Theoretical and Applied Climatology*, **117(3-4)**, pp. 521–533.
- Power, S. B., M. Haylock, R. Colman, and X. Wang, 2006: The predictability of interdecadal changes in ENSO activity and ENSO teleconnections. *Journal of Climate*, **19(19)**, pp. 4755–4771.
- Qi, L., L. M. Leslie, and S. Zhao, 1999: Cut-off low pressure systems over southern Australia: Climatology and case study. *International Journal of Climatology*, **19**, pp. 1633–1649.
- Quinting, J. F., M. J. Reeder, and J. L. Catto, 2019: The intensity and motion of hybrid cyclones in the Australian region in a composite potential vorticity framework. *Quarterly Journal of the Royal Meteorological Society*, **145(718)**, pp. 273–287.
- Rayner, N. A., D. Parker, E. Horton, C. Folland, L. Alexander, D. Rowell, E. Kent, and A. Kaplan, 2003: Global analyses of sea surface temperature, sea ice, and night marine air temperature since the late nineteenth century. *Journal of Geophysical Research*, **108**.
- Risbey, J. S., M. J. Pook, P. C. McIntosh, C. C. Ummenhofer, and G. Meyers, 2009: Characteristics and variability of synoptic features associated with cool season rainfall in southeastern Australia. *International Journal of Climatology*, **29(11)**, pp. 1595–1613.
- Risbey, J. S., M. J. Pook, P. C. McIntosh, M. C. Wheeler, and H. H. Hendon, 2009: On the remote drivers of rainfall variability in Australia. *Monthly Weather Review*, **137(10)**, pp. 3233–3253.
- Risbey, J. S., P. C. McIntosh, and M. J. Pook, 2013: Synoptic components of rainfall variability and trends in southeast Australia. *International Journal of Climatology*, **33(11)**, pp. 2459–2472.
- Ropelewski, C. and P. Jones, 1987: An extension of the Tahiti-Darwin Southern Oscillation Index. *Monthly Weather Review*, **115**, pp. 2161–2165.
- Saji, N. H. and T. Yamagata, 2003: Possible impacts of Indian Ocean Dipole mode events on global climate. *Climate Research*, **25(2)**, pp. 151–169.

- Scherrer, S. C., M. Croci-Maspoli, C. Schwierz, and C. Appenzeller, 2006: Two-dimensional indices of atmospheric blocking and their statistical relationship with winter climate patterns in the Euro-Atlantic region. *International Journal of Climatology*, **26**(2), pp. 233–249.
- Schwierz, C., M. Croci-Maspoli, and H. C. Davies, 2004: Perspicacious indicators of atmospheric blocking. *Geophysical Research Letters*, **31**(6).
- Shields, C. A., J. J. Rutz, L.-Y. Leung, F. M. Ralph, M. Wehner, B. Kawzenuk, J. M. Lora, E. McClenny, T. Osborne, A. E. Payne, P. Ullrich, A. Gershunov, N. Goldenson, B. Guan, Y. Qian, A. M. Ramos, C. Sarangi, S. Sellars, I. Gorodetskaya, K. Kashinath, V. Kurlin, K. Mahoney, G. Muszynski, R. Pierce, A. C. Subramanian, R. Tome, D. Waliser, D. Walton, G. Wick, A. Wilson, D. Lavers, A. Collow, H. Krishnan, G. Magnusdottir, and P. Nguyen, 2018: Atmospheric River tracking method intercomparison project (ARTMIP): project goals and experimental design. *Geoscientific Model Development*, **11**(6), pp. 2455–2474.
- Sodemann, H, C. Schwierz, and H. Wernli, 2008: Interannual variability of Greenland winter precipitation sources: Lagrangian moisture diagnostic and North Atlantic Oscillation influence. *Journal of Geophysical Research*, **113**.
- Sprenger, M. and H. Wernli, 2015: The LAGRANTO Lagrangian analysis tool - version 2.0. *Geoscientific Model Development*, **8**(8), pp. 2569–2586.
- Sprenger, M., G. Fragkoulidis, H. Binder, M. Croci-Maspoli, P. Graf, C. M. Grams, P. Knippertz, E. Madonna, S. Schemm, B. Škerlak, and H. Wernli, 2017: Global climatologies of Eulerian and Lagrangian flow features based on ERA-Interim. *Bulletin of the American Meteorological Society*, **98**(8), pp. 1739–1748.
- Stefanon, M., F. Dandrea, and P. Drobinski, 2012: Heatwave classification over Europe and the Mediterranean region. *Environmental Research Letters*, **7**(1).
- Taschetto, A. S. and M. H. England, 2009: El Niño Modoki impacts on Australian rainfall. *Journal of Climate*, **22**(11), pp. 3167–3174.
- Timbal, B. and W. Drosowsky, 2013: The relationship between the decline of southeastern Australian rainfall and the strengthening of the subtropical ridge. *International Journal of Climatology*, **33**(4), pp. 1021–1034.
- Trenberth, K. E., 1997: The definition of El Niño. *Bulletin of the American Meteorological Society*, **78**(12), pp. 2771–2778.
- Ulbrich, U., G. C. Leckebusch, and J. G. Pinto, 2009: Extra-tropical cyclones in the present and future climate: a review. *Theoretical and Applied Climatology*, **96**(1), pp. 117–131.

- Ummerhofer, C. C., M. H. England, P. C. McIntosh, G. A. Meyers, M. J. Pook, J. S. Risbey, A. S. Gupta, and A. S. Taschetto, 2009: What causes southeast Australia's worst droughts?. *Geophysical Research Letters*, **36(4)**.
- Ummerhofer, C. C., A. S. Gupta, P. R. Briggs, M. H. England, P. C. McIntosh, G. A. Meyers, M. J. Pook, M. R. Raupach, and J. S. Risbey, 2011: Indian and Pacific Ocean influences on southeast Australian drought and soil moisture. *Journal of Climate*, **24(5)**, pp. 1313–1336.
- Van Rensch, P., J. Arblaster, A. J. E. Gallant, W. Cai, N. Nicholls, and P. J. Durack, 2019: Mechanisms causing east Australian spring rainfall differences between three strong El Niño events. *Climate Dynamics*, pp. 1–19.
- Wang, G. and H. H. Hendon, 2007: Sensitivity of Australian rainfall to inter-El Niño variations. *Journal of Climate*, **20(16)**, pp. 4211–4226.
- Wang, X., W. Tan, and C. Wang, 2018: A new index for identifying different types of El Niño Modoki events. *Climate Dynamics*, **50(7-8)**, pp. 2753–2765.
- Wernli, H. and P. Knippertz, 2019: Warm conveyor belts and tropical moisture exports, and their relationship to atmospheric rivers. In: *Atmospheric Rivers: Two Decades of Research*, Eds. Ralph, M. F., M. Dettinger, J. J. Rutz, and D. E. Waliser, in press.
- Wernli, H. and C. Schwierz, 2006: Surface cyclones in the ERA-40 dataset (1958–2001). Part I: Novel identification method and global climatology. *Journal of the Atmospheric Sciences*, **63(10)**, pp. 2486–2507.
- Wernli, H. and M. Sprenger, 2007: Identification and ERA-15 climatology of potential vorticity streamers and cutoffs near the extratropical tropopause. *Journal of the Atmospheric Sciences*, **64(5)**, pp. 1569–1586.
- Westra, S., B. Renard, and M. Thyer, 2015: The ENSO-precipitation teleconnection and its modulation by the Interdecadal Pacific Oscillation. *Journal of Climate*, **28(12)**, pp. 4753–4773.
- Wright, W. J., 1989. *A synoptic climatological classification of winter precipitation in Victoria*.
- Wright, W. J., 1997: Tropical-extratropical cloudbands and Australian rainfall: I. Climatology. *International Journal of Climatology*, **17**, pp. 807–829.

# List of abbreviations

<b>AR</b>	Atmospheric River
<b>DMI</b>	Dipole Mode Index
<b>ECMWF</b>	European Centre for Medium-Range Weather Forecasts
<b>ENSO</b>	El Niño-Southern Oscillation
<b>EOF</b>	Empirical orthogonal function
<b>IOD</b>	Indian Ocean Dipole
<b>IPO</b>	Interdecadal Pacific Oscillation
<b>ITCZ</b>	Innertropical Convergence Zone
<b>NOAA</b>	National Oceanic and Atmospheric Administration
<b>OLR</b>	Outgoing longwave radiation
<b>PDO</b>	Pacific Decadal Oscillation
<b>RWT</b>	Rossby wave train
<b>SAM</b>	Southern Annular Mode
<b>SOI</b>	Southern Oscillation Index
<b>SPCZ</b>	South Pacific Convergence Zone
<b>TPI</b>	Tripole Mode Index



# Acknowledgement

Many people contributed to the final version of my thesis and now it's time to thank them personally.

I would like to express my gratitude to my supervisor Dr. Julian Quinting for the incredibly exciting topic and the unwavering support from the day one. Julian, your knowledge and passion for meteorology is inspiring and you have motivated me to continue in the research field. I want to thank you immensely for giving me the opportunity to complete a research stay at Monash University (Melbourne), which enabled me to develop professionally and personally.

Furthermore, I am deeply thankful to my supervisor, main referent and group leader Dr. Christian Grams for the admission in his research group 'Large-scale Dynamics and Predictability' at IMK-TRO. Christian, thank you for your suggestions and ideas through our countless discussions, for motivating me to keep going, and for your exemplary knowledge of atmospheric dynamics which has played a significant role to this thesis.

I want to thank my co-supervisors Prof. Peter Knippertz and Prof. Andreas Fink for their supervision and helpful discussions on my topic. This work would not have been possible without your constructive feedback, ideas and comments along the way. Andreas, thank you for the kind acceptance to do the proof reading and for constructive feedback on an earlier version of this thesis.

I would also like to acknowledge Dr. Dominik Büeler, Jan Wandel and Moritz Pickl from the young investigator group 'Large-scale Dynamics and Predictability'. I am deeply appreciative of your support and feedback and our good conversations. Furthermore, I want to thank the atmospheric dynamics group of Prof. Heini Wernli at ETH Zurich for providing me their data set for the weather systems and associated flow features.

I am deeply thankful to Prof. Michael Reeder and Dr. Shayne McGregor for welcoming me to the School of Earth, Atmosphere and Environment at Monash University. My research stay has expanded my knowledge about Australian weather and climate, and I am grateful that my final thesis features many of your suggestions. I am extremely thankful to the ARC Centre of Excellence for Climate Extremes for the funding of my research stay in Melbourne.

I am deeply grateful to have so many supporting friends and family members who always believe in me and support me in every possible way. Thank you to fellow students for the coffee breaks in the social room and the uncountable hours we shared the office. To all my non-fellow student friends and Australian friends, thank you for truly believing in me and providing happy

distraction to rest my mind outside of my time at university.

Last but not least, I want to thank my closest loved ones from home for strengthening me at challenging times and for your 24/7 support. Above all, I am forever grateful for your love.

# Erklärung

Ich versichere wahrheitsgemäß, die Arbeit selbstständig verfasst, alle benutzten Hilfsmittel vollständig und genau angegeben und alles kenntlich gemacht zu haben, was aus Arbeiten anderer unverändert oder mit Abänderungen entnommen wurde sowie die Satzung des KIT zur Sicherung guter wissenschaftlicher Praxis in der jeweils gültigen Fassung beachtet zu haben.

Karlsruhe, den 25.06.2019

Seraphine Hauser